

2023

The cellular and molecular effects of ethanol in mediating skeletal patterning defects in sea urchin embryos

<https://hdl.handle.net/2144/47760>

Downloaded from OpenBU. Boston University's institutional repository.

BOSTON UNIVERSITY
GRADUATE SCHOOL OF ARTS AND SCIENCES

Dissertation

**THE CELLULAR AND MOLECULAR EFFECTS OF ETHANOL
IN MEDIATING SKELETAL PATTERNING DEFECTS
IN SEA URCHIN EMBRYOS**

by

NAHOMIE RODRIGUEZ-SASTRE

B.S., Universidad Metropolitana, 2016
M.S., Boston University, 2020

Submitted in partial fulfillment of the
requirements for the degree of
Doctor of Philosophy

2023

© 2023 by
NAHOMIE RODRIGUEZ-SASTRE
All rights reserved except for Appendix
chapter which is Copyright © 2019
Elsevier Inc.

Approved by

First Reader

Cynthia A. Bradham, Ph.D.
Associate Professor of Biology

Second Reader

Angela Ho, Ph.D.
Associate Professor of Biology

DEDICATION

Para Mami y Papi:

Gracias por hacer de mí una persona con raíces firmes y con unas alas tan fuerte que el
volar no se me hace difícil.

ACKNOWLEDGMENTS

In the last six and a half years, I have been fortunate to have met many people who supported me through this journey. Thank you to everyone who has stayed through the ups and downs of grad school.

Thank you to my advisor Dr. Cynthia Bradham. Cyndi, thank you for your support and guidance throughout my journey as a graduate student in your lab. Thank you for helping me make progress in my project, for challenging me, and for helping me become a better scientist.

I would also like to thank my thesis committee members: John “Chip” Celenza, Angela Ho, Trevor Siggers, and Andrew Emili. Thank you for your input, help, and guidance with my project. Peter Castellano, Dennis Batista, Todd Blute, Jen Correa, Eliza Givens and Christina Honeycutt were always there when I needed help with something or had any questions. The department is lucky to have you; I do not know what we would do without you.

Thank you to my wonderful graduate student lab mates: Alex, Chris, Dakota, Abbie, Dan, and James. You are brilliant, extraordinary people, and I cannot wait to see what the future holds for all of you. I appreciate your support and all the laughter and beautiful memories that I will cherish forever. Thank you to the undergraduates who helped me with this project. It was terrific working with all of you.

Thank you to the friends that have made this journey a fun one. Your friendship has been so important to me, and I am grateful for all the phone calls, the DnD/Vampire games, the karaoke sessions, beach days, dancing, board game nights, etc. I am grateful

you guys are in my life.

Thank you to my parents; I love you! Without you, I do not think I would have been able to complete this. Your constant calls, care packages, and words of encouragement kept me going. You taught me to be strong, resilient, and always finish what I started. I am a lucky girl. This is for you!

Finally, I want to thank Dr. Tom Gilmore and Chip because when I started my BU journey, it was back in 2015 with them. They have been there since day one, so thank you for your advice, all of the fun teaching moments, and for being the first ones to give me an opportunity to do research at BU. I hope I have made you proud.

**THE CELLULAR AND MOLECULAR EFFECTS OF ETHANOL
IN MEDIATING SKELETAL PATTERNING DEFECTS
IN SEA URCHIN EMBRYOS**

NAHOMIE RODRIGUEZ-SASTRE

Boston University Graduate School of Arts and Sciences, 2023

Major Professor: Cynthia A. Bradham, Associate Professor of Biology

ABSTRACT

Pattern formation ensures that tissues, organs, and structures develop in the correct place and orientation within the body. Patterning processes are at the heart of morphogenesis yet remain poorly understood due to their complexity. The sea urchin larval skeleton provides a simple model to study skeletal patterning, where the skeleton-producing primary mesenchyme cells (PMCs) receive patterning cues from the overlying ectoderm. The normal skeletal patterning process requires the PMCs to migrate within the blastocoel to specific positions. While ectodermal and endodermal signals regulate PMC positioning and differentiation, additional signals act to regulate biomineralization per se in the PMCs. However, the distinction between these effects is not well understood and new efforts have been made to identify these patterning and biomineralization cues that regulate sea urchin skeletal development. Understanding the mechanism by which PMCs interpret and transduce patterning cues into a migratory bias and/or positional information will provide insight into tissue patterning and developmental plasticity both in sea urchins and, more broadly, in deuterostomes. Ethanol is a known vertebrate teratogen that causes craniofacial defects as a component of fetal alcohol syndrome.

Perturbations to retinoic acid biosynthesis and the Hedgehog signaling pathway are thought to be causal for the fetal alcohol syndrome phenotype in vertebrates. We used the sea urchin embryo to gain evolutionary insight into how ethanol affects embryonic development in a basal deuterostome animal. We found that ethanol specifically perturbs skeletal patterning. When sea urchin embryos are exposed to ethanol, they exhibit conspicuously delayed development, and broad skeletal patterning defects that are potentially analogous to fetal alcohol syndrome associated facial patterning defects in vertebrates and humans. PMC transplantation experiments demonstrated that ethanol-induced defects are not specific to the PMCs, and instead reflect the perturbation of patterning cues. We also found that the expression of both patterning cues and PMC-specific genes was delayed by ethanol exposure. Surprisingly, our results indicate that retinoic acid and Hedgehog pathways are not functionally relevant for the teratogenic effects of ethanol in the larval skeletal patterning process, indicating a lack of evolutionary conservation of these pathways in ethanol-mediated teratogenesis among deuterostomes. Temporal transcriptome analysis revealed significant impacts of ethanol on signaling and metabolic gene expression and a disruption in the timing of expression for sea urchin specification gene regulatory network (GRN) genes. Surprisingly, multiple circuits with the GRN exhibit precocious expression while others are delayed. Taken together, our results suggest that the skeletal patterning perturbations in ethanol-treated sea urchin embryos arise from a loss of temporal synchrony within and between the instructive and responsive tissues during pattern formation.

TABLE OF CONTENTS

DEDICATION	iv
ACKNOWLEDGMENTS	v
ABSTRACT	vii
TABLE OF CONTENTS	ix
LIST OF TABLES	xii
LIST OF FIGURES	xiii
LIST OF ABBREVIATIONS AND ACRONYMS	xv
CHAPTER ONE: Introduction	1
1.1 Introduction	1
1.1.1 Sea urchin as a model organism	1
1.1.2 Sea urchin development.....	2
1.1.2 Dorsal-ventral (DV) specification	3
1.2 Role of PMCs in skeletal patterning in sea urchins	5
1.2.1 Skeletal patterning cues	8
1.3 Fetal alcohol syndrome disorder	9
1.3.1 EtOH-mediated retinoic acid synthesis perturbations	10
1.3.2 EtOH-mediated defects in Hedgehog signaling pathway	11
1.3.3 Roles of hedgehog (Hh) and retinoic acid (RA) signaling in echinoderms.....	12
1.4 Thesis rationale.....	13
CHAPTER TWO: Ethanol Exposure Perturbs Sea Urchin Development and Disrupts Developmental Timing	25
2.1 Abstract	25
2.2 Introduction	26
2.3 Material and Methods.....	28
2.3.1 Reagents.....	28
2.3.2 Chemical treatment.....	29
2.3.3 Animal, perturbations, transplant, imaging, and skeletal scoring.....	29
2.3.4 Immunostaining and confocal microscopy	30

2.3.5	Fluorescent <i>in situ</i> hybridization (FISH)	30
2.3.6	HCR FISH: probe sets, amplifiers, and buffers	30
2.3.7	Acetaldehyde Measurements	31
2.3.8	Serotonin level and spatial gene expression measurements	31
2.3.9	RNA-seq Analysis	31
2.4	Results	33
2.4.1	EtOH treatments results in skeletal patterning defects	33
2.4.2	EtOH indirectly impacts the PMCs to produce skeletal patterning defects.....	35
2.4.3	EtOH does not perturb ectodermal DV specification.	35
2.4.4	EtOH does not perturb neural specification or patterning.	36
2.4.5	EtOH perturbs temporal expression of Wnt5 ectodermal patterning cue.	37
2.4.6	EtOH perturbs PMC migration, positioning, and spatial gene expression.	38
2.4.7	EtOH-mediated skeletal patterning defects arise independently of retinoic acid perturbation.....	40
2.4.8	Inhibition of the Hh signaling pathway partially rescues the EtOH phenotype.	42
2.4.9	RNA-seq reveals temporal perturbations of GRN gene expression.	42
2.5	Discussion	45
CHAPTER THREE: Discussion and Future Directions		68
3.1	Summary of findings	68
3.2	Discussion and future directions	70
3.3	Conclusions	71
APPENDIX.....		73
A.1	Measuring Voltage and Ion Concentration in Live Embryos.....	73
A.1.1	Abstract.....	73
A.1.2	Introduction.....	74
A.1.2.1	Ion flux during development.....	74
A.1.2.2	Events immediately following fertilization are regulated by Na ⁺ and Ca ²⁺	76

A.1.2.3 Dorsal-ventral (DV) and Left-Right (LR) specification are regulated by H ⁺ /K ⁺ ATPase activity and Ca ²⁺	77
A.1.2.4 Biomineralization is dependent on ion flux	78
A.1.3 Voltage sensitive dyes	79
A.1.4 Methods	80
A.1.4.1 DiBAC ₄ /DiSBAC ₄ :	80
A.1.4.2 Fluorescent Cl ⁻ ion reporters	81
A.1.4.3 Fluorescent Na ⁺ ion reporters	82
A.1.4.4 Fluorescent pH reporters	84
A.1.5 Data Analysis	85
LIST OF JOURNAL ABBREVIATIONS	91
REFERENCES.....	95
CURRICULUM VITAE.....	127

LIST OF TABLES

	Page
Table A.1. Voltage- and ion-sensing dyes	89

LIST OF FIGURES

		Page
Figure 1.1	Sea urchins are basal deuterostomes	14
Figure 1.2	Figure 1.2 A fate map of a 60-cell stage sea urchin embryo	15
Figure 1.3	The sea urchin ectoderm gene regulatory network	16
Figure 1.4	The sea urchin endomesoderm gene regulatory network	17
Figure 1.5	Ciliary band development.	18
Figure 1.6	The sea urchin skeleton is secreted by PMCs in 1° and 2° phases.	19
Figure 1.7	VEGF or VEGFR loss-of-function blocks PMC spatial patterning and skeleton formation in sea urchin embryos.	20
Figure 1.8	Wnt5 loss-of-function blocks biomineralization.	21
Figure 1.9	RNA-seq-based screen identified skeletal patterning genes in sea urchin embryos.	22
Figure 1.10	Ethanol-mediated developmental defects are rescued by retinoic acid treatment in zebrafish embryos.	23
Figure 1.11	Sonic hedgehog loss of function severely perturbs facial development.	24
Figure 2.1	Ethanol exposure perturbs skeletal patterning between 5 and 22 hpf.	49–50
Figure 2.2	EtOH treatment does not impact neural development or ectodermal DV specification and delays normal expression of the PMC-directing signal Wnt5.	51–52
Figure 2.3	EtOH treatment results in delayed PMC ingression, migration, and Jun expression	53
Figure 2.4	EtOH-mediated defects do not arise via reduction in retinoic acid.	54–55
Figure 2.5	Inhibition of Hh signaling partially rescues the EtOH phenotype	56
Figure 2.6	EtOH treatment results in disrupted temporal synchrony.	57–58

Figure 2.7	EtOH is most effective between 5-22 hpf.	59
Figure 2.8	EtOH does not perturb ectodermal DV specification or neural patterning.	60
Figure 2.9	EtOH exposure delays the normal spatial expression of Hh, Wnt, and Jun.	61
Figure 2.10	While acetaldehyde (Ace.) treatment results in skeletal patterning defects, neither retinol (R) or retinoic acid (RA) is sufficient to rescue EtOH.	62–63
Figure 2.11	The rescue of the EtOH phenotype by Hh pathway inhibition is most effective at low doses.	64
Figure 2.12	GO term analysis show metabolism and signaling are the most affected in EtOH samples.	65
Figure 2.13	EtOH-treated embryos exhibit temporally disrupted gene expression.	66–67
Figure 3.1	A model for EtOH-mediated developmental perturbations in sea urchin embryos.	72
Figure A.1	A chart depicting membrane potential measured over time	87
Figure A.2	Structures of the indicated voltage- and ion-sensing dyes described in this chapter	88
Figure A.3	Examples of control embryos at mesenchyme blastula stage, imaged for voltage potential (A, DiBAC), protons (B, SNARF), sodium ions (C, CoroNa), or chloride ions. (D, MEQ)	89

LIST OF ABBREVIATIONS AND ACRONYMS

μg	Microgram
μl	Microliter
μM	Micromolar
μm	Micrometer
Ace	Acetaldehyde
ADH	alcohol dehydrogenase
ALDH	Aldehyde dehydrogenase
Alk	activin receptor-like kinase
ALOX	Lipoxygenase
AP	anterior-posterior
AR	anal rods
AV	animal-vegetal
BMP	bone morphogenetic protein
BR	body rod
CB	ciliary band
cDNA	complementary DNA
CNS	Central nervous system
Cyc	Cyclopamine
DE	differentially expressed
DIC	differential interference contrast
DMSO	dimethyl sulfoxide
DNA	deoxyribonucleic acid
DV	dorsal-ventral
DVC	dorsal-ventral connecting rod
EB	early blastula
EG	early gastrula

EMT	epithelial to mesenchymal transition
EtOH	Ethanol
FASD	Fetal Alcohol Syndrome
FGF	fibroblast growth factor
FGFR	fibroblast growth factor receptor
FISH	fluorescent <i>in situ</i> hybridization
Fom	Fomepizole
GRN	gene regulatory network
Hh	Hedgehog
hpf	Hours post fertilization
Lv	<i>Lytechinus variegatus</i>
MAPK	Mitogen-activated protein kinase
mM	Millimolar
MO	Morpholino
PCA	principal component analysis
PMC	Primary mesenchyme cells
Ptc	Patched
qPCR	quantitative polymerase chain reaction
RA	Retinoic Acid
RALDH	retinaldehyde dehydrogenase
RDH	retinol dehydrogenase
RNA-Seq	ribonucleic acid sequencing
RO	Retinol
RR	Recurrent rod
SE	Standard error
SEM	Standard error of the mean
ser	Serotonergic
SLC	Solute carrier

Smo	Smoothen
Sp	<i>Strongylocentrotus purpuratus</i>
SPG	Sulfate proteoglycans
synB	synaptotagmin B
TGF- β	transforming growth factor beta
VEGF	Vascular endothelial growth factor
VEGFR	Vascular endothelial growth factor receptor
VLC	Ventrolateral cluster
VT	Ventral transverse
vv	Vegetal view

CHAPTER ONE: Introduction

1.1 Introduction

1.1.1 Sea urchin as a model organism

Sea urchins belong to the animal subkingdom of Bilateria (Sodergren et al., 2006), animals with bilateral symmetry as an embryo, and are members of the phylum Echinodermata. Bilateria is divided into two major phyla depending on when the mouth forms: deuterostomes (the anus develops first), which includes vertebrates, and protostomes (the mouth develops first), which includes insects (Fig. 1.1). Deuterostomes fall into two categories: chordates and non-chordates, which corresponds with the appearance of a notochord during development, which arises in the same location as the vertebral column in the adult.

Sea urchins are non-chordates deuterostomes; therefore, they represent the basal deuterostomes that gave rise to vertebrates and mammals. Genome sequencing and analysis have revealed a surprisingly high degree of similarity of gene families between sea urchins and mammals; therefore, experimental findings from simple sea urchin embryos are often conserved in more complex vertebrates and mammals and thus often provide mechanistic insights into developmental processes (Bradham et al., 2006; Sodergren et al., 2006). Sea urchins offer a range of advantages as a developmental model organism: they produce millions to billions of gametes in a single spawn, their development is very fast, the embryos are entirely transparent, and the eggs can be fertilized *in vitro* to develop synchronously. They are regulative embryos, like vertebrates, and are therefore robust to experimental manipulations such as egg

bisections, cell dissociation, transplantation, and microinjection (Lyons et al., 2012).

As a sister group to the chordates, the urchin offers an opportunity to obtain a glimpse of the evolutionary origins of the body plan that led to vertebrate development. The sea urchin has about 23,000 genes. A comparison showed that urchin shares about 70% of their genes with humans, compared to flies, which share only 40% with humans. An analysis of developmental expression showed that while approximately 50% of the genome (approx. 12,000 of 23,000 genes) is expressed in the embryo (Samanta et al., 2006), greater than 93% of genes encoding signaling proteins (including receptors) and transcription factors are expressed during embryonic development (Beane et al., 2006; Bradham et al., 2006; Croce et al., 2006; Howard-Ashby et al., 2006; Lapraz et al., 2006; Materna et al., 2006; Walton et al., 2006). This highlights the complexity of this process and emphasizes the importance of signaling and transcription to drive embryogenesis.

1.1.2 Sea urchin development

During cleavage, the sea urchin zygote is transformed into a multicellular blastula through rapid mitotic cell divisions. The first two cleavages produce the four-cell stage and occur parallel to the animal-vegetal (AV) axis that is established prior to fertilization (Angerer and Angerer, 2003; Lyons et al., 2012; Maruyama et al., 1985). During the third, perpendicularly oriented cleavage, the separation of the animal (anterior) blastomeres from four vegetal (posterior) blastomeres result in the eight-cell stage. Then, during the fourth cleavage, the animal cells divide with cleavage planes parallel to the AV axis and give rise to eight cells called mesomeres; in contrast, the vegetal blastomeres divide with cleavage planes perpendicular to the AV axis and with mitotic

spindles asymmetrically positioned toward the vegetal pole to produce four large upper cells called macromeres and four smaller, vegetally situated cells called micromeres (Fig. 1.2) (Horstadius, 1939). During the next cleavage, the micromeres again divide asymmetrically, producing vegetal small micromeres, with large micromeres above them. The embryo continues to divide, and at the 60-cell stage, the embryo is composed of six layers of cells along the AV whose fate has been specified (Horstadius, 1939).

The micromeres and macromeres in the posterior half of the embryo give rise primarily to the endomesoderm, while the mesomeres in the anterior half give rise to ectoderm. The small micromeres become the germ-line (Yajima and Wessel, 2011), and the large micromeres give rise to the PMCs (Fig. 1.2). AV axis specification is maternally initiated prior to fertilization, while the dorsal-ventral (DV) axis is established during blastula stages and becomes determined once gastrulation has begun (Bradham and McClay, 2006; Duboc et al., 2004; Hardin et al., 1992; Horstadius, 1939; Piacentino et al., 2015). Finally, the molecular cascades that define the left-right (LR) axis are initiated during gastrulation (Duboc and Lepage, 2008; Luo and Su, 2012; Piacentino et al., 2016a).

1.1.2 Dorsal-ventral (DV) specification

Specification of the DV axis, also known as the oral-aboral axis, relies on two TGF β signaling ligand superfamily members: Nodal and BMP2/4. Nodal is a downstream target of asymmetrically active p38 MAPK (Bradham et al., 2009; Bradham and McClay, 2006; Duboc et al., 2004). The ventral (oral) territory is defined by asymmetrically expressed Nodal, which is maintained by auto-activation (Nam et al.,

2007; Range et al., 2007). The spatial restriction of Nodal expression is thought to be regulated by the Nodal target Lefty in a Turing reaction-diffusion system (Duboc and Lepage, 2008). BMP2/4 plays an essential role in the dorsal (aboral) specification in urchins (Angerer et al., 2000; Lapraz et al., 2009) since it acts as a diffusible relay molecule that signals for the specification of the dorsal ectoderm. Its signaling activity is confined due to the inhibition by Chordin (Chd) within the ventral ectoderm (Bradham et al., 2009; Lapraz et al., 2009). Other studies have proposed that a maternal redox agent cooperates with BMP2/4 to induce the expression of early dorsal regulatory markers such as Tbx2/3, IrxA, Dlx, Msx, Hmx and Hox7, that contribute to dorsal specification (Fig 1.2) (Ben-Tabou de-Leon et al., 2013; Chen et al., 2011; Coffman, 2011; Coffman et al., 2004; Modell and Bradham, 2011). Our current understanding of the AP and DV axis is captured by the current gene regulatory network (GRN) models for each territory (Fig. 1.3-1.4) (Davidson et al., 2002; Li et al., 2014; Materna et al., 2013; Peter and Davidson, 2011; Saudemont et al., 2010; Su et al., 2009).

Two additional major regions in the ectoderm are the ciliary band (CB), located at the boundary between the dorsal-ventral region, and the apical neurogenic domain (Fig. 1.5A). The ciliary band consists of apically constricted, ciliated cells along with neurons that together form an integrated tissue that functions as the larva's principal swimming organ (Yaguchi et al., 2010). Ventral Nodal and dorsal BMP2/4 signaling spatially restricts the ciliary band to the territory between the ventral and the dorsal territories that are specified by each signal (Yaguchi et al., 2010). Some ectodermal cells give rise to the larval "peripheral" nervous system, which consists of 40-50 neurons marked by

expression of the pan-neural marker synaptotagmin B (synB) that are mainly distributed along the ciliary band, in the apical plate and pharyngeal endoderm; in addition, 4-6 serotonergic "central" neurons arise in the apical plate (Bradham et al., 2009; Burke et al., 2014, 2006; Yaguchi et al., 2006).

The ciliary band is the default ectodermal state prior to DV specification (Angerer et al., 2000; Bradham et al., 2009; Duboc et al., 2004; Lapraz et al., 2009; Yaguchi et al., 2006); thus, perturbations to DV specification are hallmarked by ciliary band abnormalities (Bradham et al., 2009; Lapraz et al., 2009; Yaguchi et al., 2006). For example, in the absence of DV specification, there is a broad expansion of the ciliary band to most of the ectoderm (Fig 1.5B-C); in contrast, ventralized embryos exhibit vegetal expansion of the ciliary band (Fig. 1.4D) (Bradham et al., 2009; Lapraz et al., 2009; Yaguchi et al., 2006).

1.2 Role of PMCs in skeletal patterning in sea urchins

The sea urchin larval skeleton is composed of calcium carbonate with numerous embedded proteins and is secreted via biomineralization by the primary mesenchyme cells (PMCs) (Beniash et al., 1999; Mann et al., 2010; Wilt, 2002, 1999). The PMCs arise from the large micromeres that are produced at the posterior pole of the 32-cell stage embryo (Oliveri et al., 2003, 2002). The four large micromeres exhibit β -catenin nuclearization (Logan et al., 1998). β -catenin is necessary and sufficient for micromere specification and endomesoderm induction (Emily-Fenouil et al., 1998; Logan et al., 1998; Wikramanayake et al., 1998). β -catenin nuclearization leads to the expression of the transcription factor *Pmar1*, which then represses the transcriptional repressor *HesC*.

This double-negative regulatory switch controls the fate of these cells and allows the micromere/PMC-specific program to unfold (Oliveri et al., 2003, 2002). The relief of HesC-mediated repression in the large micromeres leads to the expression of transcriptional regulators including Ets1, Alx1, and Tbr that mediate PMC specification (Oliveri et al., 2008) as well as expression of the Early Signal (now known to be Activin B) and Delta that induce endomesoderm specification (Ransick and Davidson, 1995; Sethi et al., 2009; Sherwood and McClay, 1999).

The PMCs progenitor cells are the four large micromeres; their progeny undergo an epithelial to mesenchymal transition (EMT) and ingress into the blastocoel, after which they are referred to as PMCs (Fink and McClay, 1985; Lyons et al., 2012; Wu and McClay, 2007). PMC ingression requires the expression of transcriptional repressors Snail and Twist (Wu et al., 2008; Wu and McClay, 2007), which commonly mediate EMT in development and cancer (Hemavathy et al., 2000; Kurrey et al., 2005; Kwok et al., 2005). Snail is expressed an hour before PMC ingression and is required to repress expression of the gene encoding the cell adhesion protein Cadherin and for Cadherin endocytosis from the cell membrane, which are conserved functions for this transcription factor that result in the loss of cell-cell adhesion that accompanies EMT (Hemavathy et al., 2000; Kurrey et al., 2005; Kwok et al., 2005; Lyons et al., 2012; Wu and McClay, 2007). LvTwist is expressed just before PMC ingression and is required for timely PMC ingression and skeleton formation (Wu et al., 2008).

Once inside the blastocoel, PMCs migrate to a posterior ring with two ventrolateral (VL) clusters in response to ectodermal signals, including VEGF (Duloquin

et al., 2007). The VL clusters extend PMC cords toward the embryo's anterior region, and this ring-and-cords arrangement constitutes the primary PMC pattern.

Biom mineralization initiates as skeletal triradiates that form in the VL clusters at late gastrula stage, then extend spicules along the ring and cords to produce the primary skeleton (Fig. 1.6A2-A3) (Ettensohn and M., 1993; Lyons et al., 2012; Piacentino et al., 2016b) (Fig. 1.6A4 and B4, blue). Then, additional migration out of the 1° pattern produces the secondary (2°) elements that give rise to the long skeletal arms, anterior skeleton, and the dorsal scheidel (Fig. 1.6B4, red). Heterochronic PMC transplantations and PMC re-positioning experiments demonstrated that all the PMCs are capable of making any region of the skeleton (Ettensohn, 1990; Ettensohn and McClay, 1986).

PMC migration is driven by patterning cues from the ectoderm, as first suggested by von Ubisch in 1937, who noted that the posterior PMC ring adopted a more anterior position upon animalization of the embryo with LiCl₂ treatment (von Ubisch et al. 1937). Later, it was demonstrated that nickel-mediated skeletal patterning defects arise within the ectoderm (Armstrong et al., 1993; Hardin et al., 1992; Hardin and Armstrong, 1997; Piacentino et al., 2016b). Numerous additional experiments, some involving PMC transplantation, confirmed that patterning cues from the ectoderm regulate PMC positioning (Ettensohn, 1990; Ettensohn & McClay, 1986; Hardin & Armstrong, 1997; Tan et al., 1998). The PMCs extend filopodia that interact with the ectoderm throughout their migration, which led to the hypothesis that filopodia act as conduits for receiving information from the ectoderm (Malinda et al., 1995; Malinda and Ettensohn, 1994; Miller et al., 1995; Piacentino et al., 2016a, 2016b).

1.2.1 Skeletal patterning cues

Several ectodermal cues have been identified that are required either for biomineralization or skeletal patterning, and in one case, for both. Some of these cues include VEGF, FGF, WNT5, BMP5-8, NFL, ALOX, sulfated proteoglycans, and Univin (Adomako-Ankomah and Etensohn, 2013; Duloquin et al., 2007; Knapp et al., 2012; McIntyre et al., 2013; Piacentino et al., 2016a, 2016b, 2015; Rottinger et al., 2008). Growth factors like vascular endothelial growth factor (VEGF) and fibroblast growth factor ligand (FGF) are necessary and sufficient for skeletogenesis in some sea urchins species (Adomako-Ankomah and Etensohn, 2013; Knapp et al., 2012; Rottinger et al., 2008). They are each expressed in the ventrolateral ectoderm, with VEGF in a posterior domain adjacent to the PMC clusters at late gastrula stage, while FGF is expressed by more anterior ventrolateral ectoderm at the same stage (Adomako-Ankomah and Etensohn, 2013; Rottinger et al., 2008). VEGF signaling is required for normal PMC migration into the ring and clusters and for biomineralization (Fig 1.7) (Adomako-Ankomah and Etensohn, 2013; Duloquin et al., 2007), while FGF is dispensable for biomineralization and skeletal patterning in *L. variegatus* (Adomako-Ankomah and Etensohn, 2013; Rottinger et al., 2008). Wnt5 act as a short-range signal that establishes the expression of the transcription factor Pax2/5/8 in the posterior ventrolateral ectoderm and is required for biomineralization (Fig 1.8) (Cavalieri et al., 2011; McIntyre et al., 2013).

A screen for skeletal patterning genes in *L. variegatus* (Lv) that was performed in our lab identified the sulfate transporter SLC26a2/7 (SLC) and associated sulfated

proteoglycans as ventral patterning cues, and 5-lipoxygenase (ALOX) as a ventral and midline patterning cue (Piacentino et al., 2016b). SLC and ALOX are each required for normal skeletal organization (Fig 1.9A2-A3). SLC expression in the ventral ectoderm is responsible for maintaining a gradient of sulfated proteoglycans (sPGs) along the ventral-dorsal axis within the blastocoel (Piacentino et al., 2016b). When the sPGs gradient is inhibited, this results in loss of ventral PMCs and corresponding loss of ventral skeletal elements. We have also shown that the TGF- β signal Univin and its receptor Alk4/5/7 are required for anterior PMC positioning and anterior skeleton formation (Piacentino et al., 2015).

1.3 Fetal alcohol syndrome disorder

Ethanol (EtOH) exposure during embryonic development results in a spectrum of developmental defects referred to as Fetal Alcohol Spectrum Disorder (FASD). FASD is an umbrella term used to describe a group of conditions that reflect a wide range of developmental, morphological, and neurological defects after alcohol exposure during pregnancy (CDC, 2021; Eberhart and Parnell, 2016; Kot-Leibovich and Fainsod, 2009). Fetal Alcohol Syndrome (FAS) is a condition characterized by stereotypical facial patterning defects and disruption of neural proliferation, migration, and differentiation accompanied by excessive neural apoptosis and necrosis during the development of the central nervous system (CNS) (Blader and Strähle, 1998; Gil-Mohapel et al., 2019; Sulik, 2014). The pattern of facial perturbations that arise after fetal EtOH exposure primarily affects the facial midline and is thought to arise from aberrant neural crest cell behavior (Abramyan, 2019; Cartwright and Smith, 1995; Smith et al., 2014). The extent of

phenotypic variations in response to fetal alcohol exposure is thought to reflect individual differences in both maternal and fetal genetics, as well as the dose, pattern, and timing of alcohol exposure (Gilliam, 2014; Goodlett et al., 1989; Thomas et al., 2010). Studies in vertebrate models have determined that exposure to EtOH during early gestation (i.e., gastrulation) results in facial dystrophy (Marrs et al., 2010; Sarmah et al., 2020).

1.3.1 EtOH-mediated retinoic acid synthesis perturbations

One model for the FAS phenotype is based upon the inhibitory effect that EtOH has on retinoic acid (RA) synthesis (Shabtai et al., 2018). The biosynthesis of RA from retinol involves two successive oxidation steps performed by the retinol dehydrogenase (RDH) and retinaldehyde dehydrogenase (RALDH) enzymes. Similarly, EtOH is metabolically oxidized to acetaldehyde by the enzymatic action of alcohol dehydrogenase (ADH). Acetaldehyde is then further oxidized to acetate by aldehyde dehydrogenase (ALDH). Elevated levels of EtOH result in the competitive inhibition of RALDH by acetaldehyde, resulting in a severe reduction of RA levels (Crabb et al., 2004; Duester, 1991; Rahman and Yamauchi, 2006; Shabtai et al., 2018; Singh et al., 2015).

Experimental reduction in RA synthesis results in complex developmental phenotypes that are comparable to the FAS phenotype (Fig 1.10) (De Jonge and Zachman, 1995; Kot-Leibovich and Fainsod, 2009; Marrs et al., 2010; Mitoma et al., 2021; Serio et al., 2019; Shabtai et al., 2018; Wilson et al., 1953; Zakhari, 2006). In a parallel example, in frog embryos, EtOH exposure provokes limb defects that are hallmarked by altered RA signaling and rescued by exogenous RA (C. S. Johnson et al., 2007; Yelin et al., 2005). Here, proximally produced RA (via RALDH expressed by the somites) along with

distally produced FGF and Wnt signals have opposed signaling gradients that pattern the vertebrate limb. Although limb defects are not a typical component of FASD, these findings highlight the relationship between RA and EtOH.

1.3.2 EtOH-mediated defects in Hedgehog signaling pathway.

The hedgehog pathway (Hh) was first discovered in *Drosophila melanogaster* in a genetic screen for mutations that affect the patterning of the larval cuticle (Jia and Jiang, 2006; Nüsslein-volhard and Wieschaus, 1980). Hh signaling is triggered by the binding of Hh ligand to its receptor Patched (Ptc), resulting in the release of the transmembrane protein Smoothed (SMO) from endocytic vesicles via exocytosis. In the absence of Hh signaling, SMO is internalized in vesicles, and the associated transcription factor cubitus interruptus (Ci) is phosphorylated and cleaved, truncated Ci acts as a transcriptional repressor. Upon Hh stimulation, Ci is protected by now-available SMO from phosphorylation and cleavage; full-length Ci functions as a transcriptional activator (Hooper and Scott, 2005; Ingham and McMahon, 2001; Jia and Jiang, 2006; Lou et al., 2020; Zhang et al., 2021). This signaling cascade is highly conserved among Bilateria and is essential for embryonic development and post-developmental tissue homeostasis (Echelard et al., 1993; Jiang and Hui, 2008; Riddle et al., 1995; Zhang et al., 2021). For example, Hh functions as a long-range morphogen to specify ventral neuronal fates within the spinal cord and controls both proliferation and cell survival in the neural tube (Cayuso et al., 2006). This pathway plays a crucial role in the development of both the CNS and the face, each of which is affected in FASD (Fig. 1.11); the phenotypes of embryos exposed to EtOH are very similar to those found in embryos with defects in the

Hh signal transduction (Barresi et al., 2000; Blader and Strähle, 1998; Ingham and Placzek, 2006; Li et al., 2007). In severe cases, the EtOH-mediated defects of the face and brain fall inside the spectrum of holoprosencephaly, a hallmark of Shh loss-of-function in vertebrate embryos (Abramyan, 2019; Kietzman et al., 2014; Petryk et al., 2015; Solomon et al., 2010). Mutations in the co-receptor for Hh, *Cdon*, intensify the effects of EtOH during embryonic development, demonstrating a direct genetic interaction between EtOH and the Hh signaling pathway (Eberhart and Parnell, 2016; Hong and Krauss, 2012; Kietzman et al., 2014). Moreover, EtOH disrupts cholesterol homeostasis and thereby decreases the normal cholesterol modifications of the Hh ligand. When cholesterol is added to EtOH-exposed embryos, the phenotype is mitigated, further associating fetal EtOH exposure with suppression of Hh signaling (Li et al., 2007). Recent studies in zebrafish embryos demonstrate that agonism of Shh signaling rescues EtOH-treated embryos (Burton et al., 2022), providing strong evidence for a functionally significant impact of EtOH exposure on Shh signaling during development.

1.3.3 Roles of hedgehog (Hh) and retinoic acid (RA) signaling in echinoderms

RA and Hh signaling play essential roles in vertebrate development (Abramyan, 2019; Chatzi et al., 2013; Dubey et al., 2018; Gur et al., 2022; Janesick et al., 2015; Li et al., 2021; Sun et al., 2020). RA signaling is required for AP axis specification in vertebrates and other chordates, but its role in echinoderm development is unexplored. As described above, Hh is a crucial signal for vertebrate neural and facial development. In sea urchins, endodermally expressed Hh signals to the adjacent mesodermal lineages and is required for normal mesodermal patterning. Skeletal patterning defects arise after

perturbation of Hh signaling, which shows that Hh acts as a patterning cue for the PMCs (Walton et al., 2009). Hh signaling also contributes to left-right axis specification in sea urchin embryos, where motile cilia are required for Hh signaling transduction (Warner et al., 2016, 2014).

1.4 Thesis rationale

Although significant strides toward understanding the molecular nature of EtOH-mediated teratogenesis have been made, it is still not well understood. In this dissertation, we performed a series of experiments to understand how EtOH mediates its effects on sea urchin embryos, which offer a simple model system whose specification and patterning are relatively well-understood. We find that skeletal patterning is perturbed by EtOH treatment, while neural development is surprisingly not inhibited. We show that EtOH strongly delays morphological development. We describe how some skeletal patterning cues are affected by EtOH treatment. We tested the known targets for EtOH, RA, and Hh, and we found unexpectedly that they contributed only minimally or not at all to the teratogenic effects of EtOH in sea urchins, providing insight into the evolution of the embryonic response to EtOH. Temporal transcriptome analysis of EtOH-exposed embryos revealed both delayed and precocious gene expression within PMC-specific genes, specification GRN genes, as well as among genes encoding skeletal patterning cues. We, therefore, conclude that EtOH exposure results in dysregulation of temporal synchronization of GRN gene expression that results in disruption of development. This model provides novel insights into the mechanism underlying EtOH-mediated teratogenesis.

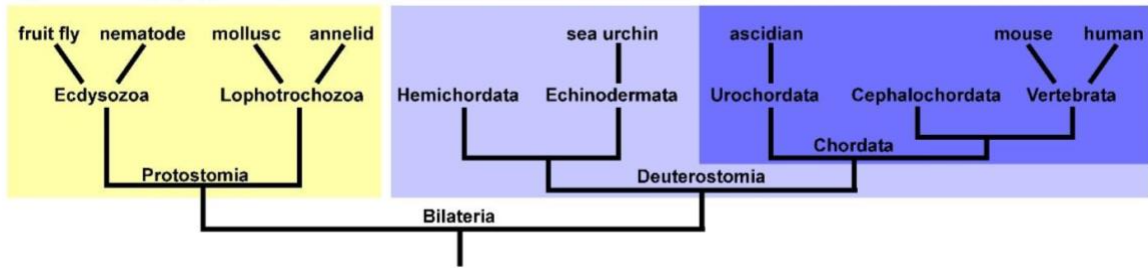


Fig. 1.1 Sea urchins are basal deuterostomes. Chordates (which possess a notochord, dark blue) are a subgroup of the Deuterostomes ("mouth second", light blue), and are distinct from Protostomes ("mouth first", yellow). From Sodergren et al 2006.

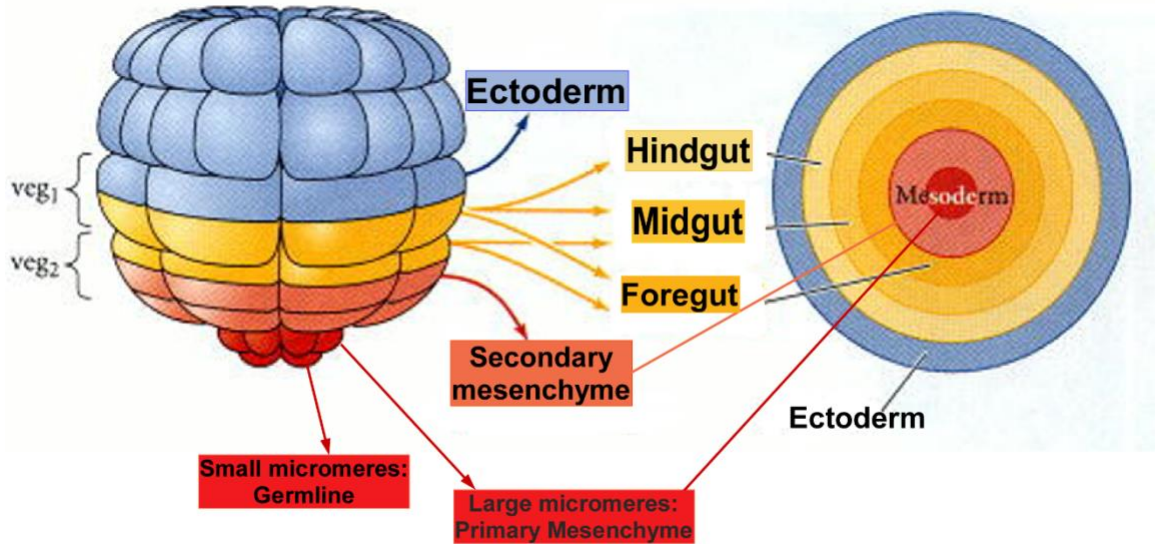


Figure 1.2 A fate map of a 60-cell stage sea urchin embryo. Blastomeres that give rise to the ectoderm are shown in blue, endoderm in yellow, mesoderm in orange, and micromere lineages in red. The small micromeres give rise to the germ line, and the large micromeres produce the PMCs. Veg1 and veg2 tiers are derived from macromeres. Adapted from S. Gilbert, *Developmental Biology* 8th Edition (Sinauer Oxford Press).

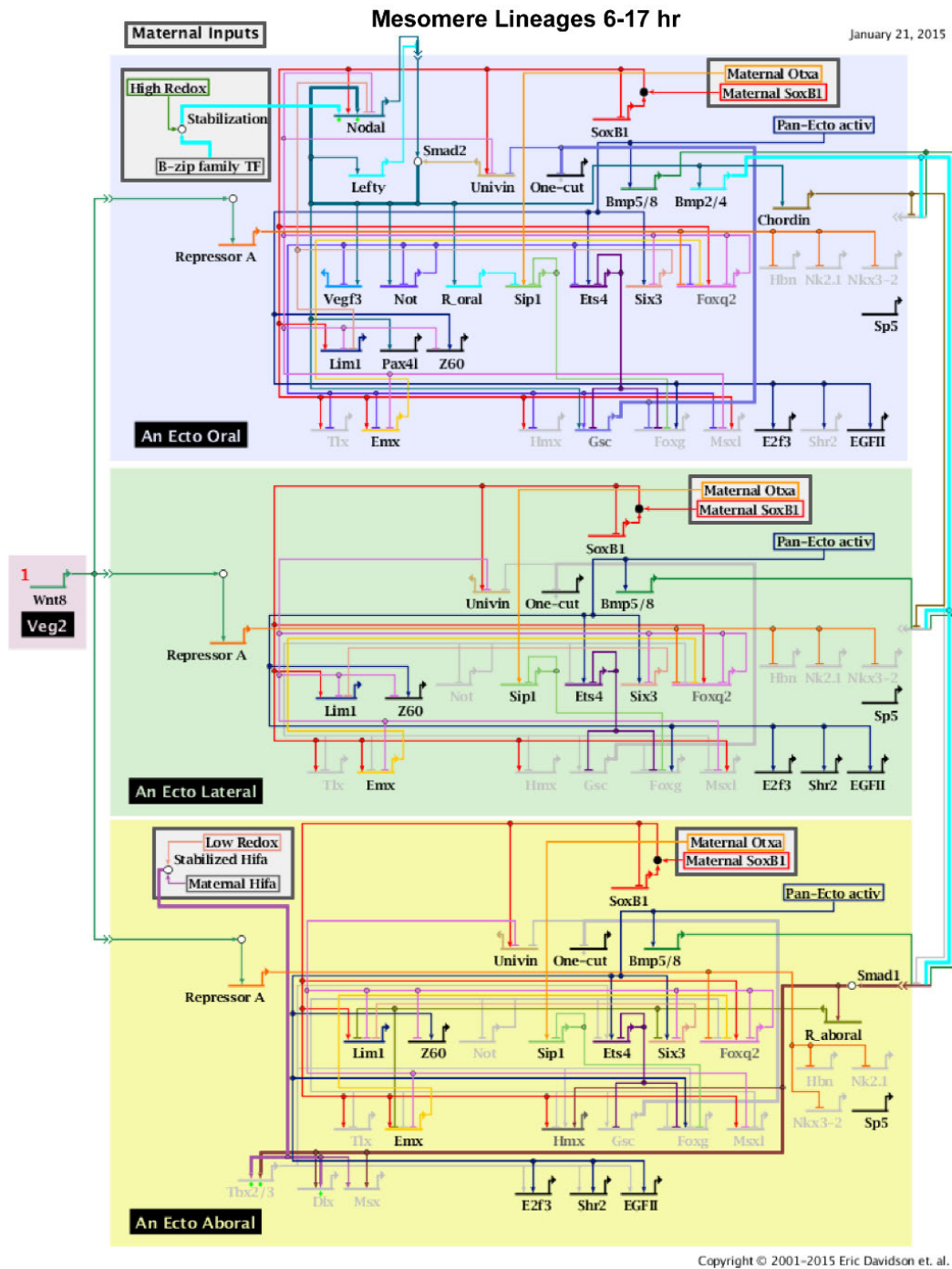


Figure 1.3 The sea urchin ectoderm gene regulatory network model. The model is a presentation of all interactions among regulatory genes governing ectoderm regulatory state. From BioTapestry online tool; Davidson Lab Gene Regulatory Networks

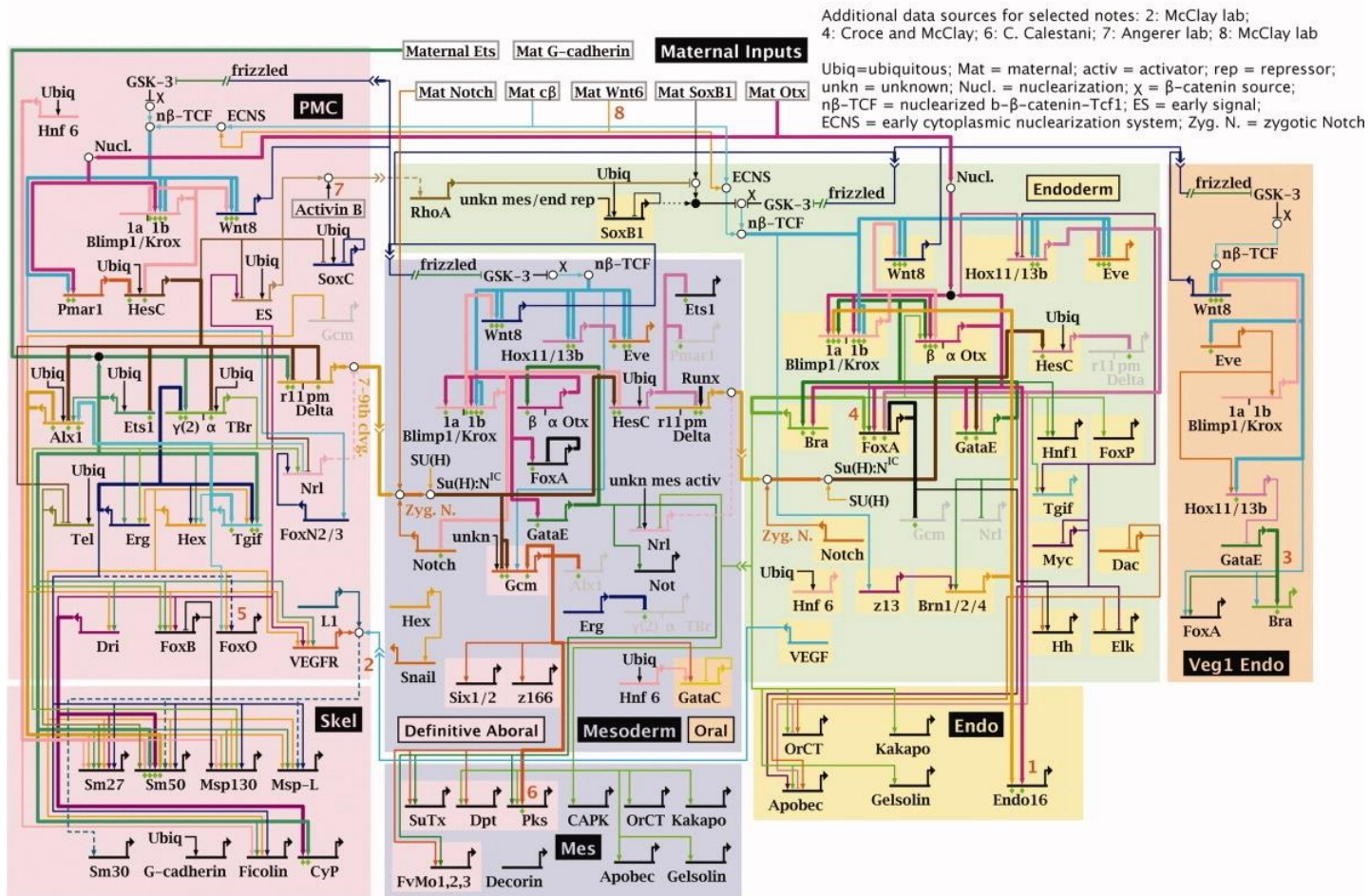


Figure 1.4 The sea urchin endomesoderm gene regulatory network model. The model is a presentation of all interactions among regulatory genes governing endomesoderm regulatory states including PMCs ("Skel"). From Li and Davidson 2009.

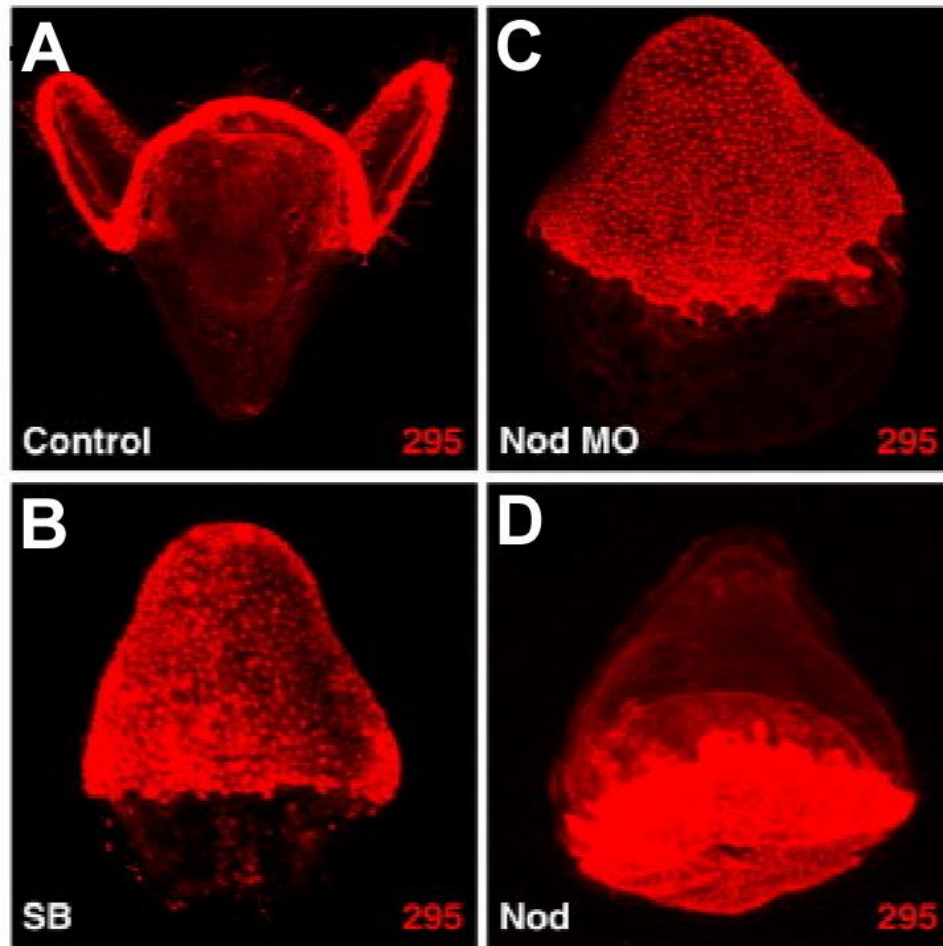


Figure 1.5. Ciliary band development. (A) The ciliary band was immunolabeled in control embryos (A), p38 MAPK-inhibited embryos (via SB203580 treatment) (B), LvNodal MO-injected embryos (C), and LvNodal mRNA-injected embryos (D), shown at 30 hpf. Adapted from Bradham et al., 2009.

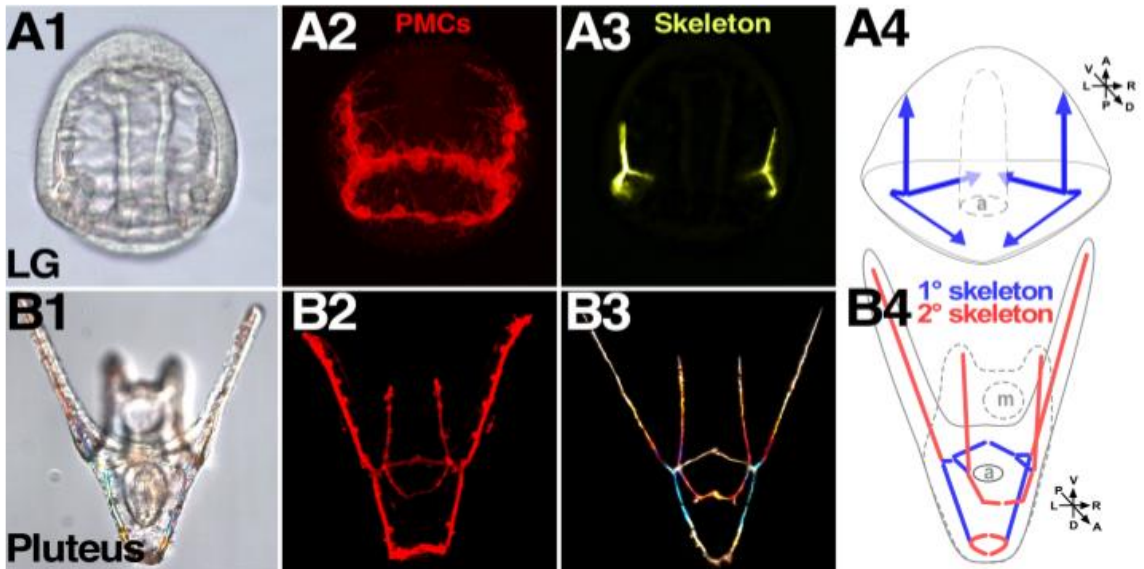


Figure 1.6. The sea urchin skeleton is secreted by PMCs in 1° and 2° phases.

Morphology (DIC, 1), PMC-specific immunostaining (2), and skeletal birefringence (3) are shown at late gastrula (LG, A) and pluteus stages (B). Schematics (4) show the 1° (blue) and 2° (red) elements.

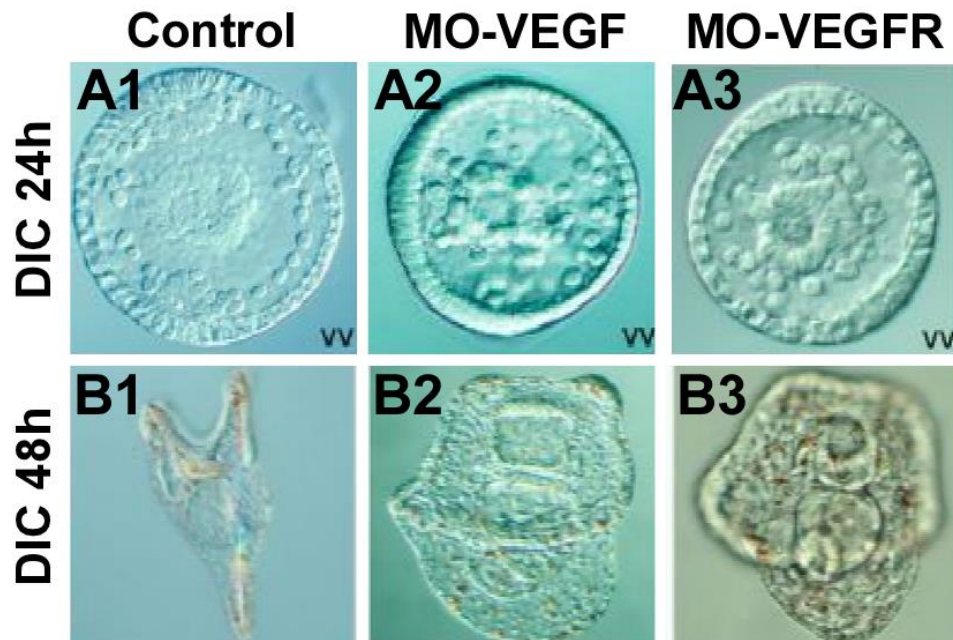


Figure 1.7. VEGF or VEGFR loss-of-function blocks PMC spatial patterning and skeleton formation in sea urchin embryos. *Paracentrotus lividus* sea urchin zygotes were injected with VEGF or VEGFR morpholino (MO) as indicated. Morphant embryos exhibit loss of PMC spatial organization (A2-3), and loss of biomineralization (B). Adapted from Duloquin et al., 2007.

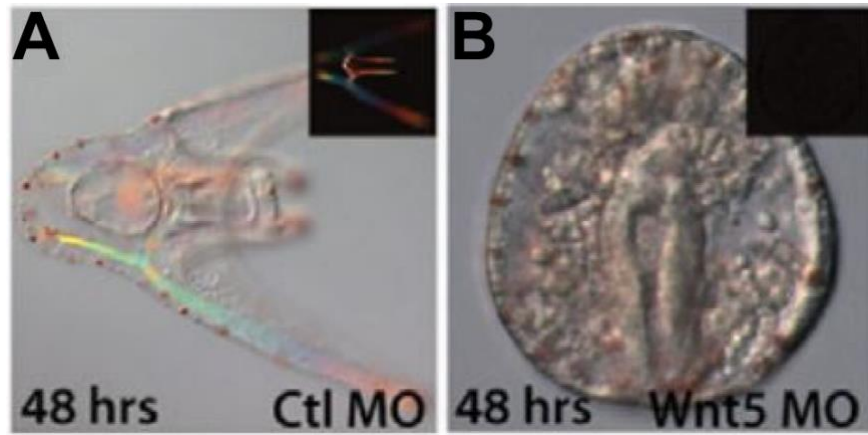


Figure 1.8. Wnt5 loss-of-function blocks biomineralization. Embryos were injected with control MO (A) or with Wnt5 MO (B), then developed to pluteus stage. Morphology (DIC) and skeletal birefringence (insets) are shown. Wnt5 morphants lack skeletons and are morphologically stalled at late gastrula stage. Adapted from McIntyre et al., 2013.

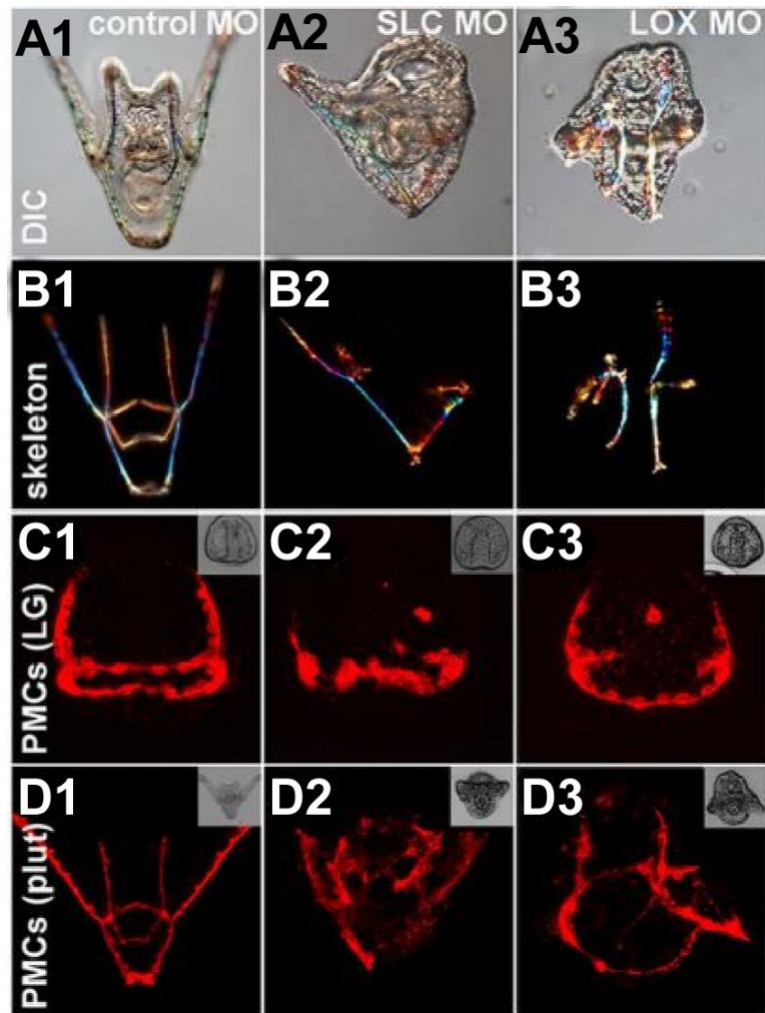


Figure 1.9. An RNA-seq-based screen identified skeletal patterning genes in sea urchin embryos. Loss-of-function analysis for *SLC26a2/7* (SLC, 2) and *ALOX* (LOX, 3) is compared to control MO (1), shown as morphology (DIC; A), skeletal pattern (B), PMC immunostaining at late gastrula stage (18 hpf; C) and at pluteus stage (48 hpf, D), with corresponding brightfield images inset. Adapted from Piacentino et al., 2016.

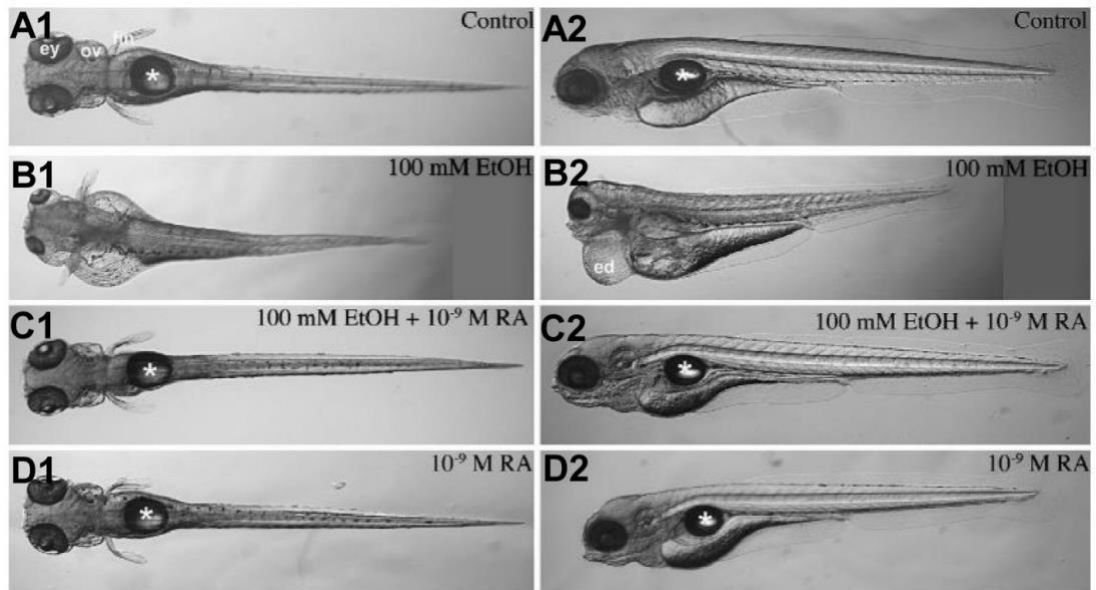


Figure 1.10. Ethanol-mediated developmental defects are rescued by retinoic acid (RA) treatment in zebrafish embryos. Control (A), EtOH- (B), EtOH+RA- (C), and RA- (D) treated embryos are shown in dorsal (1) and lateral (2) views at 4 days post-fertilization. The eye, optic vesicle (ov) and fin are indicated; asterisks and arrows indicate the swim bladder. Adapted from Marrs et al., 2010.



Figure 1.11. Sonic hedgehog loss of function severely perturbs facial development.

Mouse embryos with normal (A) and perturbed (B, C) facial morphogenesis due to heterozygous loss of Shh are shown in frontal (control and mutants, left) and lateral (mutants, right) views. Adapted from Kietzman et al., 2014.

CHAPTER TWO: Ethanol Exposure Perturbs Sea Urchin Development and Disrupts Developmental Timing

Nahomie Rodríguez-Sastre, Nicholas Shapiro, Dakota Y. Hawkins, Alexandra T. Lion, Monique Peyreau, Andrea E. Correa, Kristin Dionne, Cynthia A. Bradham¹

This chapter has been published on bioRxiv and is currently under peer review:

bioRxiv 2022.07.07.499183; doi: <https://doi.org/10.1101/2022.07.07.499183>

2.1 Abstract

Ethanol is a known vertebrate teratogen that causes craniofacial defects as a component of fetal alcohol syndrome (FAS). Our results show that sea urchin embryos treated with ethanol similarly show broad skeletal patterning defects, potentially analogous to the defects associated with FAS. The sea urchin larval skeleton is a simple patterning system that involves only two cell types: the primary mesenchymal cells (PMCs) that secrete the calcium carbonate skeleton and the ectodermal cells that provide migratory, positional, and differentiation cues for the PMCs. Perturbations in RA biosynthesis and Hh signaling pathways are thought to be causal for the FAS phenotype in vertebrates. Surprisingly, our results indicate that these pathways are not functionally relevant for the teratogenic effects of ethanol in developing sea urchins. We found that developmental morphology as well as the expression of ectodermal and PMC genes was delayed by ethanol exposure. Temporal transcriptome analysis revealed significant

¹ **NRS** performed the experiments and analysis reflected in Figures 2.1A-D, 2.2, 2.3, 2.4C-D and 2.5, 2.7, 2.8, 2.9, 2.10, 2.11. **NS, MS, and AEC** performed replicates captured in Figure 2.1-2.2, 2.7, 2.8. **ATL** performed the experiments in Figure 2.1E. **NS** performed the experiments reflected in Figure 2.1A-D, 2.4, 2.10. **MP** and **KD** establish optimal dose for EtOH. **DYH** and **CAB** performed the analysis presented in Figure 2.6, 2.12, 2.13.

impacts of ethanol on signaling and metabolic gene expression, and a disruption in the timing of GRN gene expression that includes both delayed and precocious gene expression throughout the specification network. We conclude that the skeletal patterning perturbations in ethanol-treated embryos likely arise from a loss of temporal synchrony within and between the instructive and responsive tissues.

2.2 Introduction

Pattern formation during embryonic development represents the expansion of genetically encoded biological design into tangible physical structures within the animal (Briscoe, 2019; Cang et al., 2021; Ulloa and Briscoe, 2007; Zernicka-Goetz, 2002).

Studying patterning in vertebrates is challenging, because of both their morphological and their genomic complexity. Vertebrates exhibit two ancestral genome duplication events that have resulted in significant genetic redundancy. Sea urchin embryos offer a considerably simpler model for pattern formation. First, they are morphologically quite simple, and second, because their genome was never duplicated, they lack extensive genetic redundancy (Sodergren et al., 2006), simplifying the study of gene function in this model.

The sea urchin larval skeleton is a bilaterally symmetric biomineral composed of calcium carbonate with numerous embedded proteins; the skeletal elements are secreted by the primary mesenchyme cells (PMCs) (Mann et al., 2010; Wilt, 2002). The PMCs ingress into the blastocoel at the onset of gastrulation, then migrate into stereotypical positions (Lyons et al., 2012). The PMCs receive instructive cues, mainly from the ectoderm, which direct their spatial positioning and differentiation (Adomako-Ankomah

and Ettensohn, 2013; Armstrong et al., 1993; Duloquin et al., 2007; McIntyre et al., 2013; Piacentino et al., 2016b, 2016a, 2015; Walton et al., 2009). The PMCs migrate into a primary (1°) spatial arrangement at late gastrula stage that is comprised of a posterior ring of cells around the blastopore with ventrolateral PMC clusters that extend cords of PMCs towards the embryo's anterior pole. This ring-and-cords arrangement presages the 1° skeletal pattern (Fig. 1A, blue). Then, additional PMC migration produces the secondary (2°) elements that give rise to the pluteus skeleton (Fig. 1A, red). Previous work from our lab and others has discovered numerous skeletal patterning cues that are expressed by the ectoderm; the molecules that drive skeletal patterning include conserved signaling proteins, second messengers, and extracellular matrix molecules (Armstrong et al., 1993; McIntyre et al., 2013; Piacentino et al., 2016b, 2016a, 2015). Although most patterning cues are expressed by the ectoderm, Hedgehog (Hh) signals from the endoderm also contribute to skeletal patterning (Walton et al., 2009).

Ethanol (EtOH) exposure during embryonic development in vertebrates leads to Fetal Alcohol Spectrum Disorder (FASD), which is a group of conditions that include a range of neurological and skeletal patterning defects (CDC, 2021; Eberhart and Parnell, 2016; Kot-Leibovich and Fainsod, 2009). Fetal Alcohol Syndrome (FAS) in humans is characterized by defects in the central nervous system (CNS) and facial aberrations. The patterning defects that arise after EtOH exposure primarily affect the midline of the face and are thought to arise from perturbations to the neural crest cells that produce the facial skeleton (Abramyan, 2019; Cartwright and Smith, 1995; Smith et al., 2014). Studies performed in vertebrate models have identified multiple downstream targets for EtOH,

including the Hh signaling pathway (Abramyan, 2019; Ahlgren et al., 2002; Li et al., 2007) and the retinoic acid signaling pathway (Hong and Krauss, 2017; Kot-Leibovich and Fainsod, 2009; Shabtai et al., 2018). Although these pathways contribute to the FASD phenotype, the overall mechanism underlying the FASD phenotypes, including their variable penetrance and severity, is still not well understood (Eberhart and Parnell, 2016; Sarmah et al., 2020; Serio et al., 2019).

When we exposed sea urchin zygotes and embryos to EtOH, we observed skeletal patterning defects, including midline and rotational defects, with no apparent effects on neural development or patterning. Surprisingly, we found that RA or Hh signaling perturbation does not account for the EtOH phenotype in sea urchins. We found that migration of the skeletogenic PMCs was delayed in EtOH-treated embryos, as was the expression of some PMC genes and ectodermal patterning cues. Temporal transcriptome analysis revealed that other such genes exhibited precocious expression, indicating that ethanol treatment results in temporally disrupted developmental gene expression; this broad asynchrony may underlie the intercellular communication-based patterning process in sea urchin embryos.

2.3 Material and Methods

2.3.1 Reagents

Dose-response experiments were performed to determine the optimal working doses for each perturbation reagent, which include EtOH, Acetaldehyde, Retinol, Retinoic Acid, Fomepizole (Sigma-Aldrich or Fisher Scientific), Cycloamine (Enzo Life Sciences), and SAG (Santa Cruz Biotechnology). All other chemicals were obtained from

Sigma-Aldrich or Fisher Scientific unless otherwise noted.

2.3.2 Chemical treatment

Embryos were cultured in artificial sea water (ASW) at a density of 500 embryos/mL in a 24 well plates and incubated in humid chamber at 23°C. EtOH- and Acetaldehyde-treated embryos were cultured in a separate well-plate and humid chamber to prevent vapor-mediated cross-contamination. Highly volatile and reactive retinol was reconstituted in DMSO, aliquoted, and added to embryo cultures inside an oxygen-free glove box.

2.3.3 Animal, perturbations, transplant, imaging, and skeletal scoring

Lytechinus variegatus sea urchins were obtained from the Duke University Marine Laboratory (Beaufort, NC) or from Reeftopia (Miami, FL). Gamete harvesting, fertilizations, and embryo culturing were performed as previously described (Bradham et al., 2006). Transplant experiments were performed as described (Piacentino et al., 2016b), using donor embryos labeled with tetramethyl rhodamine methyl ester (TMRM, Fisher Scientific). Larval morphology was imaged using DIC; larval skeletal birefringence was imaged in multiple focal planes using plane-polarized light on a Zeiss Axioplan inverted microscope at 200x magnification. Focal planes were then manually assembled into montage images using CanvasX (Canvas GFX, Inc.) to present the complete larval skeleton in focus. All focal planes were used for scoring with our in-house scoring rubric (Piacentino et al., 2016b) which captures element shortening, lengthening, loss, or duplication, spurious element production, abnormal element orientations, as well as whole embryo-level defects such as midline defects, and

orientation defects.

2.3.4 Immunostaining and confocal microscopy

Immunolabeling was performed as described (Bradham et al., 2006). Primary antibodies were PMC-specific 6a9 (1:5; from Charles Ettensohn, Carnegie Mellon University, Pittsburgh, PA), neural-specific 1e11 (1:10, from Robert Burke, University of Victoria, BC, Canada) and anti-serotonin (Sigma), and ciliary band-specific 295 (undiluted; from David McClay, Duke University, Durham, NC). Confocal imaging was performed using an Olympus FV10i laser-scanning confocal microscope. Confocal z-stacks were projected using Fiji, and full z-projections are presented.

2.3.5 Fluorescent *in situ* hybridization (FISH)

Full-length probes for LvJun, LvVEGF, LvVEGFR, LvHh, and LvWnt5a were transcribed using SP6 or T7 RNA polymerases (New England BioLabs) and labeled with digoxigenin (Roche). In situ hybridization was performed as previously described (Piacentino et al., 2015). FISH probe for Hedgehog, VEGF, VEGFR, and Wnt5 were previously described (McIntyre et al., 2013; Piacentino et al., 2015; Walton et al., 2009).

2.3.6 HCR FISH: probe sets, amplifiers, and buffers

Embryos were collected and fixed in 4 % paraformaldehyde at 18 hours post-fertilization (hpf). The published hybridization chain-reaction (HCR) single molecule FISH protocol (Choi et al., 2018, 2016) was performed using fluorescently labeled amplifiers (hairpins with either Alexa488, Alexa 546, or Alexa647 labels), buffers, and probe sets from Molecular Instruments, Inc. (Los Angeles, CA). The detection step was performed in 0.5 mL microcentrifuge tubes at 37° C; embryos were then transferred to a

96-well plate for the amplification step. Embryos were incubated in the hairpin solution for ~2.5 hours or overnight in the dark at room temperature, washed with 5X SSCT, then mounted in PBS/glycerol for imaging. Probe sets were designed from the open reading frames by Molecular Instruments, Inc. (Los Angeles, CA).

2.3.7 Acetaldehyde Measurements

Embryos were cultured at a density of 1500 embryos/mL until 18 hpf when the culture supernatant was collected. Acetaldehyde measurements was performed with a kit (Megazyme, Inc.) according to the manufacturer's instructions.

2.3.8 Serotonin level and spatial gene expression measurements

Fiji was used to process all confocal z-stacks. For measurements of serotonin levels from immunostained images, regions of interest (ROIs) were manually drawn in Fiji around each neural cell body, then the fluorescence intensity was measured as the total relative fluorescent units (RFU) per cell. Comparisons were limited to controls and treated embryos that were prepared together and imaged using identical settings. For spatial measurements of gene expression territories from FISH images, a threshold was applied to z-projections images in Fiji to produce a binary image. ROIs were then automatically defined using the Analyze Particles function in Fiji after adjusting the size range to most accurately capture the data. The resulting area values were normalized to the total area of the z-projected embryo.

2.3.9 RNA-seq Analysis

Total RNA was prepared from 10,000 embryos per sample using TRIzol (Invitrogen) and precipitated along with glycogen carrier (Ambion) from control and

ethanol-treated embryos at 15, 18 and 21 hpf, from three independent biological replicates. Library preparation and transcriptome sequencing were performed using DNA nanoball (DNB)-seq (BGI, Inc.) to generate 100 bp paired end reads. Quality control was performed using *fastp* to trim low-quality bases and remove low quality and low complexity reads (Chen et al., 2018). Reads were then aligned to the *Lvar* 3.0 genome (Davidson et al., 2020) using STAR (Dobin et al., 2013) and read counts were calculated using *featureCounts* (Liao et al., 2014). Raw *fastq* files and the processed count matrix are available at GEO (accession number GSE207100). Multiple gene models mapping to a single gene annotation were collapsed to a single entry by summing read accounts across models. Differential expression analysis and library normalization was performed using DESeq2 (Love et al., 2014), with batch set as a covariate during differential expression analysis. For downstream analysis, normalized counts were batch corrected using COMBAT from the *sva* R package (W. E. Johnson et al., 2007; Leek et al., 2012). Principal component analysis was performed using the *prcomp* R function with the corrected counts. GO enrichment analysis was performed using ssGSEA from the *gsva* R package (Barbie et al., 2009; Hänzelmann et al., 2013), and the top 20 up and down pathways were ranked by p-value following a Wilcoxon Rank-sum test. The top 20 enriched and depleted GO terms were manually binned using custom-defined categories (Hogan et al., 2020). Gene regulatory network (GRN) and skeletal patterning cue gene expression levels were analyzed in time-matched and heterochronic comparisons; in time-matched comparison, genes were considered to be early/elevated or late/reduced if the average expression level in EtOH-treated embryos deviated from control embryos by

$\geq 18\%$. Potential GRN circuits connecting genes whose expression was similarly impacted by EtOH were manually mapped onto known and predicted edges in an integrated version of the specification network (Hogan et al., 2020).

2.4 Results

2.4.1 EtOH treatments results in skeletal patterning defects

To test whether EtOH has teratogenic effects on developing sea urchins, we exposed zygotes to a range of EtOH doses, then assessed their larval phenotypes. Using a systematic scoring approach (Piacentino et al., 2016b), we found that treatment with 1.7% (369 mM) EtOH induces dramatic skeletal patterning defects that include element losses, spurious elements, and rotational defects, with anterior and ventral elements most frequently perturbed, and both 1° and 2° elements affected (Fig. 2.1A-C). Most skeletal elements exhibited losses in EtOH-treated embryos (Fig. 2.1C). Anterior-posterior rotational defects were the most common orientation defect in EtOH-treated embryos. The treated embryos also showed unusual defects, including a high frequency of spurious elements, long anonymous rods, and midline losses (Fig. 2.1C); these latter defects were not observed with perturbations to other known patterning cues or their receptors, including *Univin/Alk4/5/7*, *VEGF/VEGFR*, *SLC26a2/7*, or *BMP5-8* (Adomako-Ankomah and Ettensohn, 2013; Duloquin et al., 2007; McIntyre et al., 2013; Piacentino et al., 2016b, 2016a, 2015).

To determine the time dependence of EtOH-mediated defects, first, we treated embryos at different time points ranging from fertilization to 30 hours post-fertilization (hpf), then scored the resulting pluteus larvae for patterning defects at 48 hpf. The results

show that an inflection point occurred between 22 and 24 hpf when the fraction of perturbed embryos dramatically declined (Fig. 2.1D1, left; Fig. 2.7A, 2.7B1-4). This indicates that EtOH is most effective before 24 hpf. This timepoint overlaps with both 1° and 2° skeletal patterning processes, in keeping with the broad skeletal defects induced by EtOH (Fig. 2.1A-C), although 1° skeletogenesis is well-underway at 24 hpf (Piacentino et al., 2016b, 2016a, 2015). Next, to define when EtOH begins to have an effect, we treated embryos at fertilization, removed EtOH hourly over a range of time points, then scored the resulting larvae at pluteus stage. We found an inflection point at 5 hpf, indicating that EtOH effects initiate between 4 and 5 hpf (Fig. 2.1D2; Fig. 2.7A, 2.7B5-6). This time point is surprisingly early, before the onset of Nodal expression and ectodermal dorsal-ventral specification (Bradham et al., 2006). These results indicate that EtOH perturbs skeletal patterning between 5 and 24 hpf.

Because EtOH treatment caused a broad range of skeletal patterning defects, we evaluated whether any defects predominated for different intervals of EtOH exposure during the overall window of sensitivity to EtOH by scoring skeletal defects in embryos treated with EtOH for the same defined temporal windows. Our results show that 2° elements and rotational defects are most sensitive to EtOH at 17 hpf, while 1° defects are most penetrant at 18 hpf (Fig. 2.7C1). We used the same approach to assess EtOH wash-out embryos, and the results show that 2° elements and rotational defects are most sensitive to EtOH after 6 hpf (Fig. 2.7C2). These data demonstrate that EtOH is most effective between 7 and 17 hpf regarding specific perturbations to the 2° elements and rotational defects, while impacts on the 1° elements are most pronounced after 18 hpf.

2.4.2 EtOH indirectly impacts the PMCs to produce skeletal patterning defects.

To determine whether the EtOH-mediated defects arise from perturbation of the ectoderm or the PMCs, we performed PMC transplantation experiments (Armstrong et al., 1993; Etensohn and McClay, 1986; Piacentino et al., 2016b) to produce chimeric embryos in which either the PMCs or the remaining hulls were treated with EtOH (Fig. 2.1E1). When we transplanted EtOH-treated PMCs into control hulls, this resulted in embryos with normal skeletons (Fig. 2.1E2). In contrast, when we performed the reciprocal experiment in which control PMCs were transplanted into EtOH-treated hulls, the embryos developed skeletal patterning defects characteristic of EtOH treatment (Fig. 2.1E3). These results demonstrate that EtOH acts on PMCs indirectly via impacts on other tissues such as the ectoderm. This is consistent with EtOH treatment perturbing the expression of skeletal patterning cues rather than directing perturbing the PMCs.

2.4.3 EtOH does not perturb ectodermal DV specification.

The ectoderm is the source of most skeletal patterning cues (Piacentino et al., 2016b). This tissue is subdivided into dorsal and ventral regions during early development by TGF- β signaling (Duboc et al., 2004); DV perturbations produce radialized embryos and skeletons (Armstrong et al., 1993; Bradham and McClay, 2006; Hardin et al., 1992; Piacentino et al., 2016a, 2015). While the patterning defects elicited by EtOH do not resemble radialization, we nonetheless tested whether DV specification of the ectoderm is affected by EtOH treatment. We performed immunostains to examine the ectodermal ciliary band (CB), a distinct region that is spatially restricted to the boundary between the dorsal and ventral ectodermal regions by the DV specifying TGF- β

signals in sea urchin embryos. When those signals are disrupted, the ciliary band is either posteriorly positioned or spatially unrestricted (Bradham et al., 2009; Duboc et al., 2004; Yaguchi et al., 2010). Our results show that the CB was both restricted normally and appropriately positioned within the context of the perturbed morphology induced by EtOH treatment (Fig. 2.2A, 2.8A). These results suggest that EtOH exposure does not affect ectodermal DV specification. This finding was corroborated by evaluating gene expression for the dorsal marker *Lv-IrxA* and ventral marker *Lv-Chd* via single-molecule FISH. The spatial expression of both genes was normal in EtOH-treated embryos (Fig. 2.2B), confirming that EtOH exposure does not perturb ectodermal DV specification.

2.4.4 EtOH does not perturb neural specification or patterning.

EtOH is a well-known neural teratogen that leads to intellectual impairment and reduced brain size in vertebrates and humans (Hoyme et al., 2005; Khalid et al., 2014). To test whether neural defects are a conserved response to embryonic EtOH exposure, we visualized synaptotagmin B (*synB*)-positive and serotonergic neurons using immunostaining (Fig. 2.2C, Fig. 2.8B). Surprisingly, we did not detect any losses of serotonergic neurons in the EtOH-treated embryos (Fig. 2.2C, 2.2D1), nor any significant losses of *synB* neurons (Fig. 2.2C, 2.8B). Instead, we found a statistically significant increase in serotonin levels in EtOH-treated embryos compared to controls (Fig. 2.2C, D2; see also Fig. 2.8B). These results indicate that EtOH exposure does not disrupt neural specification or patterning in sea urchin embryos but increases the serotonin expression level within the nervous system.

2.4.5 EtOH perturbs temporal expression of Wnt5 ectodermal patterning cue.

The ectoderm is required for normal PMC positioning and biomineralization since it provides instructive cues that are detected by the PMCs (Armstrong et al., 1993; Duloquin et al., 2007; Etensohn and McClay, 1986; McIntyre et al., 2013; Piacentino et al., 2016a, 2016b, 2015; von Ubisch, 1937). Thus, our next step was to ask whether EtOH exposure perturbs the expression of ectodermal skeletal patterning cues, including Lv-Wnt5 and Lv-VEGF. Lv-VEGF is an ectodermal cue that is expressed in the ectoderm that overlies ventrolateral PMC clusters at the late gastrula stage (Fig. 2.2E1) and is required for normal PMC cluster formation and biomineralization; at later time points, VEGF is required for skeletal patterning (Adomako-Ankomah and Etensohn, 2013; Duloquin et al., 2007; Piacentino et al., 2016b). Lv-Wnt5 is also expressed in the ectoderm that overlies the PMC clusters (Fig. 2.2F1) and is required for biomineralization (McIntyre et al., 2013). We found that the expression of both Lv-VEGF and Lv-Wnt5 appears to be spatially expanded to an abnormally broad ectodermal expression pattern in EtOH-treated embryos, with VEGF expression expanded laterally, and Wnt5 expression expanded both laterally and apically (Fig. 2.2E2, 2.2F2). We also assessed the expression pattern for Lv-Hh, which is expressed by the endoderm and contributes to skeletal patterning (Walton et al., 2009). Since gastrulation is delayed by EtOH treatment, the morphology of the developing archenteron differs from controls such that the gut tube is shorter and wider, making a qualitative assessment of Hh expression domain size challenging (Fig. 2.2G). Quantitation of their expression areas shows that among these three skeletal patterning cues, only Wnt5 expression is significantly spatially perturbed

by EtOH exposure at 18 hpf (Fig. 2.2H).

To test whether the differences in gene expression might reflect a developmental delay, we compared their expression over time. Those results show that Lv-Hh and Lv-Wnt5 expression patterns match controls with a 3- to 6-hour delay (Fig. 2.9A-D). Hh expression appears mildly delayed with EtOH treatment compared to controls (Fig. 2.9A-B). Wnt5 exhibits broad ectodermal expression in controls at 13 and 15 hpf, spatially contracts to bilateral posterior ventrolateral regions of expression at 18 and 21 hpf, then displays a distinct dorsal expression domain at 24 hpf (Fig. 2.9C). In EtOH-treated embryos, Wnt5 expression similarly contracts to the posterior VL ectoderm at 21 hpf, 3 hours later than controls, while simultaneously exhibiting the dorsal expression domain, 3 hours earlier than controls (Fig. 2.9C-D).

Taken together, these results show that the patterning cues Hh and Wnt5 exhibit temporally abnormal spatial expression in EtOH-treated embryos. While this change to Wnt5 might be responsible for the perturbations to skeletal patterning that occur with EtOH exposure, this seems less likely to account for the patterning defects since Wnt5 loss of function blocks biomineralization rather than patterning per se (McIntyre et al., 2013). The effects on Hh are more likely to contribute to patterning defects since Hh signaling is required for normal 2° skeletal patterning (Walton et al., 2009).

2.4.6 EtOH perturbs PMC migration, positioning, and spatial gene expression.

Given the effects of EtOH on Wnt5 and Hh expression, we next examined the skeletogenic PMCs in EtOH-treated embryos using immunostaining. PMCs in control embryos ingress at the mesenchyme blastula stage (~13 hpf) (Fig. 2.3A1), become

organized into the 1° ring-and-cords pattern during gastrulation (~15-18 hpf) (Fig. 2.3A2-A3), then initiate biomineral secretion in the ventrolateral PMC clusters at late gastrula stage (~18 hpf) (Fig. 2.3A3). In EtOH-treated embryos, PMC ingress and migration were delayed by approximately 3 hours compared to controls, although the cells eventually adopted relatively normal spatial positions by 24 hpf (Fig. 2.3B1-B5). During skeletal secretion, PMCs located in distinct regions express different genes (Sun and Ettensohn, 2014; Zuch and Bradham, 2019) reflecting their diversification during skeletal patterning. We next asked whether the spatial expression of known PMC subset genes is perturbed in response to EtOH exposure using a combination of FISH and PMC immunostaining. Lv-VEGFR is generally expressed in the PMCs and is elevated in the PMC clusters at late gastrula stage (Fig 3C1), adjacent to the VEGF signal that is expressed in the posterior ventrolateral ectoderm (Fig. 2.2E) (Adomako-Ankomah and Ettensohn, 2013; Duloquin et al., 2007; Schatzberg et al., 2015; Sun and Ettensohn, 2014). Lv-Jun is a transcription factor that is expressed primarily in the PMC clusters (Fig. 2.3D1, E1) (Sun and Ettensohn, 2014). In EtOH-treated embryos, VEGFR exhibits spatial expanded expression into non-cluster PMCs (Fig. 2.3C), while Jun is not expanded in the PMCs but interestingly is ectopically expressed in the ectoderm (Fig. 2.3D-E). We also assessed two additional genes enriched in the VL cluster PMCs, Lv-Frp and Lv-Otop. Neither Frp nor Otop exhibited changes in spatial expression with EtOH exposure (Fig. 2.3F-G). This observation of perturbed spatial expression of some PMC subset genes is consistent with the perturbation of some patterning cues and agrees with our previous results, suggesting that the EtOH-induced skeletal defects reflect

perturbations to patterning cues.

Given that PMC ingression and migration are delayed in response to EtOH, and that patterning cue expression is also delayed, we next evaluated how Jun expression changes with time. The results show that ectodermal expression of Jun normally occurs at 15 hpf in control embryos, while a similar expression pattern was observed in EtOH-treated embryos at 18 hpf, consistent with the general delay in PMC development with EtOH (Fig. 2.9E-F). As with migration, Jun expression appears normally restricted to the PMC clusters in EtOH-treated embryos at later time points (Fig. 2.9F4-5). Together, these results show delays induced by EtOH exposure in the spatial expression of ectodermal and endodermal patterning cues and a PMC subset gene, as well as delayed PMC ingression, migration, and differentiation.

2.4.7 EtOH-mediated skeletal patterning defects arise independently of retinoic acid perturbation.

A central mechanism that has been identified for FAS phenotypes in vertebrates is the loss of retinoic acid (RA) production and signaling (Kot-Leibovich and Fainsod, 2009; Nelson et al., 2013). This occurs because EtOH is normally metabolized to acetaldehyde by alcohol dehydrogenase (ADH); acetaldehyde then competitively binds and inhibits retinaldehyde dehydrogenase (RALDH), causing the reduced synthesis of retinoic acid (RA) (Shabtai et al., 2018) (Fig. 2.4A, blue). To test whether this mechanism is conserved in sea urchins, we first examined whether acetaldehyde is sufficient to phenocopy EtOH. We found that treatment with acetaldehyde caused skeletal patterning defects that are similar but not identical to the defects produced by

EtOH (Fig. 2.10A-C, 2.10E). Acetaldehyde embryos also showed a similar delay in PMC migration and positioning (Fig. 2.10C3-C5). We also tested the time dependence of the effects of acetaldehyde and found that the inflection point is delayed compared to EtOH to 25 hpf (data not shown), consistent kinetically with a model in which EtOH perturbs sea urchin development by increasing acetaldehyde levels that result in diminished RA levels, as in vertebrates.

To test this model, we performed two key experiments. In the first set of experiments, we attempted to rescue the EtOH phenotype by adding RA or retinol at fertilization. We tested a range of doses and found surprisingly that neither RA nor retinol rescued EtOH (Fig. 2.4B, Fig. 2.10D). Next, we attempted to rescue EtOH with fomepizole (4-methylpyrazole), an inhibitor of ADH that blocks acetaldehyde production (Fig. 2.4A, red). We tested the inhibitory activity of fomepizole on EtOH-mediated acetaldehyde production and confirmed its inhibitory effects in sea urchin embryos (Fig. 2.10F). However, we found that fomepizole did not rescue the EtOH phenotype over a wide range of doses (Fig. 2.4C-D), indicating that acetaldehyde production is not required for the defects produced by EtOH. This result is consistent with the lack of rescue of the EtOH phenotype by either RA or retinol. Taken together, these unexpected findings indicate that while acetaldehyde is sufficient to perturb skeletal patterning, neither acetaldehyde production, ADH activation, nor RA reduction account for the mechanism by which EtOH exposure produces skeletal patterning defects in sea urchin embryos. Thus, the role for the RA pathway in vertebrate EtOH teratogenesis is not conserved throughout deuterostomes.

2.4.8 Inhibition of the Hh signaling pathway partially rescues the EtOH phenotype.

The Hh signaling pathway is causally implicated downstream from EtOH in FASD in vertebrate embryos (Abramyan, 2019; Eberhart and Parnell, 2016; Hong and Krauss, 2017; Li et al., 2007; Sidik et al., 2021). Since Hh signaling is also implicated in sea urchin skeletal patterning (Walton et al., 2009), we next asked whether perturbed Hh signaling can explain the EtOH-mediated defects by testing whether the Hh pathway inhibitor cyclopamine or agonist SAG (Chen et al., 2002b, 2002a; Frank-Kamenetsky et al., 2002) can rescue EtOH-treated embryos. Neither cyclopamine nor SAG alone elicited patterning defects (Fig. 2.5A2-3). When combined with EtOH, cyclopamine provided a modest but statistically significant rescue, while SAG treatment did not. (Fig. 2.5A4-6, 2.5B). Interestingly, increasing the dose of cyclopamine did not improve the rescue effect, and cyclopamine was the least effective at the highest tested dose (Fig. 2.11). Similarly, higher doses of SAG did not improve the rescue effect (Fig. 2.11). These results show that antagonism but not agonism of Hh signaling is sufficient to partially rescue the EtOH phenotype, but only at low doses and with a weak effect.

2.4.9 RNA-seq reveals temporal perturbations of GRN gene expression.

We used RNA-seq to query the global effects of EtOH on development by comparing the transcriptomes of control and EtOH-treated embryos at 15, 18, and 21 hpf. We found many differentially expressed (DE) genes at 15 and 18 hpf, but at 21 hpf, far fewer DE genes were identified (Fig. 2.12A). We analyzed differential GO pathway activity using ssGSEA to identify functional categories of genes affected by EtOH exposure. The top 20 enriched and depleted GO terms for each pair-wise comparison

were binned into broad categories (Fig. 2.6A, 2.12B). Those results show that metabolism and signaling were the GO term categories most impacted in EtOH-treated embryos in time-matched comparisons, accounting for 55-70% of the enriched and 35-55% of depleted GO terms (Fig. 2.6A). Heterochronic comparisons revealed additional differences in chromatin and protein trafficking while still exhibiting a majority of differences in signaling and metabolism (Fig. 2.12B).

The first two components of a principal component analysis (PCA) accounted for 62% of the overall variation in the data. PC1 appears to sort on treatment for the earlier time points but does not separate control and EtOH at 21 hpf (Fig 2.6B), consistent with the few DE genes identified at 21 hpf. PC2 appears to sort on time, with EtOH samples being temporally offset from controls, aside from 21 hpf. Given the mild temporal displacements in the PCA results and the conspicuous morphological delays in development for EtOH-treated embryos, we further assessed EtOH-mediated temporal perturbations by comparing the expression of genes in the known gene regulatory network (GRN) specification models for sea urchins, focusing on genes whose expression changes between 15 and 21 hpf in *L. variegatus* embryos and their regulators (Davidson et al., 2002; Hogan et al., 2020; Li et al., 2014; Materna et al., 2013; Peter and Davidson, 2011; Saudemont et al., 2010; Su et al., 2009), using a cut-off threshold of $\geq 18\%$ change. Surprisingly, of the 49 genes we evaluated, only 30% exhibited late or reduced expression, with 47% of genes instead displaying early or elevated expression, while the remaining 22% were unaffected by EtOH treatment (Fig. 2.6C). Temporally perturbed genes were present in each of the germ layers (Fig. 2.13).

These results suggested that some GRN subcircuits are independently activated and therefore insulated from other circuits. To obtain a clearer view, we mapped the late/reduced genes and the early/elevated genes onto a network model and indicated previously known connections that could potentially integrate these changes. Several plausible circuits emerged from this analysis, including elevated or early expression of ectodermal *Univin*, *Nodal*, *Lefty*, *Not1*, *Vegf3*, *BMP2/4*, *Tbx2/3*, and *IrxA* (Fig. 2.6D). Curiously, *Nodal* is known to activate *Lefty*, *Chordin (Chd)*, *Goosecoid (Gsc)*, and *BMP2/4*, but both *Chd* and *Gsc* exhibit late or reduced expression rather than early or elevated expression in response to EtOH, implying additional regulators for these genes (Fig. 2.6D). Similarly, early, or elevated expression interconnects the PMC genes *Ets1/2*, *Alx1*, *Tbr*, *Erg*, *FoxB*, and *VEGFR*. As with the ectoderm, some known targets of *Alx1* and *Ets1/2* are not affected or are delayed/reduced, including *SM50*, *SM30b*, *Snail*, and *Twist* (Fig. 2.6D), once again implying additional unknown regulators for those genes. Interestingly, the clearest circuits interconnecting genes that are delayed or reduced by EtOH are in the endomesoderm and include β -catenin, *GataE*, *Blimp1*, *Bra*, *FoxA*, *Hh*, *LOX*, and *Cdx*. The delayed or reduced expression of these genes could explain the delay in gastrulation in EtOH-exposed embryos; perhaps the timing of gastrulation sets the pace for development overall, leading to the morphological delay despite the presence of genes whose expression is early or elevated rather than delayed or reduced. Finally, we evaluated the expression of known patterning genes from the RNA-seq data (Fig. 2.6E). Those results indicated early or elevated expression for *BMP5-8*, *Univin*, *SLC*, *VEGF*, *VEGFR*, and *Ptc*, late expression for *Hh*, and unaffected expression for *Wnt5*. These

findings agree with our FISH results for VEGF and Wnt5, particularly that normal expression is achieved at late timepoints, as well as supporting the weak rescue effects we obtained when Hh signaling was perturbed along with EtOH treatment.

2.5 Discussion

In this study, we show that EtOH exposure is teratogenic to sea urchin embryos; more specifically, EtOH perturbs skeletal patterning but not neural development. We further show that the defective skeletal patterns in EtOH-treated embryos arise from perturbation to patterning cues rather than from the direct effects of EtOH on the PMCs and are not explained by the RA or Hh pathways that are implicated in vertebrate fetal alcohol syndrome disorders. Finally, we observed temporal perturbations in developmental gene expression in EtOH-treated embryos that potentially account for their aberrant pattern formation.

Although skeletal patterning defects were observed that could be considered to be analogous to the facial perturbations in FASD, neural patterning was not perturbed in sea urchins after the exposure to EtOH. Levels of serotonin were increased by EtOH treatment, but the number of ser neurons was not affected. Studies in mice, fish, and frogs have shown that EtOH exposure disrupts every step of CNS development, including neural proliferation, migration, and differentiation, as well as directly leading to neural apoptotic and necrotic cell death (Blader and Strähle, 1998; Gil-Mohapel et al., 2019; Sulik, 2014). The absence of evident neural specification or patterning defects in EtOH-treated sea urchin embryos suggests that the neural developmental vulnerability to ethanol is a vertebrate novelty whereas the impact of ethanol on skeletal patterning is

more deeply conserved among deuterostomes.

Previous studies have linked FASD abnormalities, both neural and facial, to perturbations of the Hh and RA signaling pathways (Ahlgren et al., 2002; Cayuso et al., 2006; Cohen and Sulik, 1992; Petrelli et al., 2019; Reimers et al., 2004; Smith et al., 2014), each of which plays important roles in the development of both the CNS (Chatzi et al., 2013; Janesick et al., 2015; Li et al., 2021) and the facial skeleton (Abramyan, 2019; Dubey et al., 2018; Gur et al., 2022; Sun et al., 2020). Our results show that RA signaling does not play a role in EtOH-mediated perturbations, and Hh plays only a minor role in sea urchin embryos. We found that acetaldehyde also results in skeletal patterning defects, implying that other downstream pathways that are shared by ethanol and acetaldehyde, but that do not impinge upon RA levels, are responsible for their overlapping patterning phenotypes in sea urchins. These shared downstream effects potentially include metabolic pathways, which clearly are affected by EtOH treatment (Fig. 2.6A); for example, both EtOH and acetaldehyde exert inhibitory effects on mitochondrial β -oxidation (Latipää et al., 1986; Ontko, 1973; You and Arteel, 2019). Thus, the contributions of the RA and Hh pathways to the phenotypic effects of embryonic EtOH exposure surprisingly are not evolutionarily conserved in sea urchins.

Our results show that EtOH perturbs skeletal patterning by affecting patterning cues rather than directly impacting the skeletogenic PMCs. One of the most conspicuous defects in EtOH-treated embryos is a three-hour morphological delay in development. This delay is echoed by the expression of numerous genes, including delays or reductions in the level of expression or the normal spatial pattern for some genes that encode

skeletal patterning or differentiation cues, such as Wnt5 and Hh, or PMC subset genes, such as Jun. However, other genes encoding patterning cues exhibit early expression, including BMP5-8, SLC26a2/7, and VEGF3, while still others are unaffected. Temporal discrepancies are present throughout the GRN; those genes exhibit mostly early or elevated expression in response to EtOH, with a minority being unaffected. Together, this suggests that the EtOH-induced phenotype might arise from temporal mismatches between the instructive ectoderm and endoderm tissues and the responsive PMCs, reflecting an overall loss of synchronization across the embryo. Asynchronous intraembryonic development is clearly implied by plausible circuits connecting genes whose expression is early or elevated by EtOH exposure in the ectoderm and PMCs, alongside plausible circuits for genes whose expression is late or reduced by EtOH in the endomesoderm; in each of these tissues, genes with all three temporal profiles are present but not readily explained, implying the existence of still-unknown network components. Temporal loss of registration could also explain why our attempts to rescue the EtOH phenotype have met with limited success since that model suggests a more complex cause for the EtOH-mediated defects than the simple loss of a signal or set of signals. It will be interesting to determine whether these effects are conserved by testing whether EtOH exposure mediates similar temporal disruption in other species.

Overall, our study offers a novel model to study EtOH-mediated teratogenesis that separates the impact on skeletal patterning from the effects on neuronal survival, providing insight into the evolution of the embryonic response to EtOH and revealing a novel dysregulation of temporal synchronization of GRN gene expression that is induced

during EtOH-mediated teratogenesis.

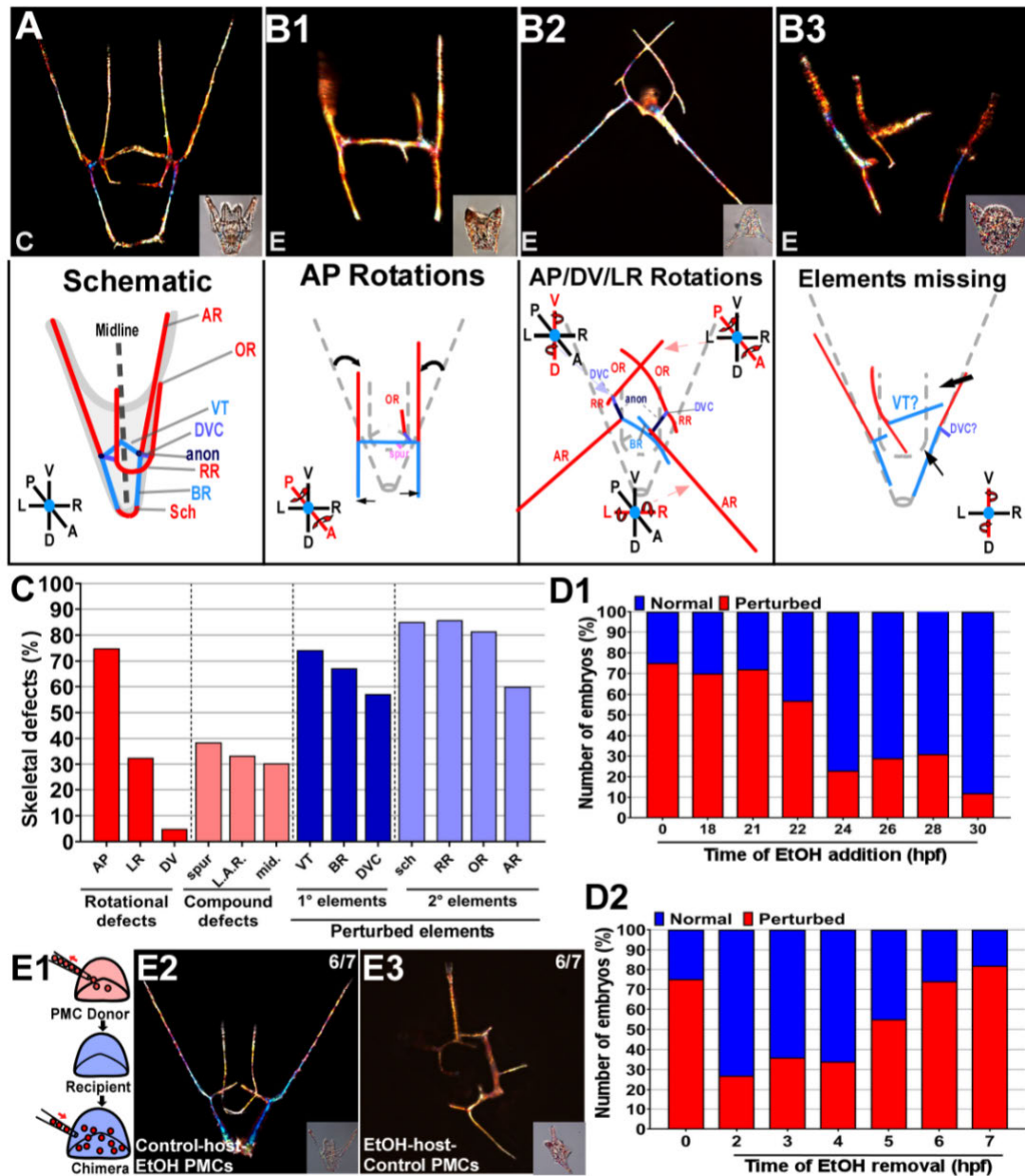


Figure 2.1. Ethanol exposure perturbs skeletal patterning between 5 and 22 hpf.

A-B. Representative skeletal morphology (birefringence, top) and schematics (bottom) of control (C, A) and EtOH-treated (E, B1-3) embryos are shown at 48 hpf (pluteus stage); the corresponding DIC images are inset, and body axes are indicated. The primary skeletal elements (A, blue) include the initial triradiate that gives rise to the ventral

transverse rods (VTs), the dorsoventral connecting rods (DVCs), and the anonymous rods (anon); the latter branch to produce the dorsal body rods (BRs). Secondary elements (A, red) include the posterior aboral rods (ARs) that branch from the anons, as well as the anterior oral rods (ORs) and the recurrent rods (RRs) that branch from the DVC, and finally the scheidtel (sch) that branches from the tips of the BRs at the dorsal extreme. The perturbed skeletons in EtOH-treated embryos exhibit abnormal rotations of skeletal elements about one of the body axes (B1), sometimes in combinations (B2), as well as element losses (B3). Arrows show rotations (B1, B2) and absent elements (B3). **C.** Skeletal patterning defects including rotational defects, compound defects, and element losses are plotted as the percentage of embryos exhibiting the indicated effect. Spur, spurious elements; LAR, long anonymous rods; mid, midline losses; $n > 60$. **D.** The percentage of embryos that were normal (blue) or perturbed (red) after adding (D1) or removing (D2) EtOH at different time points is shown; $n > 50$ per time point. **E.** The approach for PMC transplantation to produce chimeric embryos is shown schematically (E1). Chimeric embryos are shown as morphology (DIC, 1) and skeletal pattern (birefringence, 2) for EtOH-treated PMCs in control hulls (E2), or the reciprocal control PMCs in EtOH-treated hulls (E3) at 40 hpf (pluteus stage). The results shown were obtained in 6/7 trials. See also Fig. 2.7.

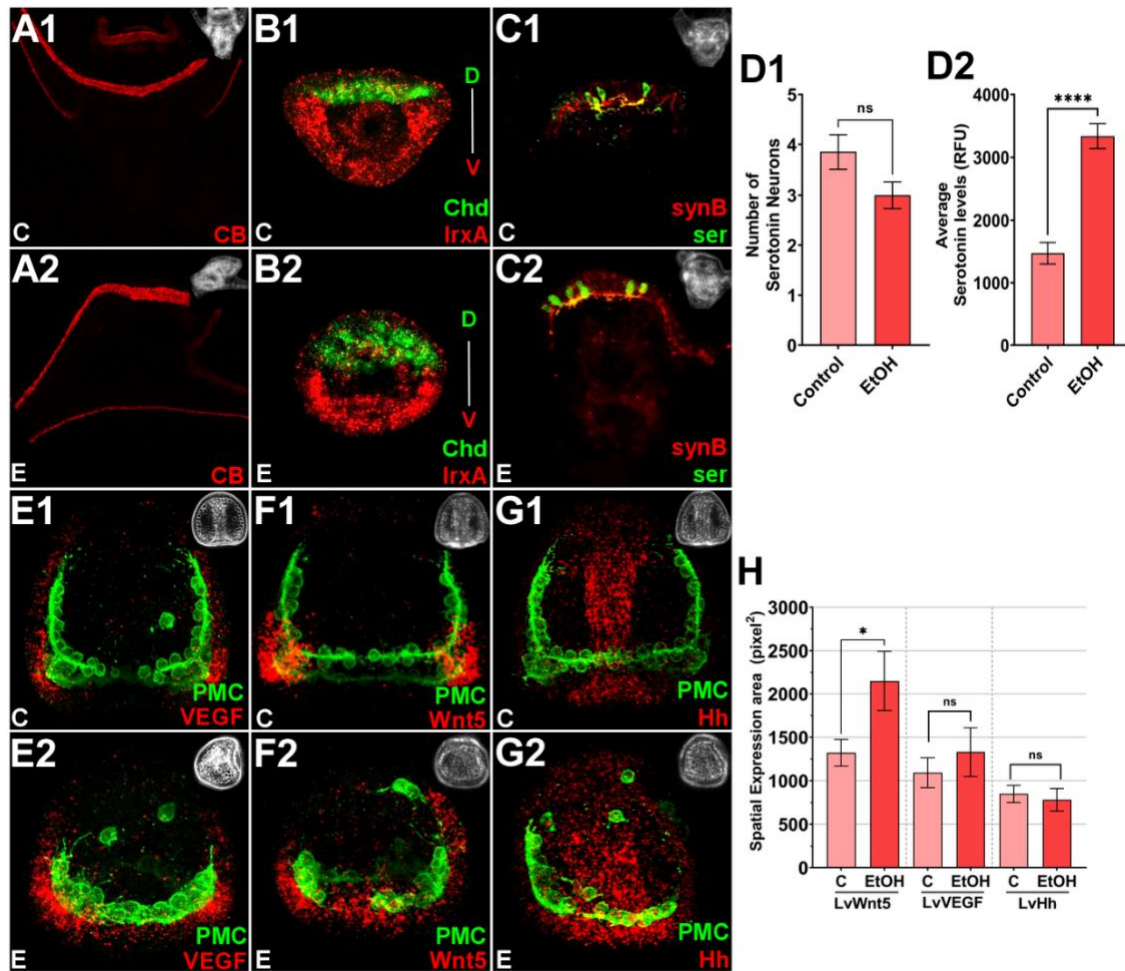


Figure 2.2. EtOH treatment does not impact neural development or ectodermal DV specification and delays normal expression of the PMC-directing signal Wnt5. A.

The ciliary band was visualized via immunostaining in controls (A1) and EtOH-treated (A2) embryos at 48 hpf. B. HCR-FISH for ventral Chd (green) and dorsal IrxA (red) expression is shown in control (B1) and EtOH-treated embryos (B2) at 18 hpf (late gastrula stage); the DV axis is indicated. C. Neural-specific immunostaining for serotonin (ser, green) and pan-neural synaptotagmin B (synB, red) is shown in control (C1) and EtOH-treated (C2) anterior structures at 48 hpf (pluteus stage); corresponding phase contrast images are inset. D. The number of neurons (D1) and the relative level of the

serotonin signal (D2) is shown as the average per embryo \pm s.e.m.; $n = 15$; ****, $p \leq 0.0001$ (student t-test). E-G. The expression of the signals VEGF (E), Wnt5 (F), and Hh (G) is shown along with PMC immunostains in control (1) and EtOH-treated (2) embryos at 18 hpf. Embryos are oriented with anterior at the top. H. The total expression area for the indicated signals in control (C) and EtOH (E) is shown as the mean summed area \pm s.e.m; * $p < 0.05$ (student t test, $n=15$ per condition). See also Fig. 2.8.

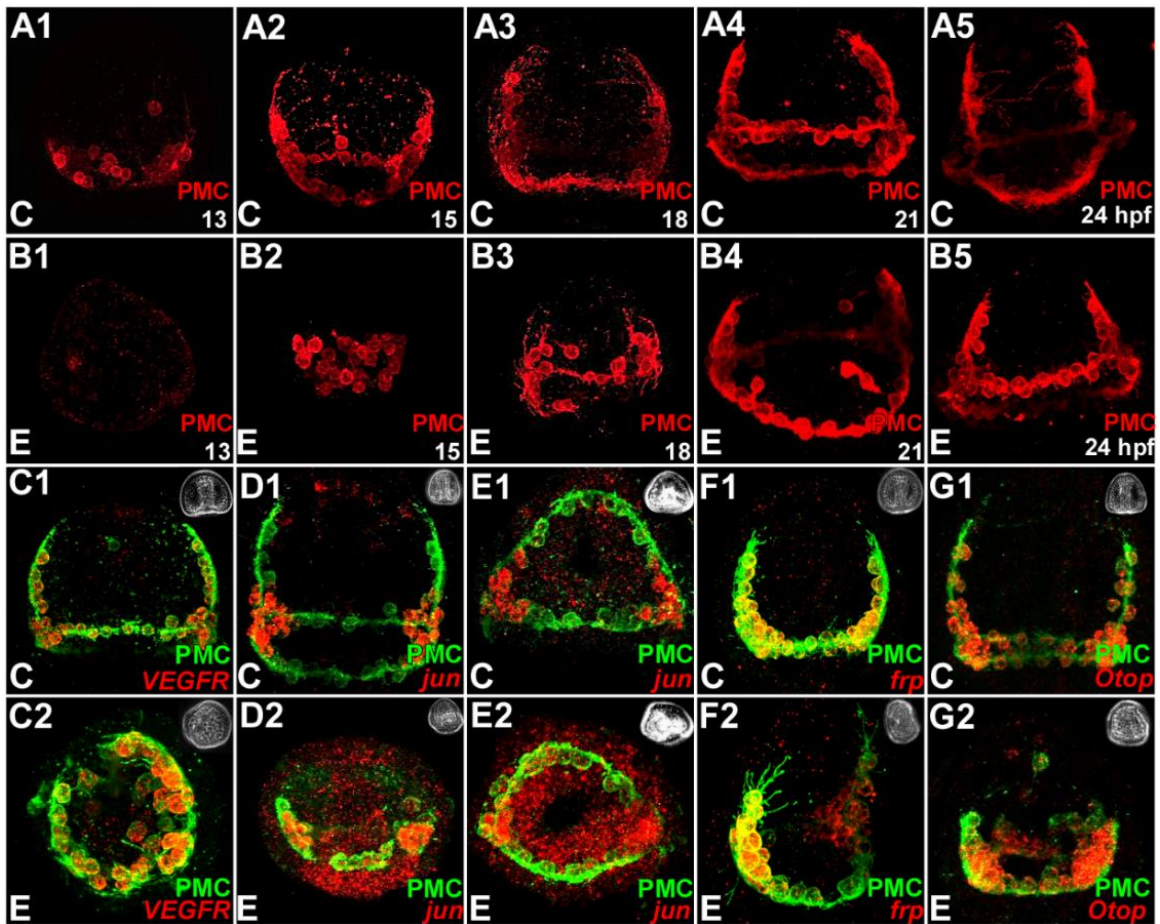


Figure 2.3. EtOH treatment results in delayed PMC ingress, migration, and Jun expression. A-B. PMCs were immunolabeled in control (A) and EtOH-treated embryos (B) that were fixed at 13 (1), 15 (2), 18 (3), 21 (4) or 24 (5) hpf during gastrulation. All embryos are oriented with anterior upward. C-G. Gene expression was detected using HCR-FISH and PMCs were immunolabeled in control (1) and EtOH treated (2) embryos at 18 hpf (late gastrula stage). PMC-specific genes detected are Lv-VEGFR (C), Lv-Jun (D-E), Lv-Frp (F), and Lv-Otop (G). All embryos are oriented with anterior upward except C2 and E1-2 shown in vegetal views. See also Fig. 2.9.

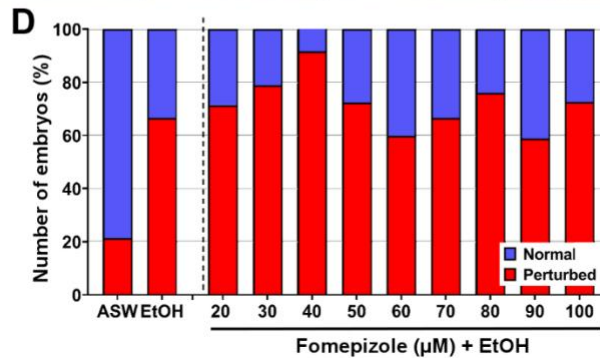
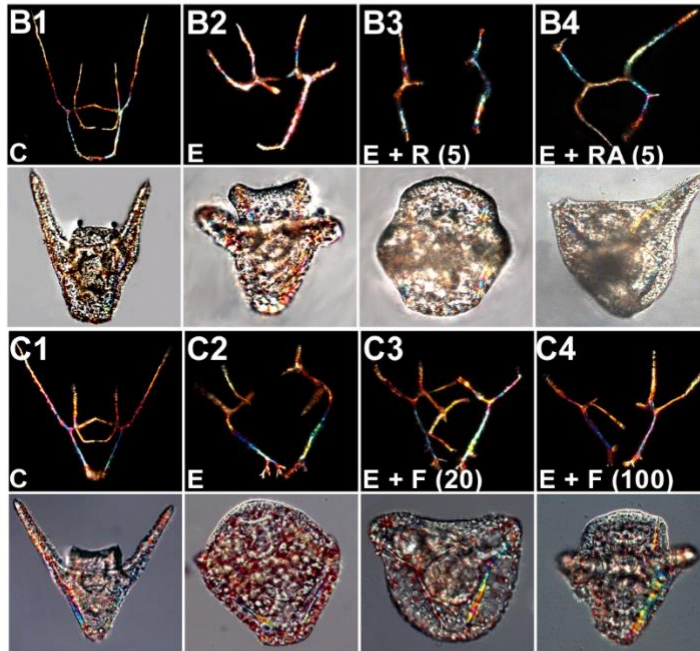
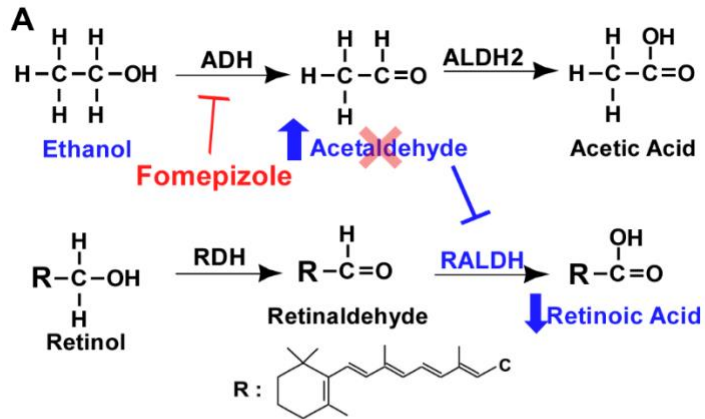


Figure 2.4. EtOH-mediated defects do not arise via reduction in retinoic acid. A.

EtOH metabolism results in reduced RA synthesis via acetaldehyde-mediated inhibition

of RALDH (blue). Fomepizole inhibits ADH and thereby reduces acetaldehyde production from EtOH (red). B-C. Skeletons (birefringence, upper panels) and morphology (DIC, lower panels) are shown at 48 hpf for embryos subjected to treatments with 5 μ M Retinol (R) or Retinoic Acid (RA) with or without EtOH (E), or with EtOH (E) and Fomepizole (F) at 20 μ M or 100 μ M. D. The fraction of perturbed embryos is plotted for the indicated treatments; $n \geq 100$ per condition. ADH, alcohol dehydrogenase; ALDH2, Aldehyde dehydrogenase; ASW, artificial sea water; F, fomepizole; R, retinol; RA, retinoic acid; RDH, retinol dehydrogenase; RALDH, retinaldehyde dehydrogenase. See also Fig. 2.10.

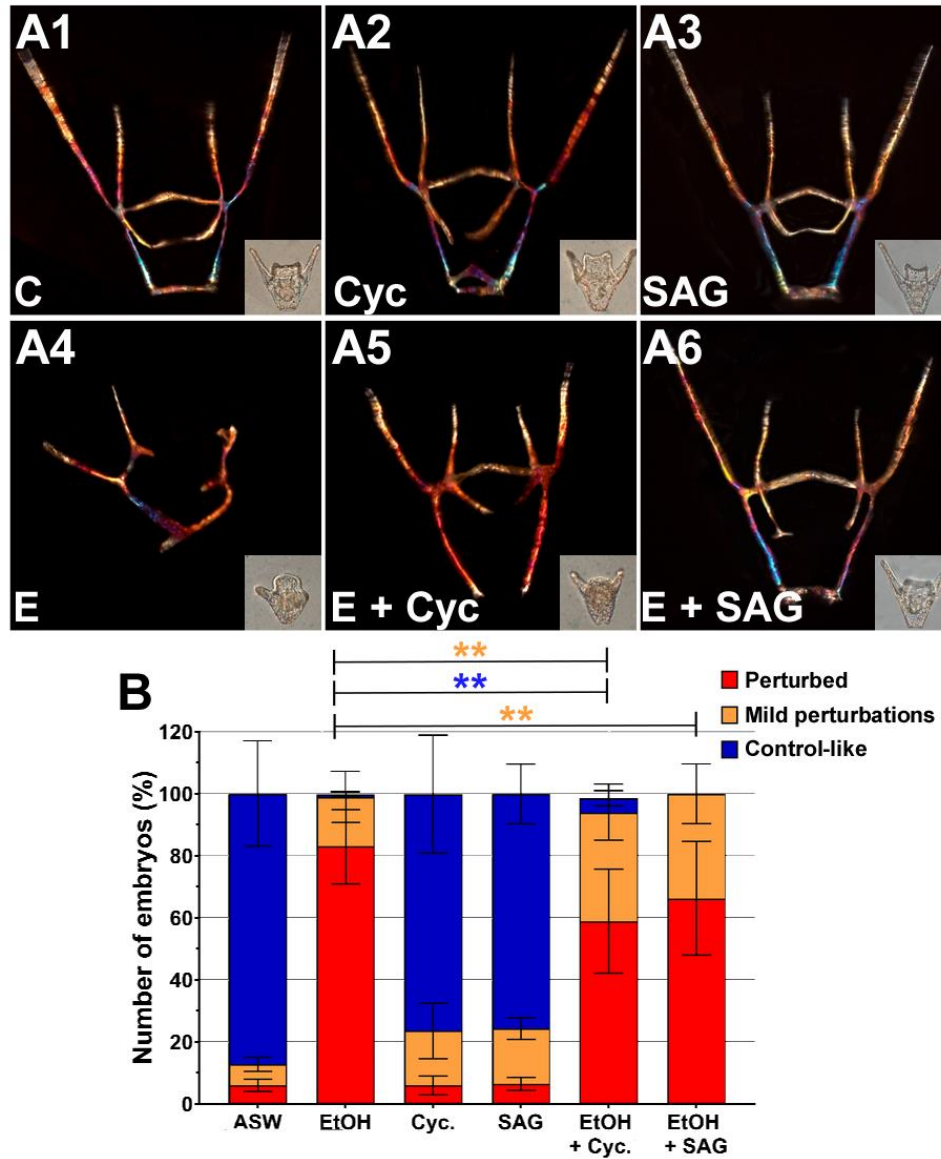


Figure 2.5. Inhibition of Hh signaling partially rescues the EtOH phenotype.

A. Skeletal birefringence and morphology (DIC, inset) are shown at 48 hpf for embryos treated with cyclopamine (cyc, 0.2 μ M) or with SAG (0.3 μ M) with or without EtOH (E).

B. The fraction of normal and perturbed embryo is plotted for the indicated conditions as the average \pm s.e.m.; $n \geq 150$ per condition; * $p < 0.05$; n.s., not significant (t test). Mild perturbations are illustrated by panels A5 and A6. See also Fig. 2.11.

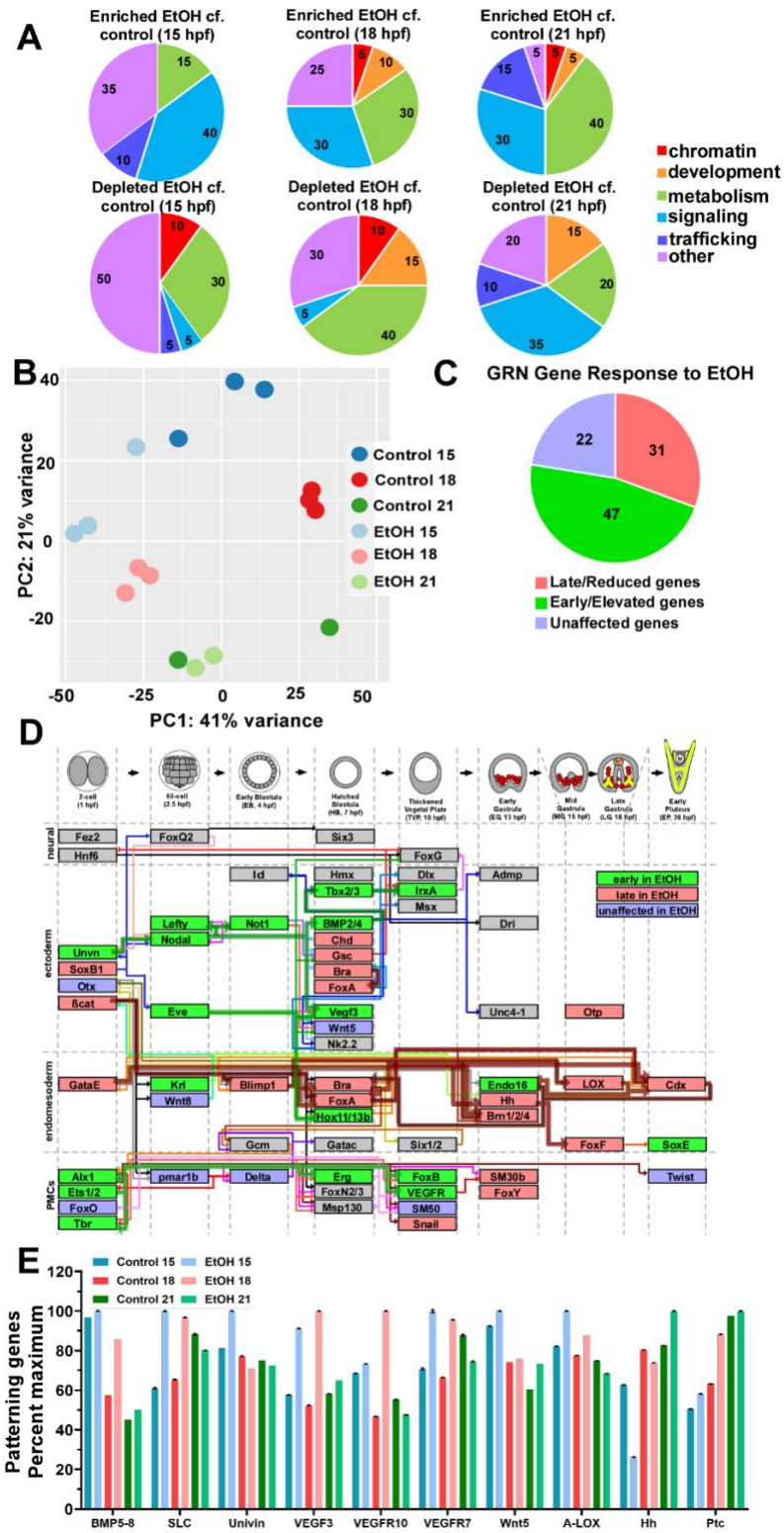


Figure 2.6. EtOH treatment results in disrupted temporal synchrony.

A. Broad categories for the top 20 GO terms enriched or depleted in EtOH-treated embryos compared to time-matched controls are shown; their relative percentages are indicated. B. 2-D principal component analysis (PCA) compares control and EtOH-treated replicates. C. The effects of EtOH on the expression of 49 GRN genes at three time points is shown by their distribution into late/reduced, early/elevated, and unaffected bins; percentages are indicated. D. An overview of the sea urchin specification GRN model is separated vertically into major tissues, and horizontally by time, with genes positioned according to their onset of expression (adapted from Hogan 2020). Colored nodes indicate late or reduced genes (red), early or elevated genes (green), and unaffected genes (blue). Plausible circuit connections are indicated as thick, transparent edges. E. The expression levels of genes encoding known patterning cues in control and EtOH-treated embryos at 15, 18, 21 hpf are shown as the average \pm s.e.m. with values scaled to the maximum expression level for each gene. See also Fig. 2.12-2.13.

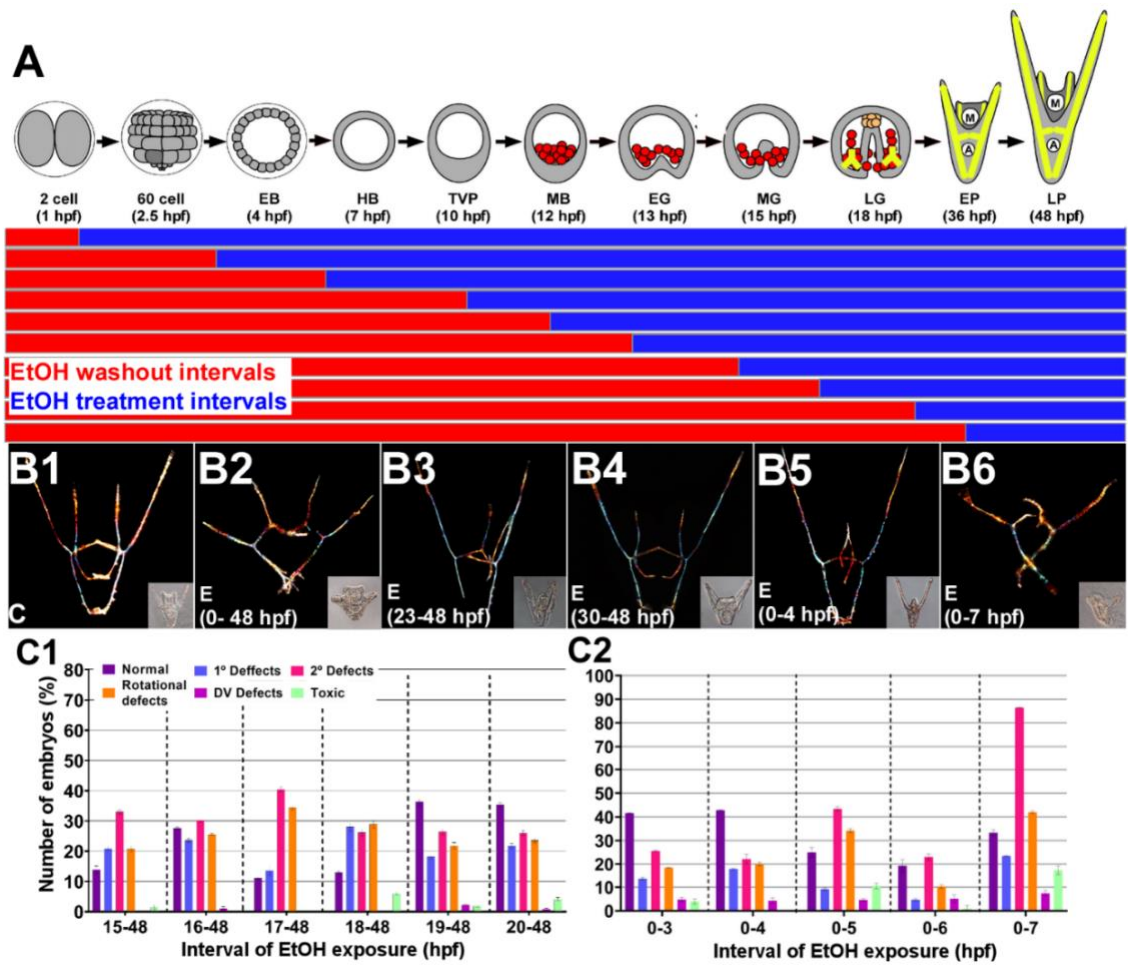


Figure 2.7. EtOH is most effective between 5-22 hpf. **A.** A schematic of the developmental time course for sea urchin embryos (top), and the temporal treatment regimen (bottom). **B.** Skeletal birefringence and DIC morphology (inset) are shown at 48 hpf for controls (C) and embryos treated with EtOH (E) during the indicated intervals. **C.** Skeletal patterning defects were scored for the indicated groups of EtOH-treated embryos, comparing defects with variable times of EtOH addition (C1) or removal (C2); $n \geq 30$ per condition. See also Fig. 2.1. Panel A was adapted from Hogan et al. 2020.

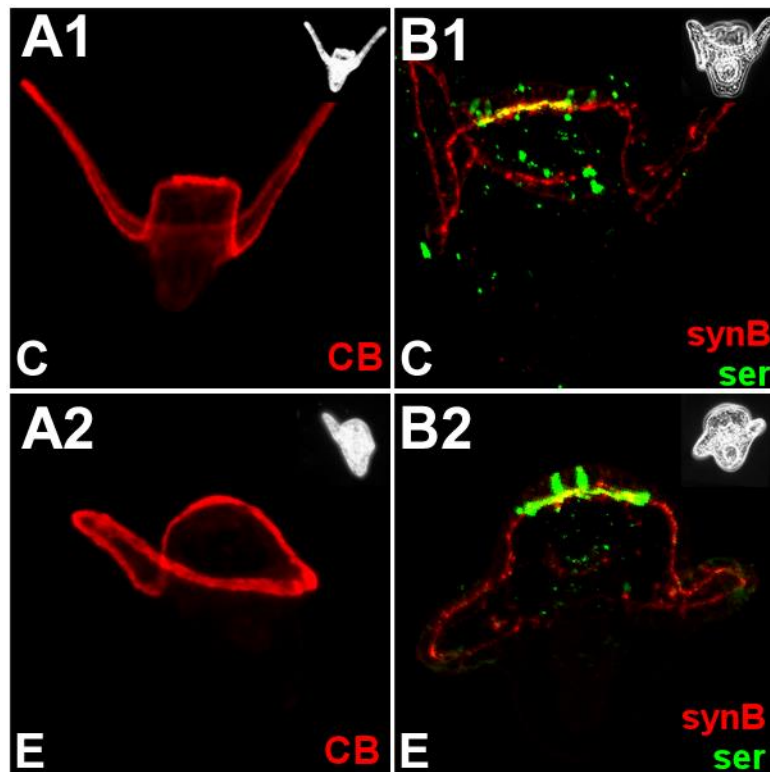


Figure 2.8. EtOH does not perturb ectodermal DV specification or neural patterning. A-B Ciliary band (CB, A) and synB- (red) and ser- (green) positive neurons (B) were immunolabeled in controls (1) and EtOH-treated (2) embryos at pluteus stage (48 hpf) and are shown at 100x magnification to capture their complete morphology. Corresponding phase-contrast images are inset. See also Fig. 2.2.

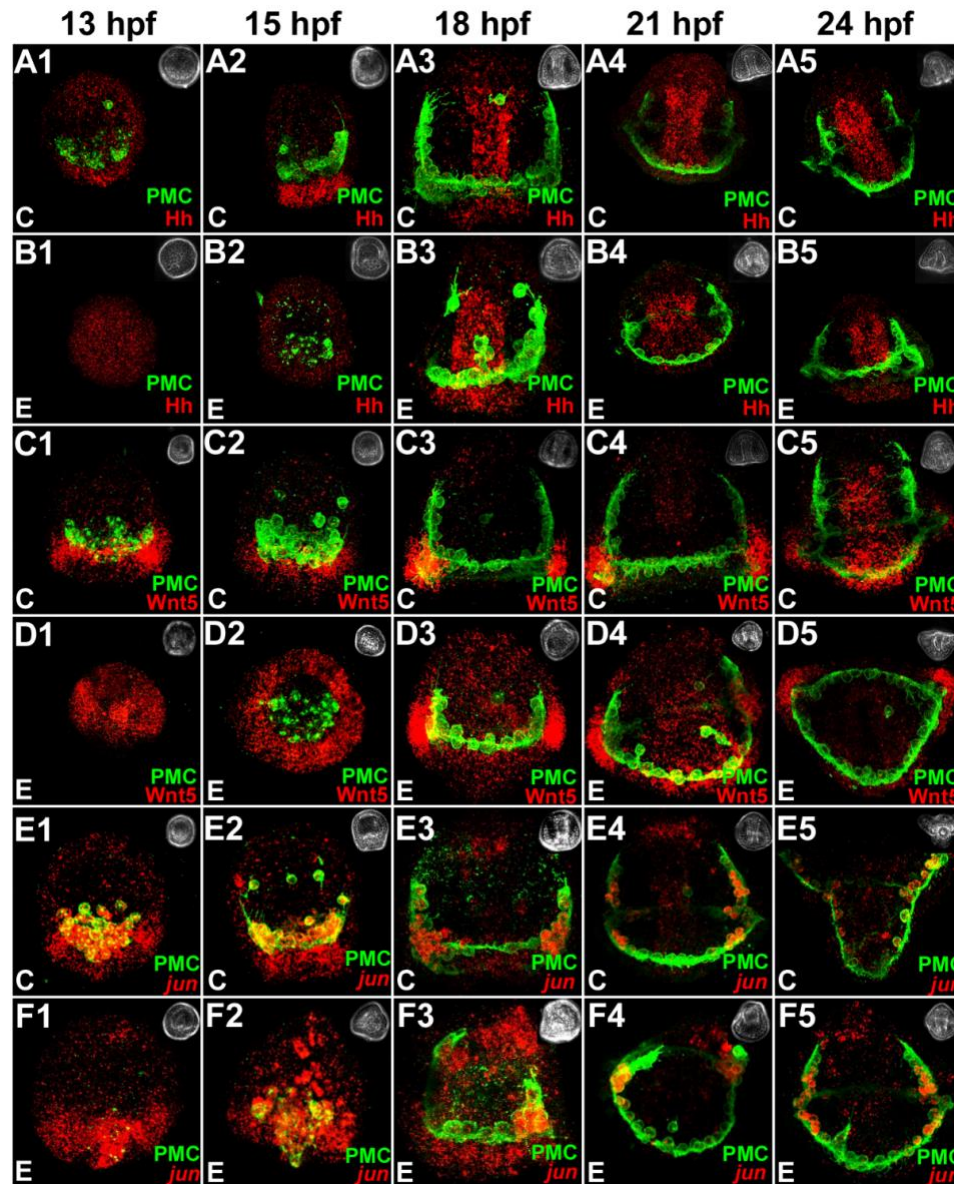


Figure 2.9. EtOH exposure delays the normal spatial expression of Hh, Wnt, and **Jun**. Embryos were collected at indicated time points then subjected to fluorescence in situ hybridization for Lv-Hh (A-B), Lv-Wnt5 (C-D), and Lv-Jun (E-F), (red) along with immunolabeling for the PMCs (green). Embryos are shown with anterior oriented upward, except A5, B4, B5, C5, E5, and F5, shown with ventral upward, and F2, in a vegetal view. See also Fig. 2.3.

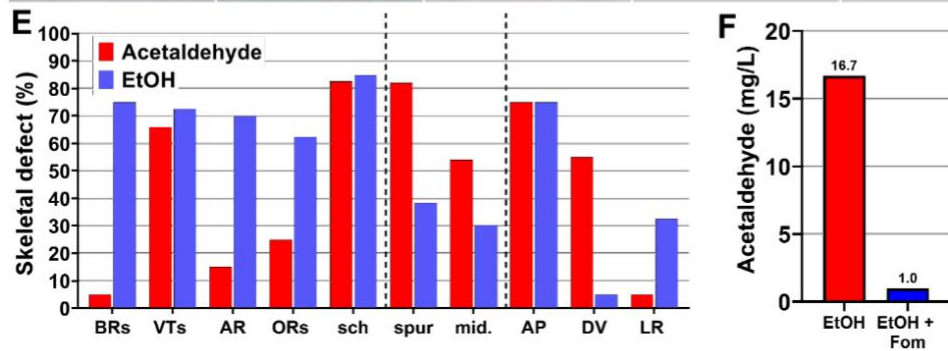
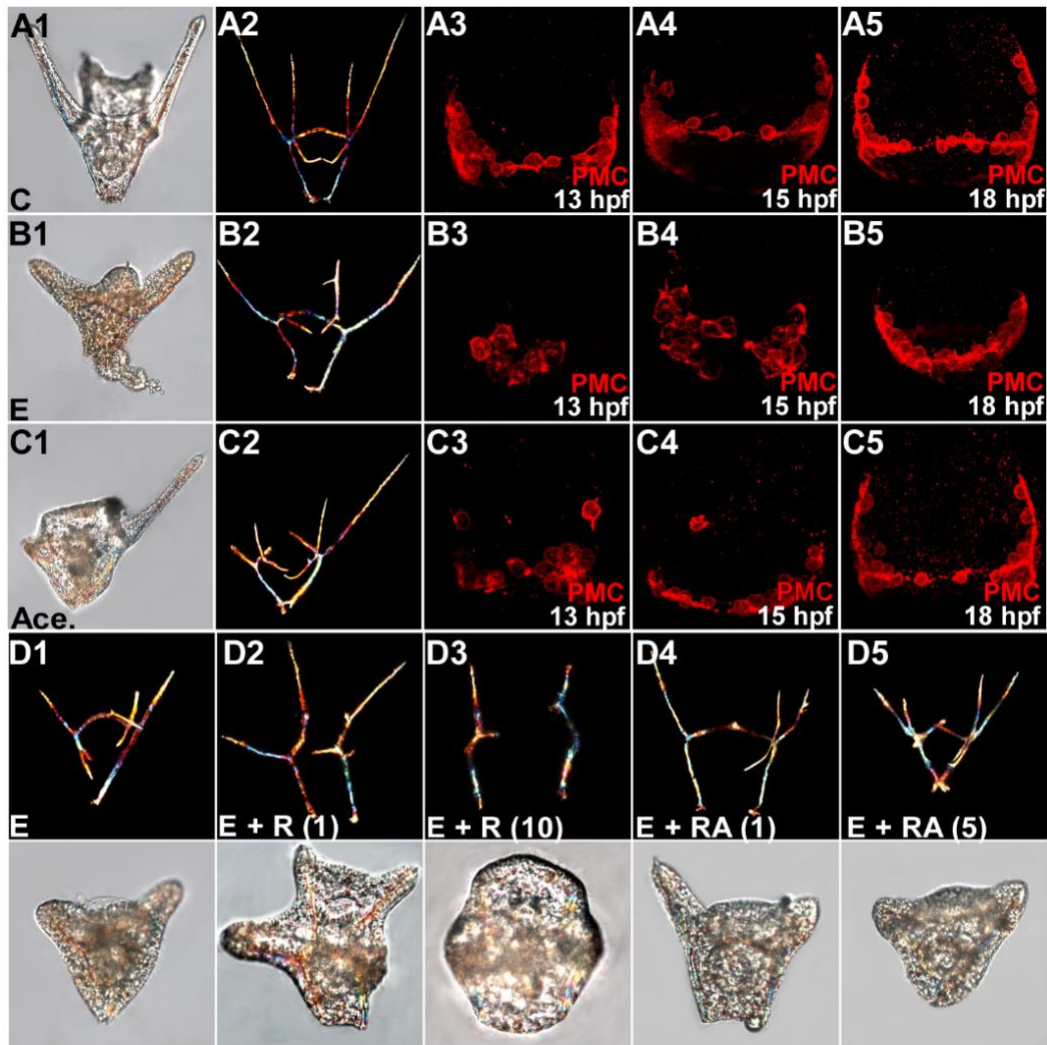


Figure 2.10. While acetaldehyde (Ace.) treatment results in skeletal patterning defects, neither retinol (R) or retinoic acid (RA) is sufficient to rescue EtOH. A.-C.

Representative morphology (DIC, 1), skeletal birefringence (2) and PMC

immunolabeling are shown at 48 hpf (A, B) or at the indicated time points (C) for control (C, A), EtOH- (E, B, 369 mM), and acetaldehyde- (Ace, C, 891 μ M) treated embryos. D. Skeletal birefringence (upper panels) and corresponding morphology (DIC, lower panels) is shown at 48 hpf for embryos treated with EtOH (E) and either retinol (R) at 1 μ M (D2) or 10 μ M (D3), or retinoic acid (RA) at 1 μ M (D4) or 5 μ M (D5) E. Skeletal patterning defects were scored for embryos treated with EtOH or acetaldehyde, including element losses (see Fig. 1A for abbreviations), spurious elements (spur), midline defects (mid) and rotational defects (AP, DV, and LR; see Fig. 1A–B), and are plotted as the percentage of embryos exhibiting the indicated effect; n > 60. F. Acetaldehyde assays confirm the effectiveness of the ADH inhibitor fomepizole (Fom, 100 μ M) in sea urchin embryos. The density of embryos for each sample was 1000 embryos/ml. See also Fig. 2.4.

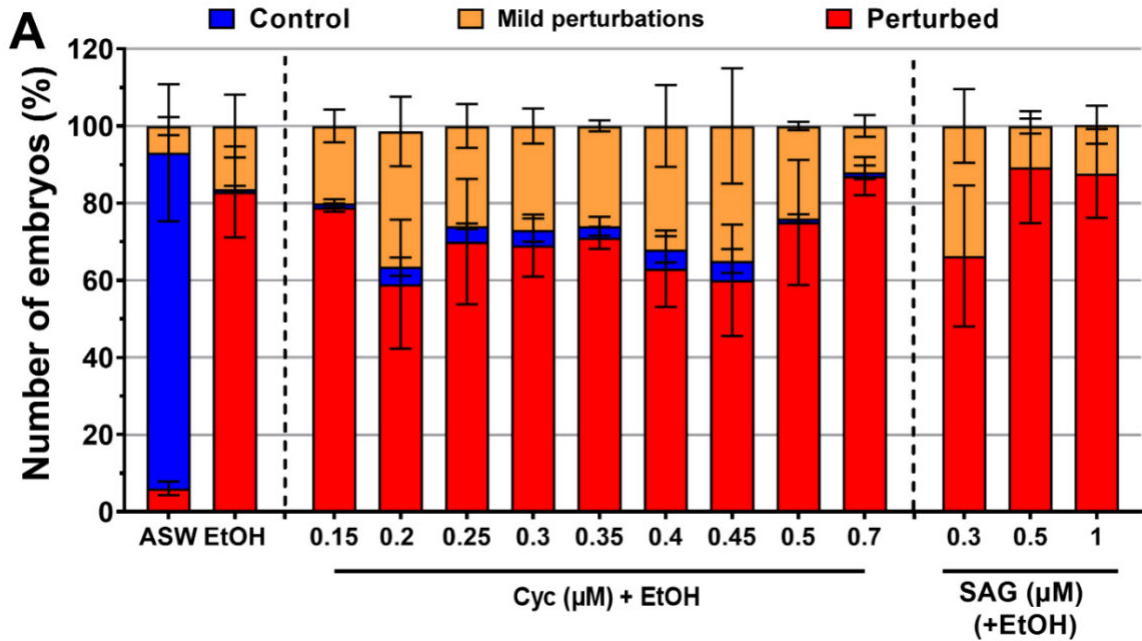


Figure 2.11. The rescue of the EtOH phenotype by Hh pathway inhibition is most effective at low doses. A. The fraction of skeletal patterning defects is shown for the combinations of EtOH and cyclopamine or SAG at the indicated doses as the average \pm s.e.m; $n = 150$ per condition. See also Figure 2.5.

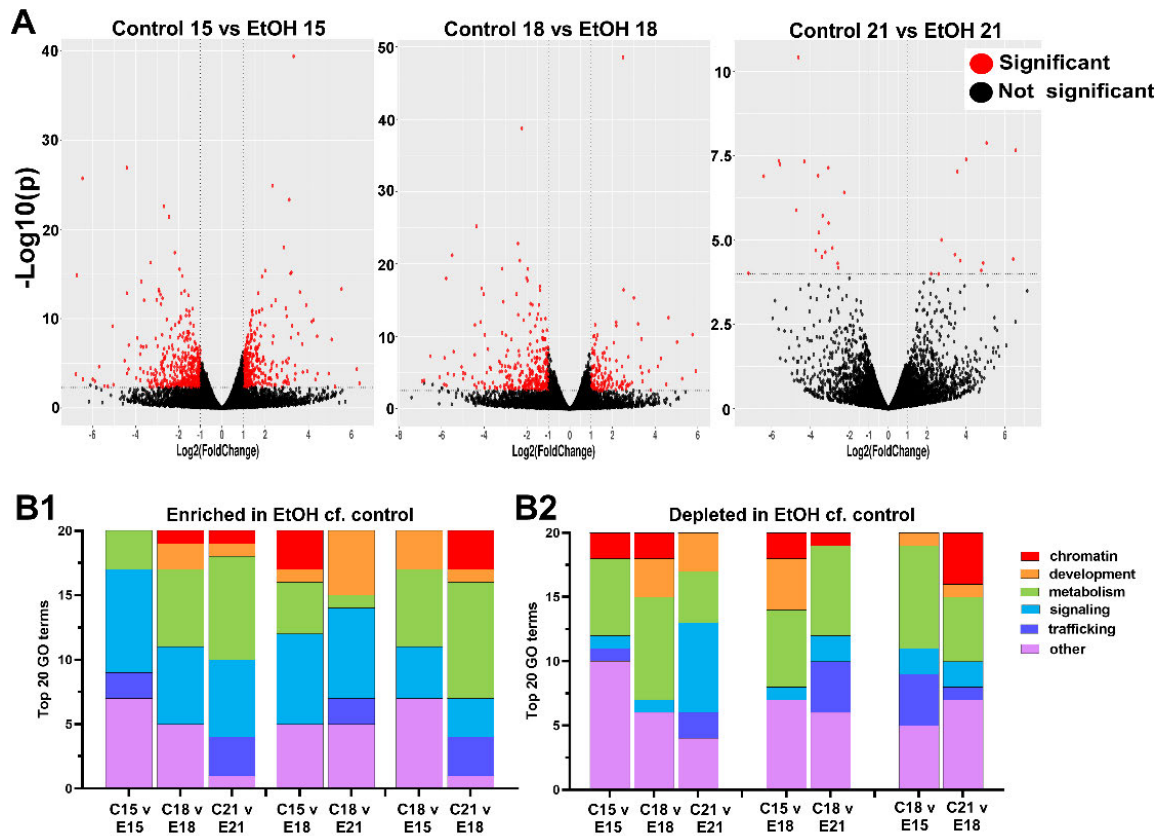


Figure 2.12. GO term analysis show metabolism and signaling are the most affected in EtOH samples. A. Volcano plots show significant DE genes (red) between EtOH and control transcriptomes at each sequenced time point. **B.** The top 20 enriched (B1) or depleted (B2) GO terms, binned into broad categories, are shown for the indicated time-matched or heterochronic comparisons of EtOH to controls. See also Figure 2.6.

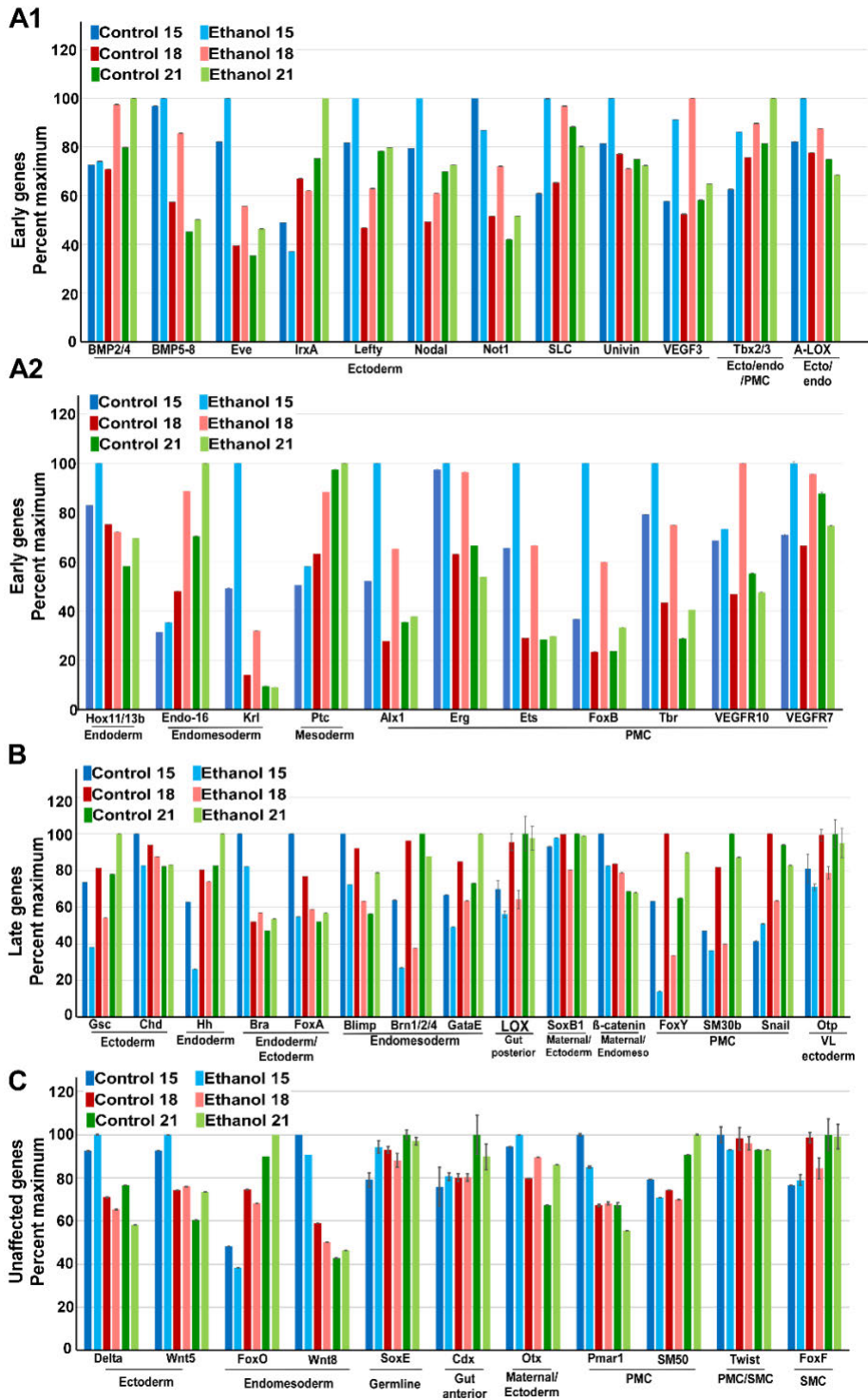


Figure 2.13. EtOH-treated embryos exhibit temporally disrupted gene expression.

GRN genes whose expression is either early or elevated (A), late or reduced (B), or

unaffected (C) by EtOH treatment are shown as the average \pm s.e.m. with expression scaled to the maximum expression level for each gene. The early/elevated group is divided into ectodermal (A1) and endomesodermal (A2) genes. The germ layer in which each gene is expressed is indicated. See also Figure 2.6.

CHAPTER THREE: Discussion and Future Directions

3.1 Summary of findings

This thesis aims to provide a molecular fingerprint for the effects of EtOH during sea urchin development that explain its mechanism of action regarding its perturbation of normal skeletal patterning. The sea urchin embryo offers a model for embryonic patterning that is comparatively simple, and significant work has been done to understand the molecular regulation of larval skeletal patterning in this model. In particular, several transcription factors and signaling ligands have been identified that are required for PMC positioning and biomineralization (Adomako-Ankomah and Ettensohn, 2013; Armstrong and McClay, 1994; Duloquin et al., 2007; McIntyre et al., 2013; Piacentino et al., 2016a, 2016b, 2015; Walton et al., 2009).

Our results are consistent with a complex, multi-pathway mechanism for ethanol-mediated larval skeletal perturbation. Skeletal patterning defects were observed that could be considered analogous to the facial perturbations that arise in FASD, particularly since many of the skeletal elements support and surround the larval mouth (Piacentino et al., 2016a, 2016b, 2015). Interestingly, the absence of distinct neural patterning defects or losses in EtOH-treated sea urchin embryos suggests that the neural developmental vulnerability to EtOH is a vertebrate novelty. In contrast, the impact of EtOH on skeletal patterning is more deeply conserved among deuterostomes.

We tested whether the effects of EtOH on the RA signaling pathway is conserved between vertebrates and sea urchins. In vertebrates, metabolites of EtOH suppress the production of RA, and exogenous RA is sufficient to rescue EtOH-mediated teratogenesis

(Marrs et al., 2010). Although both EtOH and its metabolite acetaldehyde each suffice to produce similar skeletal patterning defects in sea urchin embryos, inhibition of acetaldehyde production, via pharmacological ADH inhibition, was functionally irrelevant for skeletal patterning in this model. Similarly, treatment with retinol or RA was insufficient to rescue EtOH-mediated skeletal patterning defects in sea urchin embryos. Together, these results indicate that the inhibition of RA by increased levels of acetaldehyde is not responsible for skeletal patterning defects induced by EtOH in sea urchin larvae.

We also tested the conservation of the role of Shh signaling downstream from EtOH by attempting to rescue the EtOH phenotype by pharmacological activation or inhibition of the Hh pathway. Our results show that the inhibition of this pathway provided a modest but statistically significant rescue, while the activation did not. Because the rescue was quite mild, we conclude that Hh is not a major component of the response to EtOH in sea urchins.

One of the most striking defects in EtOH-treated embryos is a three-hour morphological delay in development. This delay was also seen in the spatial expression pattern of some genes that encode skeletal patterning or differentiation cues, such as *Wnt5* and *Hh*, as well as for some PMC subset genes, such as *Jun*. From temporal transcriptome sequencing, we found that the set of known specification genes exhibits both early and late expression within each embryonic tissue. These results suggest that the EtOH-induced phenotype arises from temporal discontinuities both within and between the instructive ectoderm and endoderm tissues and the responsive PMCs,

reflecting an overall loss of temporal synchronization across the embryo. General desynchronization might also explain why our attempts to rescue the EtOH phenotype have met with only limited success in the case of Hh, and none in the case of RA, since our model suggests a more complex cause for the EtOH-mediated defects than a simple loss or gain of a signal or set of signals.

3.2 Discussion and future directions

The apparent discrepancy between our findings that acetaldehyde is sufficient to induce skeletal patterning defects, yet the inhibition of RA synthesis is not responsible for EtOH-perturbations in sea urchin embryos, led us to hypothesize that there is an alternative explanation for these results. In metabolizing ethanol to acetate, two moles of reduced NADH are generated per mole of ethanol oxidized (You and Arteel, 2019). Thus, ethanol exposure leads to an increase in the NADH: NAD⁺ ratio within the cell, favoring the inhibition of mitochondrial β -oxidation (Ontko, 1973). Thus, EtOH and acetaldehyde might each inhibit β -oxidation, which could in turn be responsible for mediating patterning defects. If true, this could account for the phenotypes induced by acetaldehyde that do not depend on RA. Since the role of mitochondrial β -oxidation has not previously been explored in sea urchin embryos, this is a potential area for further study.

As described above, the RNA-seq analysis revealed temporal discrepancies throughout the specification GRN for sea urchin embryos, reflecting an overall loss of synchronization across the embryo. Testing this model for EtOH-mediated teratogenesis presents a challenge both for sufficiency tests, since imposing similar temporal disruptions would be experimentally challenging given the large number of genes

involved, and for requirement tests, since an approach for mediating a rescue of broad and variable temporal disruption is unclear. Future studies that focus on understanding how patterning cues are integrated into the GRN and whether these circuits can be manipulated could provide avenues for testing the mechanism. Single cell RNA-seq experiments that compare control and EtOH-treated embryos over time would also provide valuable insights into the complexity of the ectodermal and endodermal sources of patterning cues and could similarly provide avenues for nuanced experimental manipulation of the system. Finally, multi-omics studies that compare control and EtOH-treated embryonic proteomes, phospho-proteomes, and metabolomes over the range of time points would systematically define the post-translational and metabolic targets of EtOH. Validation and testing of candidate genes and pathways thereby identified would significantly contribute to determining the complex mechanism that underlies EtOH-induced teratogenesis in sea urchin embryos.

3.3 Conclusions

In this thesis, we used cellular, molecular, and systems-level approaches to understand the molecular mechanism of action for EtOH-mediated patterning defects in sea urchin embryos. Sea urchin development is an intricate, signal-dependent process whose large number of regulatory inputs seem to fall out of synchrony during EtOH exposure, leading to developmental patterning defects. Given the biomedical importance of fetal alcohol syndrome disorders in humans, it will be of significant interest to determine whether similar EtOH-mediated temporal disruptions are conserved in other vertebrates and in mammals.

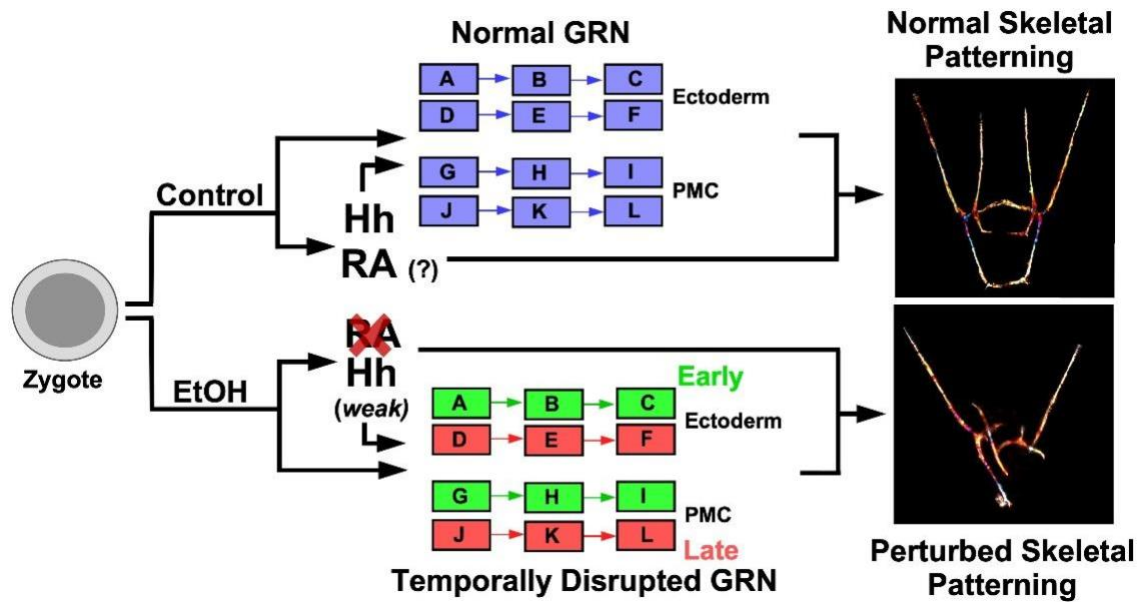


Figure 3.1. A model for EtOH-mediated developmental perturbations in sea urchin embryos. In this model, the major effect of EtOH exposure is a temporally disrupted gene regulatory network (GRN) whose asynchrony leads to perturbations in skeletal patterning. Hh signaling makes a minor contribution to the EtOH phenotype and may be partially upstream from the impacts of EtOH on the GRN, while RA signaling surprisingly does not contribute.

APPENDIX

A.1 Measuring Voltage and Ion Concentration in Live Embryos

This work has been published in Elsevier as:

Rodriguez-Sastre, N., Thomas, C. F., & Bradham, C. A. (2019). Measuring voltage and ion concentrations in live embryos. In *Methods in Cell Biology* (Vol. 151, pp. 459–472). Academic Press Inc. <https://doi.org/10.1016/bs.mcb.2019.01.007>

A.1.1 Abstract

Homeostasis of charged particles in biological systems is fundamental for life. Indeed, the efficient synthesis of ATP is predicated on an electrochemical gradient. Ion pumps and channels act as conduits that regulate membrane potential by controlling ion flux. This phenomenon is critical for the generation of action potentials in excitable cells such as neurons and muscle fibers, and for acidification of lysosomes in all cells. However, the production of action potentials or pH differentials is merely one facet of bioelectricity. Increasing evidence has shown that ion channels and pumps also play critical roles in other cellular processes: cell cycle regulation, wound healing, regeneration, and symmetry breaking during development. In recent years, the functional roles of ion channels have been explored in echinoderm development. The application of fluorescence-based ion and voltage sensitive dyes allows for measurements of ion concentrations with both spatial and temporal resolution. In this chapter, we describe the use of such dyes for interrogating and visualizing ion and voltage gradients in sea urchin embryos.

A.1.2 Introduction

The membrane potential of a cell describes the difference in electrical potential between the inside and outside of the cell. Resting cells maintain a dynamic ionic equilibrium by balancing the electrochemical forces that drive ions into or out of the cell (Sundelacruz et al., 2009). Ions are unable to move freely across the membrane due to the hydrophobic nature of the lipid bilayer. Thus, the passage of ions is controlled by transmembrane proteins known as ion channels and pumps (Rasband et al. 2010).

Cells generally have a resting potential of -70 mV, meaning that the cytosol is negatively charged compared to the external solution. This electrical potential, which is negative inside the cell compared to the outside, is created by actively pumping ions across the membrane (Reid and Zhao, 2014). When the cell undergoes a change in charge distributions, making it less negative (more positive) compared to the external solution, the cell is depolarized (Figure 1). The cell is hyperpolarized when the membrane potential becomes more negative internally. Neuronal action potentials involve a rapid depolarization followed by a restorative hyperpolarization. All cells, excitable or otherwise, exhibit a membrane potential. In some cases, membrane potential dynamics on a smaller, slower scale occur in cells that are not classically considered to be excitable, and, interestingly, functional studies show that bioelectrical changes are required for wound healing, regeneration, and left-right axis specification during embryonic development.

A.1.2.1 Ion flux during development

Studies of ion and voltage gradients have revealed a regulatory role for membrane

potential in cell cycle control. For example, hyperpolarization arrests the cell cycle in vascular endothelial cells (Wang et al., 2003), while ENaC Na⁺ channel overexpression induces proliferation in the mouse colonic epithelium (Canady et al., 1990; Orr et al., 1972; Wilson and Chiu, 1993).

Researchers have used cornea and skin as wound-healing models to demonstrate that these tissues exhibit an endogenous transepithelial electrical field. When wounded, the wound edges in skin short-circuit the field, and produce an outward current, measured at 4 $\mu\text{Amps}/\text{cm}^2$ (Zhao et al., 2006). The wounded cornea similarly generates an electric field that, in turn, directs nerve growth and the rate of epithelial wound healing closure (Reid and Zhao, 2014; Song et al., 2004). The change in ion currents after wounding suggests that electrical changes are an active response to injury (Vieira et al., 2011). In wounded cornea endothelial monolayers, membrane potential depolarization occurs at the leading edge of wounds and gradually extends inward toward the neighboring cells (Chifflet et al., 2005). Similar gradients of membrane potential are observed in wounded skin monolayers. Artificially reversing the endogenous current in wound edges causes them to separate rather than merge (Zhao et al., 2006).

Studies with ion channel inhibitors have revealed the importance of their functional requirements during regeneration. For example, H⁺/K⁺-ATPase activity is required for limb regeneration in frogs, which depends on depolarization of the blastema, and for anterior gene expression and head formation during anterior regeneration in Planaria, in which depolarization suffices to drive anterior regeneration (Beane et al., 2011; Luxardi et al., 2014). The H⁺/K⁺-ATPase is a pump that exports protons in

exchange for imported potassium ions. Interestingly, H⁺ flux driven by the V-ATPase pump is similarly required for tail regeneration in *Xenopus* tadpoles (Adams et al., 2007). The V-ATPase also pumps protons out of the cell or into vesicles, but at the expense of ATP rather than in exchange for Na⁺. The specific role and mechanism for differential potential in regeneration remains unclear; however, it seems likely that potential changes in the blastema may promote local proliferation as a prerequisite for the regenerative response.

Bioelectrical signals are also essential in establishing the left-right body axis during embryonic development (Yost, 2001). In chick and frog models, LR asymmetry determination depends on the early differential ion flux created by H⁺/K⁺-ATPase activity (Levin et al., 2002). The asymmetric expression of H⁺/K⁺-ATPase on the right but not the left side of the primitive streak and developing node maintains a left-right gradient of cell membrane potential in chick embryos that is required for the directed transport of left-specifying Nodal proteins (Levin et al., 2002; Soukup et al., 2015).

A.1.2.2 Events immediately following fertilization are regulated by Na⁺ and Ca²⁺

Numerous events involving ion channel activity occur following fertilization. Prior to fertilization, the sea urchin egg is in an inactive state during which protein synthesis is decreased and DNA synthesis is suspended (Johnson et al., 1976; Steinhardt and Epel, 1974). Upon fertilization, the egg undergoes several critical events that both block polyspermy and render the egg metabolically active. First, the fast block to polyspermy occurs in which the electric potential of the egg cell membrane is increased from -70 mV to about +20 mV (Longo et al., 1986). This change in membrane potential

is mediated by Na⁺ influx into the egg (Shen and Steinhardt, 1978). Next, the slow block to polyspermy occurs during which the exocytosis of cortical granules promotes the elevation of the fertilization envelope. This slow block is mediated by a dramatic increase in cytosolic Ca²⁺ from the endoplasmic reticulum, which initiates the fusion of the cortical granules to the egg cell membrane (Mazia, 1937). In addition to mediating the slow block to polyspermy, Ca²⁺ flux initiates the first phase of egg activation by activating translation (Grainger and Winkler, 1987; Steinhardt and Epel, 1974). The second phase of activation requires an increase in intracellular pH and is mediated by a second influx of Na⁺ (Johnson et al., 1976). Endogenous Na⁺/H⁺ antiporters on the egg cell membrane exchange H⁺ for Na⁺ (Michael and Walt, 1999; Nishioka and McGwin, 1980). This efflux of H⁺ results in the alkalization of the egg (Michael and Walt, 1999; Shen and Steinhardt, 1978). Thus, the concerted movements of calcium, sodium, and hydrogen ions tightly control the earliest stages of development in the sea urchin embryo.

A.1.2.3 Dorsal-ventral (DV) and Left-Right (LR) specification are regulated by H⁺/K⁺ ATPase activity and Ca²⁺

Calcium ions are potent regulators of both the DV and LR axes in sea urchin embryos (Akasaka et al., 1997; Hibino et al., 2006). Inducing a global increase of cytosolic Ca²⁺ abolishes the ectodermal DV axis (Akasaka et al., 1997; Hibino et al., 2006), while treatment with Ni²⁺ ventralizes the ectoderm (Hardin et al., 1992), an effect likely due to inhibition of calcium channels. Globally increasing Ca²⁺ perturbs the LR axis and dysregulates both LR specific gene expression and placement of the adult rudiment (Hibino et al, 2006). Similarly, inhibiting H⁺/K⁺ ATPase disrupts both the normal

expression patterns of LR asymmetric genes and placement of the adult rudiment (Hibino et al, 2006). Furthermore, immunohistochemistry revealed an asymmetric distribution of H⁺/K⁺ ATPase antigens in the cleavage-stage embryo, consistent with this channel playing a role in LR symmetry breaking (Hibino et al, 2006).

A.1.2.4 Biomineralization is dependent on ion flux

Sea urchin larvae possess a calcite endoskeleton made up of both calcium carbonate and numerous embedded proteins (Killian and Wilt, 2008). The calcium carbonate is first accumulated within PMC vesicles as amorphous calcium carbonate (ACC) (Beniash et al., 1997). The vesicles are then trafficked to the PMC membrane and the accumulated ACC is deposited onto the growing skeleton. The formula for the formation of ACC is:



Because the generation of ACC and H⁺ occur concomitantly, intracellular pH (pHi) regulation and calcification are inherently linked. PMCs possess pHi regulatory mechanisms that allow for skeletogenesis even in acidified extracellular media (Stumpp et al., 2012). This regulatory machinery is dependent on the presence of both Na⁺ and HCO³⁻ (Stumpp et al., 2012). ACC precipitation also requires H⁺/K⁺ ATPase activity (Schatzberg et al., 2015). Inhibition of H⁺/K⁺ ATPase initially perturbs H⁺ concentration, but later results in compensatory changes to both Cl⁻ and Na⁺ levels within PMCs while H⁺ levels normalize; H⁺/K⁺ ATPase activity is required for ACC precipitation and biomineralization, with an impact on Na⁺- or Cl⁻-mediated carbonate transport implicated as the most probable cause (Schatzberg et al., 2015). Altogether,

these studies highlight the importance of ionic flux during sea urchin embryonic development.

A.1.3 Voltage sensitive dyes

Neurons communicate electrically and therefore scientist have relied on measuring their membrane potential to understand how this is happening. Traditionally, microelectrodes have been used; however, this comes with a disadvantage of being mechanically invasive, lacking in reproducibility, and resulting in high mortality (Mazari et al., 2014; Peterka et al., 2011). This drove scientists to find other noninvasive methods to measure voltage in developing embryos. For example, in 1976, Neher and Sakman developed the patch clamp techniques used to study ion-channel activities in cells; patch clamps can have the resolution of a single channel (Conforti, 2012). However, path clamps perform poorly on ciliated cells since the cilia disrupt the seal between the patch clamp and the cell membrane.

Another technique for measuring voltage is the usage of fluorescent dyes. Voltage-sensitive dyes, in particular small molecule fluorophores, provide rapid and accurate measurements of membrane potential dynamics. The dyes can be divided into two classes, fast and slow response dyes. Fast dyes (i.e., electrochromic dyes) provide a rapid response rate but low sensitivity, which makes them ideal for monitoring rapid voltage changes such as action potentials. Slow dyes are often based on voltage-dependent accumulation or redistribution and can display much larger changes in fluorescence and are thus more sensitive (Miller, 2016), appropriate for measuring lower amplitude, longer duration voltage changes that occur in non-neuronal cell types. For the

purpose of this chapter, we will focus on the slow response dyes, since they provide a better measurement of the differences in membrane potential in developing embryos.

A.1.4 Methods

A.1.4.1 DiBAC₄/DiSBAC₄:

Bis-(1,3-dibutylbarbituric acid)trimethine oxonol or DiBAC₄(3) (DiBAC) was identified as a slow-response probe that presents a moderate sensitivity towards membrane potential. Bis-(1,3-diethylthiobarbituric acid)trimethine oxonol or DiSBAC₂(3) (DiSBAC) is a related oxonal dye with similar voltage-response properties. Both oxonal dyes are small, negatively charge fluorophores that preferentially enters depolarized cells; their fluorescence also increases in response to depolarization (Epps et al., 1994; Wolff et al., 2003). DiBAC₄(3) produces green fluorescence (excitation maxima at 490 nm and emission maxima of 516 nm), while DiSBAC₄(3) produces red fluorescence (excitation maxima at 535 nm and emission maxima of 560 nm).

Preparation and application of DiBAC₄/DiSBAC₄:

1. 0.5-1 mg/ml stock solutions of DiBAC₄(3) (DiBAC) and DiSBAC₄(3) (DiSBAC) are convenient, and DMSO is a common solvent.
 - a. For sea urchin embryos, 0.5 µg/ml is a useful working concentration.
2. Prior to each experiment, prepare an adequate volume of 2x DiBAC or DiSBAC in sea water, and store in the dark.
3. Load embryos with DiBAC or DiSBAC by combining one volume of embryos with one volume of DiBAC or DiSBAC.

i. If embryos are drug-treated, include the drug in the 2x working dye solution.

a. Incubate 1 hour at room temperature in the dark. Embryos can be held in a drawer or covered with foil, for example.

4. Wash embryos in sea water, then mount and image the embryos using confocal microscopy.

a. In our hands, DiBAC and DiSBAC quench rapidly; we typically collect only a single high-resolution slice per embryo, after determining the optimal focal plane using fast scanning.

b. For quantitative comparisons, it is important to maintain the same image capture settings for each embryo.

c. Mount live embryos on a slide in physiological buffer with some air bubbles, apply coverslip, and seal (i.e., use VALAP) to prevent the sample from drying out.

d. VALAP is 1:1:1 vaseline, lanolin, and paraffin. Melt to combine, then aliquot into screw cap jars. Melt on heat block to use and apply a swab or toothpick to seal cover slip.

e. Mounting fewer embryos is preferred so that oxygen demands are not exceeded.

A.1.4.2 Fluorescent Cl⁻ ion reporters

MEQ-AM: MEQ [6-Methoxy-N-ethylquinolinium iodide] is a chloride ion-sensitive fluorescent dye that provides a reliable method to measure changes in chloride ion

concentration (Wolff et al., 2003). MEQ-AM is modified with an Acetoxymethyl (AM) moiety to improve its membrane permeability; the AM group is removed by esterase in the cytosol, which promotes its cytoplasmic retention. Unlike other ion-sensitive dyes, Cl⁻ quenches MEQ fluorescence; thus, MEQ fluorescence is inversely proportional to Cl⁻ concentration.

Preparation and application of MEQ-AM

1. Make stock DMSO aliquots.
 - i. Make single use aliquots of MEQ-AM in DMSO at ~250 mM store at -20°C.
 - ii. Dilute MEQ AM prepared in DMSO to 5 mM with sea water (10X working stock). Load embryos by combining 1 volume of 5 mM MEQ AM with 9 volumes of embryos.
 - iii. Incubate for 1-2 hours at physiological temperature in the dark.
2. Mount and image using a confocal microscope, using the FITC channel (excitation maxima at 390 nm and emission maxima of 440nm)
 - i. Image using the same approach as described above for DiBAC (Step 4).

A.1.4.3 Fluorescent Na⁺ ion reporters

CoroNa Green, AM: CoroNa acetoxymethyl ester is a member of a class of cation-sensitive fluorescent indicators based on benzoannelated crown systems (Martin et al., 2005). It is a derivative of CoroNa, with the significant addition of an acetoxymethyl ester group, which facilitates its uptake and retention in cells. Upon entering the cell,

intracellular esterases catalyze the cleavage the acetate moiety rendering the probe sensitive to sodium ions, as well as membrane-impermeant. CoroNa AM is maximally excited at 492 nm and emits at 516 nm. As a consequence of its relatively large K_d (~80 mM), CoroNa AM is particularly well suited to measuring large changes in sodium ion concentrations. Measurements can be taken using any instrument that possesses the optical filter sets designed for detection of fluorescein (FITC) or AlexaFluor 488. *In situ* calibration can be carried out by exposing CoroNa AM loaded cells to 2-10 μ M gramicidin, a sodium ion ionophore, in solutions of known sodium ion concentrations (Amorino and Fox, 1995; Harootunian et al., 1989; Negulescu and Machen, 1990).

Preparation of concentrated CoroNa AM stock solutions:

- Dry stocks of CoroNa AM should be stored at -20°C .
- Before opening each stock, bring to room temperature in the dark to prevent hygroscopy.
- Prepare 5 mM (1000x) stocks with anhydrous DMSO.
- Store single-use aliquots (e.g., 2 μ l) of the 5 mM stock at -20°C in the dark

Loading embryos with CoroNa AM:

- The working dilution range suggested by the manufacturers is 0.5 – 10 μ M.
 - *This serves only as a suggestion and may require optimization for the model of interest.*
- Treat embryos with an appropriate dose of CoroNa AM, then incubate for 60 minutes at a physiologically appropriate temperature in the dark.
- Wash the loaded embryos with the appropriate physiological buffer.

- *If embryos are being treated with a pharmacological inhibitor or other reagent, maintain the concentration of that reagent throughout the staining, washing, and imaging steps.*

Imaging CoroNa-loaded embryos:

1. *Image using the same approach as described above for DiBAC (Step 4).*

A.1.4.4 Fluorescent pH reporters

SNARF: Fluorescence-based methods can also be used to measure changes in pH. 5-(and-6)-carboxy SNARF-1 acetoxymethyl ester, acetate (SNARF-1 AM) is a pH-sensitive fluorescent reporter. SNARF-1 AM is a dual-emission probe, with excitation at between 488 nm and 530 nm and emission at 580 nm and 640 nm. This reporter is ratiometric; therefore, the relative pH is measured as the ratio of the emissions. This ratiometric property eliminates multiple fluorescence measurement artifacts: photobleaching, cell thickness, instrument stability, leakage, and non-uniform loading of the dye. *In situ* calibration can be carried out by exposing SNARF-1 AM loaded cells to 10-50 μM nigericin, a H^+/K^+ ionophore, in the presence of 100 – 150 mM K^+ and solutions of known pH (Negulescu and Machen, 1990; Owen, 1992).

Preparation of concentrated SNARF-1 stock solutions:

- Dry stocks of SNARF-1 AM acetate should be stored at -20°C .
- Before opening each stock, bring to room temperature in the dark to prevent hygroscopy.
- Prepare ~ 5 mM (1000x) stocks with anhydrous DMSO.
- Store single-use aliquots (e.g., 2 μl) of the 5 mM stock at -20°C in the dark.

Loading embryos with SNARF-1:

- The working dilution range cited by the manufacturers is 1 – 20 μM .
 - *This serves only as a suggestion and may require optimization for the model of interest.*
- Treat embryos with an appropriate dose of SNARF-1 AM, then incubate for 30 minutes at a physiologically appropriate temperature in the dark.
- Wash the loaded embryos with the appropriate physiological buffer.
 - *If embryos are being treated with a pharmacological inhibitor or other reagent, maintain the concentration of that reagent throughout the staining, washing, and imaging steps.*

Imaging SNARF-1 AM loaded embryos:

2. *Image using the same approach as described above for DiBAC (Step 4).*

- Excite the dye at either 488 nm or 514 nm and use settings appropriate for the detection of ~580 nm and ~640 nm.

A.1.5 Data Analysis

For qualitative analysis of raw data for DiBAC₄/DiSBAC₄, CoroNA Green, MEQ, and SNARF ratio images, use image editing software e.g., Fiji, Canvas, or Photoshop to pseudocolor the images. Differences in the signal can be better visualized with pseudocoloring; a look-up table (LUT) can be applied using an image editor. Our in-house rainbow LUT (Canvas) is shown in Figure 4. First, convert the images to grayscale. Prior to pseudocoloring, brightness and contrast may be adjusted; such adjustments should be applied uniformly across each image and to all the images in a

given dataset. In our hands, these adjustments are performed primarily to darken the background. In addition, Gaussian blur filters may be applied to smooth images that are overly pixelated. Again, such filters must be applied uniformly across each image and across the dataset.

For quantitative analysis, image editing software (Fiji, Canvas, Photoshop, MATLAB) can be used to manually draw regions of interest (ROIs) within the image. We typically draw rectangular ROIs smaller than individual cells and produce numerous such ROIs around the circumference of the embryonic ectoderm, within the endoderm, and within the mesodermal populations (depending on the age of the embryo), within the blastocoel, and outside the embryo in the background. For each ROI, a spreadsheet is generated with the fluorescence intensity within each ROI as well as the area of the ROI. Fluorescence per pixel can thus be calculated (fluorescence per unit area). We typically subtract the fluorescence in the background (averaged from several background ROIs) to produce the net fluorescence for each ROI, then make comparisons between different regions of the embryo.

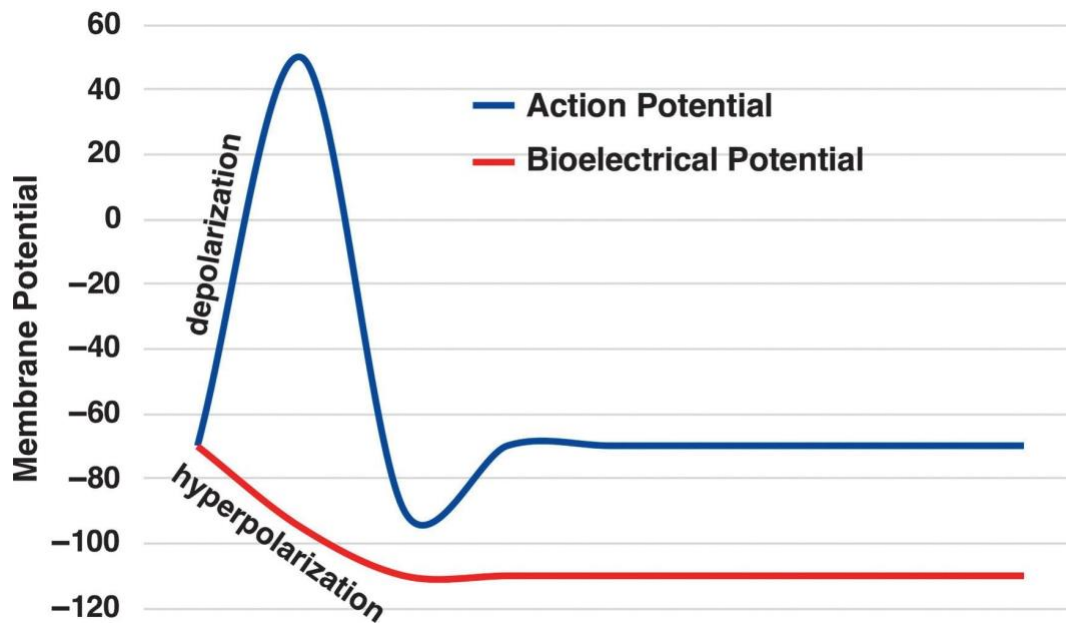


Fig A.1. A chart depicting membrane potential measured over time. A typical action potential of high amplitude and short duration (blue) is compared with a typical bioelectrical signature (red), which is lower amplitude and longer duration than an action potential. The bioelectrical potential here is shown as a hyperpolarization for clarity; it is as likely to instead be a depolarization event.

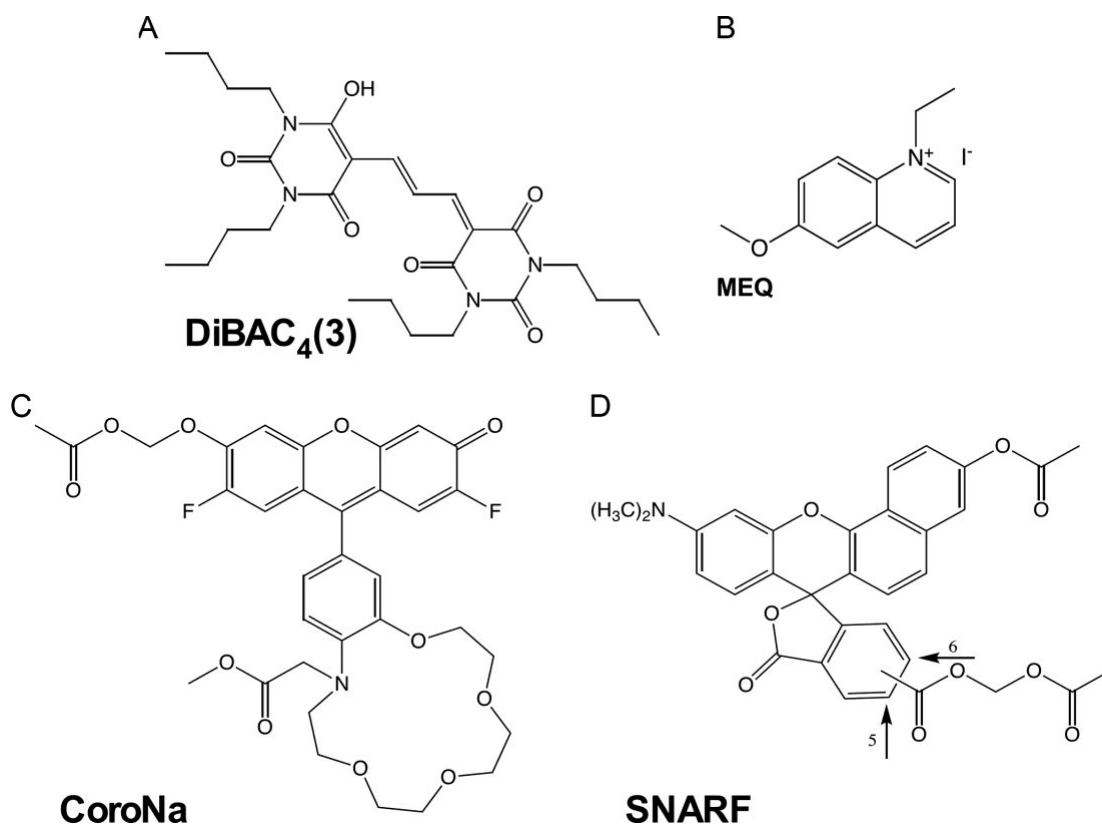


Fig. A.2. Structures of the indicated voltage- and ion-sensing dyes described in this Chapter.

Table A.1. Voltage- and ion-sensing dyes.

Dye	Ion detected	Working concentration	Loading time	Imaging parameters
CoroNa	Sodium ions	0.5–10 μM	1 h	<i>Excitation: 492 nm</i> <i>Emission: 516 nm</i>
SNARF	pH (hydrogen ions)	1–20 μM	30 min	<i>Excitation: 488–530 nm</i> <i>Emission: 580–640 nm</i>
DiBAC ₄ /DiSBAC ₄	Membrane voltage	0.5 $\mu\text{g/mL}$	1 h	<i>Excitation: 490 nm</i> <i>Emission: 516 nm</i> (DiSBAC ₄)
MEQ-AM	Chloride ions	500 μM	1 h	<i>Excitation: 488 nm</i> <i>Emission: 440–460 nm</i>

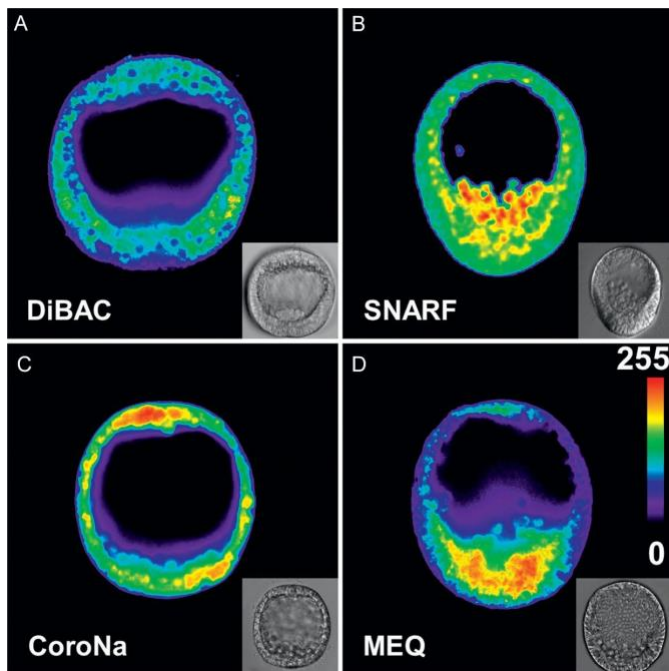


Fig. A.3. Examples of control embryos at mesenchyme blastula stage, imaged for voltage potential (A, DiBAC), protons (B, SNARF), sodium ions (C, CoroNa), or chloride ions (D, MEQ). Each image is pseudocolored using the inset look-up table. For DiBAC, red corresponds to depolarization, while blue corresponds to hyperpolarization. For SNARF, red is alkaline, and blue is acid. For CoroNa, red reflects the highest sodium ion levels, while for MEQ, red reflects the lowest chloride ion levels.

*Adapted from Schatzberg, D., Lawton, M., Hadyaniak, S. E., Ross, E. J., Carney, T., Beane, W.S., et al. (2015). H^+/K^+ ATPase activity is required for biomineralization in sea urchin embryos. *Developmental Biology*, 406, 259–270.*

LIST OF JOURNAL ABBREVIATIONS

Adv Exp Med Biol	Advances in Experimental Medicine and Biology
Adv Wound Care	Advances in Wound Care
Alcohol Clin Exp Res	Alcoholism, Clinical and Experimental Research
Alcohol Res Heal	Alcohol Research & Health
Am J Anat	American Journal of Anatomy
Am J Med Genet Part C Semin Med Genet	American Journal of Medical Genetics. Part C, Seminars in Medical Genetics
Am J Physiol – Cell Physiol	American Journal of Physiology. Cell Physiology
Anal Biochem	Analytical Biochemistry
Biochim Biophys Acta (BBA) Lipids Lipid Metab	Biochimica et Biophysica Acta (BBA) – Lipids and Lipid Metabolism
Biol Rev	Biological Reviews of the Cambridge Philosophical Society
Bioorganic Med Chem Lett	Bioorganic & Medicinal Chemistry Letters
Birth Defects Res Part A – Clin Mol Teratol	Birth Defects Research. Part A, Clinical and Molecular Teratology
Birth Defects Res Part C – Embryo Today Rev	Birth Defects Research. Part C, Embryo Today: Reviews
BMC Biol	BMC Biology
Cancer Res	Cancer Research
Cell Biochem Funct	Cell Biochemistry & Function
Cell Mol Life Sci	Cellular and Molecular Life Sciences: CMLS
Chem Biol	Chemistry & Biology
Chem Rev	Chemical Reviews
Chem Phys Lipids	Chemistry and Physics of Lipids

Curr Opin Chem Biol	Current Opinion in Chemical Biology
Curr Top Dev Biol	Current Topics in Developmental Biology
Curr Top Med Chem	Current Topics in Medicinal Chemistry
Dev Biol	Developmental Biology
Dev Cell	Developmental Cell
Dev Dyn	Developmental Dynamics
Dev Genes Evol	Development Genes and Evolution
Dev Growth Differ	Development, Growth & Differentiation
DMM Dis Model Mech	Disease Models & Mechanisms
FASEB J	FASEB Journal
Front Cell Dev Biol	Frontiers in Cell and Developmental Biology
Front Genet	Frontiers in Genetics
Gene Expr Patterns	Gene Expression Patterns: GEP
Genes Dev	Genes & Development
Genome Biol	Genome Biology
Genome Biol Evol	Genome Biology and Evolution
Gynecol Oncol	Gynecologic Oncology
Handbk Clin Neurol	Handbook of Clinical Neurology
Int J Environ Res Public Health	International Journal of Environmental Research and Public Health
Int Rev Cytol	International Review of Cytology
Integr Biol	Integrative Biology
J Am Chem Soc	Journal of the American Chemical Society
J Biol	Journal of Biology

J Biol Chem	Journal of Biological Chemistry
J Biomol Screen	Journal of Biomolecular Screening
J Cell Comp Physiol	Journal of Cellular and Comparative Physiology
J Cell Sci	Journal of Cell Science
J Comp Neurol	Journal of Comparative Neurology
J Comput Biol	Journal of Computational Biology
J Craniofac Genet Dev Biol	Journal of Craniofacial Genetics and Developmental Biology
J Dev Biol	Journal of Developmental Biology
J Exp Zool	Journal of Experimental Zoology
J Exp Zool Part B Mol Dev Evol	Journal of Experimental Zoology. Part B, Molecular and Developmental Evolution
J Hepatol	Journal of Hepatology
J Lipid Res	Journal of Lipid Research
J Neurosci Res	Journal of Neuroscience Research
J Physiol	Journal of Physiology
J Struct Biol	Journal of Structural Biology
Lab Investig	Laboratory Investigation
Methods Enzymol	Methods in Enzymology
Mol Biol Evol	Molecular Biology and Evolution
Mol Cell Biol	Molecular and Cellular Biology
Mol Reprod Dev	Molecular Reproduction and Development
Nat Rev Genet	Nature reviews. Genetics
Nat Rev Mol Cell Biol	Nature Reviews. Molecular Cell Biology
Pediatr Res	Pediatric Research

PLoS Biol	PLoS Biology
PLoS Comput Biol	PloS Computational Biology
PLoS Genet	PloS Genetics
Proc Natl Acad Sci USA	Proceedings of the National Academy of Sciences of the United States of America
Proc Nutr Soc	Proceedings of the Nutrition Society
Proc R Soc B Biol Sci	Proceedings of the Royal Society of London. Series B, Biological Sciences
Proteome Sci	Proteome Science
Sci Rep	Scientific Reports
Stem Cell Res	Stem Cell Research
Stem Cell Rev Reports	Stem Cell Reviews and Reports
Wiley Interdiscip Rev Dev Biol	Wiley Interdisciplinary Reviews. Developmental Biology
Z Wiss Zool	Zeitschrift für Wissenschaftliche Zoologie
Zoolog Sci	Zoological Science

REFERENCES

- Abramyan, J., 2019. Hedgehog signaling and embryonic craniofacial disorders. *J. Dev. Biol.* 7(2), 9. <https://doi.org/10.3390/JDB7020009>
- Adams, D.S., Masi, A., Levin, M., 2007. H⁺ pump-dependent changes in membrane voltage are an early mechanism necessary and sufficient to induce *Xenopus* tail regeneration. *Development* 134, 1323–1335. <https://doi.org/10.1242/dev.02812>
- Adomako-Ankomah, A., Ettensohn, C.A., 2013. Growth factor-mediated mesodermal cell guidance and skeletogenesis during sea urchin gastrulation. *Development* 140, 4214–4225. <https://doi.org/10.1242/dev.100479>
- Ahlgren, S.C., Thakur, V., Bronner-Fraser, M., 2002. Sonic hedgehog rescues cranial neural crest from cell death induced by ethanol exposure. *Proc. Natl. Acad. Sci. U. S. A.* 99, 10476–10481. <https://doi.org/10.1073/pnas.162356199>
- Akasaka, K., Uemoto, H., Wilt, F., Mitsunaga-Nakatsubo, K., Shimada, H., 1997. Oral-aboral ectoderm differentiation of sea urchin embryos is disrupted in response to calcium ionophore. *Dev. Growth Differ.* 39, 373–379.
<https://doi.org/10.1046/j.1440-169X.1997.t01-2-00013.x>
- Amorino, G.P., Fox, M.H., 1995. Intracellular Na⁺ measurements using sodium green tetraacetate with flow cytometry. *Cytometry* 21, 248–256.
<https://doi.org/10.1002/cyto.990210305>
- Angerer, L.M., Angerer, R.C., 2003. 4 Patterning the sea urchin embryo: Gene regulatory networks, signaling pathways, and cellular interactions. *Curr. Top. Dev. Biol.* 53, 159–198. [https://doi.org/10.1016/s0070-2153\(03\)53005-8](https://doi.org/10.1016/s0070-2153(03)53005-8)

- Angerer, L.M., Oleksyn, D.W., Logan, C.Y., McClay, D.R., Dale, L., Angerer, R.C.,
2000. A BMP pathway regulates cell fate allocation along the sea urchin animal-
vegetal embryonic axis. *Development* 127, 1105–1114.
<https://doi.org/10.1242/dev.127.5.1105>
- Armstrong, N., Hardin, J., McClay, D.R., 1993. Cell-cell interactions regulate skeleton
formation in the sea urchin embryo. *Development* 119(3), 833–840.
<https://doi.org/10.1242/dev.119.3.833>
- Armstrong, N., McClay, D.R., 1994. Skeletal pattern is specified autonomously by the
primary mesenchyme cells in sea urchin embryos. *Dev. Biol.* 162, 329–338.
<https://doi.org/10.1006/dbio.1994.1090>
- Barbie, D.A., Tamayo, P., Boehm, J.S., Kim, S.Y., Moody, S.E., Dunn, I.F., Schinzel,
A.C., Sandy, P., Meylan, E., Scholl, C., Fröhling, S., Chan, E.M., Sos, M.L., Michel,
K., Mermel, C., Silver, S.J., Weir, B.A., Reiling, J.H., Sheng, Q., Gupta, P.B.,
Wadlow, R.C., Le, H., Hoersch, S., Wittner, B.S., Ramaswamy, S., Livingston,
D.M., Sabatini, D.M., Meyerson, M., Thomas, R.K., Lander, E.S., Mesirov, J.P.,
Root, D.E., Gilliland, D.G., Jacks, T., Hahn, W.C., 2009. Systematic RNA
interference reveals that oncogenic KRAS-driven cancers require TBK1. *Nature*
462, 108–112. <https://doi.org/10.1038/nature08460>
- Barresi, M.J.F., Stickney, H.L., Devoto, S.H., 2000. The zebrafish slow-muscle-omitted
gene product is required for Hedgehog signal transduction and the development of
slow muscle identity. *Development* 127, 2189–2199.
<https://doi.org/10.1242/dev.127.10.2189>

- Beane, W.S., Morokuma, J., Adams, D.S., Levin, M., 2011. A chemical genetics approach reveals H,K-ATPase-mediated membrane voltage is required for planarian head regeneration. *Chem. Biol.* 18, 77–89.
<https://doi.org/10.1016/j.chembiol.2010.11.012>
- Beane, W.S., Voronina, E., Wessel, G.M., McClay, D.R., 2006. Lineage-specific expansions provide genomic complexity among sea urchin GTPases. *Dev. Biol.* 300, 165–179. <https://doi.org/10.1016/j.ydbio.2006.08.046>
- Ben-Tabou de-Leon, S., Su, Y.H., Lin, K.T., Li, E., Davidson, E.H., 2013. Gene regulatory control in the sea urchin aboral ectoderm: Spatial initiation, signaling inputs, and cell fate lockdown. *Dev. Biol.* 374, 245–254.
<https://doi.org/10.1016/j.ydbio.2012.11.013>
- Beniash, E., Addadi, L., Weiner, S., 1999. Cellular control over spicule formation in sea urchin embryos: A structural approach. *J. Struct. Biol.* 125, 50–62.
<https://doi.org/10.1006/jsbi.1998.4081>
- Beniash, E., Aizenberg, J., Addadi, L., Weiner, S., 1997. Amorphous calcium carbonate transforms into calcite during sea urchin larval spicule growth. *Proc. R. Soc. B Biol. Sci.* 264, 461–465. <https://doi.org/10.1098/rspb.1997.0066>
- Blader, P., Strähle, U., 1998. Ethanol impairs migration of the prechordal plate in the zebrafish embryo. *Dev. Biol.* 201, 185–201. <https://doi.org/10.1006/dbio.1998.8995>
- Bradham, C.A., Foltz, K.R., Beane, W.S., Arnone, M.I., Rizzo, F., Coffman, J.A., Mushegian, A., Goel, M., Morales, J., Geneviere, A.M., Lapraz, F., Robertson, A.J., Kelkar, H., Loza-Coll, M., Townley, I.K., Raisch, M., Roux, M.M., Lepage, T.,

- Gache, C., McClay, D.R., Manning, G., 2006. The sea urchin kinome: A first look. *Dev. Biol.* 300, 180–193. <https://doi.org/10.1016/j.ydbio.2006.08.074>
- Bradham, C.A., McClay, D., 2006. p38 MAPK is essential for secondary axis specification and patterning in sea urchin embryos. *Development* 133, 21–32. <https://doi.org/10.1242/dev.02160>
- Bradham, C.A., Oikonomou, C., Kühn, A., Core, A.B., Modell, J.W., McClay, D.R., Poustka, A.J., 2009. Chordin is required for neural but not axial development in sea urchin embryos. *Dev. Biol.* 328, 221–233. <https://doi.org/10.1016/j.ydbio.2009.01.027>
- Briscoe, J., 2019. Understanding Pattern Formation in Embryos: Experiment, Theory, and Simulation. *J. Comput. Biol.* 26, 696–702. <https://doi.org/10.1089/cmb.2019.0090>
- Burke, R.D., Moller, D.J., Krupke, O.A., Taylor, V.J., 2014. Sea urchin neural development and the metazoan paradigm of neurogenesis. *Genesis*. <https://doi.org/10.1002/dvg.22750>
- Burke, R.D., Osborne, L., Wang, D., Murabe, N., Yaguchi, S., Nakajima, Y., 2006. Neuron-specific expression of a synaptotagmin gene in the sea urchin *Strongylocentrotus purpuratus*. *J. Comp. Neurol.* 496, 244–251. <https://doi.org/10.1002/cne.20939>
- Burton, D.F., Boa-Amponsem, O.M., Dixon, M.S., Hopkins, M.J., Herbin, T.A., Toney, S., Tarpley, M., Rodriguez, B. V., Fish, E.W., Parnell, S.E., Cole, G.J., Williams, K.P., 2022. Pharmacological activation of the Sonic hedgehog pathway with a Smoothened small molecule agonist ameliorates the severity of alcohol-induced

- morphological and behavioral birth defects in a zebrafish model of fetal alcohol spectrum disorder. *J. Neurosci. Res.* 1–17. <https://doi.org/10.1002/jnr.25008>
- Canady, K.S., Ali-Osman, F., Rubel, E.W., 1990. Extracellular potassium influences DNA and protein syntheses and glial fibrillary acidic protein expression in cultured glial cells. *Glia* 3, 368–374. <https://doi.org/10.1002/glia.440030508>
- Cang, Z., Wang, Y., Wang, Q., Cho, K.W.Y., Holmes, W., Nie, Q., 2021. A multiscale model via single-cell transcriptomics reveals robust patterning mechanisms during early mammalian embryo development. *PLoS Comput. Biol.* 17, e1008571. <https://doi.org/10.1371/journal.pcbi.1008571>
- Cartwright, M.M., Smith, S.M., 1995. Increased Cell Death and Reduced Neural Crest Cell Numbers in Ethanol-Exposed Embryos: Partial Basis for the Fetal Alcohol Syndrome Phenotype. *Alcohol. Clin. Exp. Res.* 19, 378–386. <https://doi.org/10.1111/j.1530-0277.1995.tb01519.x>
- Cavalieri, V., Guarcello, R., Spinelli, G., 2011. Specific expression of a TRIM-containing factor in ectoderm cells affects the skeletal morphogenetic program of the sea urchin embryo. *Development* 138, 4279–4290. <https://doi.org/10.1242/dev.066480>
- Cayuso, J., Ulloa, F., Cox, B., Briscoe, J., Marti, E., 2006. The Sonic hedgehog pathway independently controls the patterning, proliferation and survival of neuroepithelial cells by regulating Gli activity. *Development* 133, 517–528. <https://doi.org/10.1242/dev.02228>
- CDC, 2021. Basics about FASDs | CDC [WWW Document]. *Natl. Cent. Birth Defects Dev. Disabil.* URL <https://www.cdc.gov/ncbddd/fasd/facts.html> (accessed 1.24.22).

- Chatzi, C., Cunningham, T.J., Duester, G., 2013. Investigation of retinoic acid function during embryonic brain development using retinaldehyde-rescued Rdh10 knockout mice. *Dev. Dyn.* 242, 1056–1065. <https://doi.org/10.1002/dvdy.23999>
- Chen, J.H., Luo, Y.J., Su, Y.H., 2011. The dynamic gene expression patterns of transcription factors constituting the sea urchin aboral ectoderm gene regulatory network. *Dev. Dyn.* 240, 250–260. <https://doi.org/10.1002/dvdy.22514>
- Chen, J.K., Taipale, J., Cooper, M.K., Beachy, P.A., 2002a. Inhibition of Hedgehog signaling by direct binding of cyclopamine to Smoothened. *Genes Dev.* 16, 2743–2748. <https://doi.org/10.1101/gad.1025302>
- Chen, J.K., Taipale, J., Young, K.E., Maiti, T., Beachy, P.A., 2002b. Small molecule modulation of smoothened activity. *Proc. Natl. Acad. Sci. U. S. A.* 99, 14071–14076. <https://doi.org/10.1073/pnas.182542899>
- Chen, S., Zhou, Y., Chen, Y., Gu, J., 2018. Fastp: An ultra-fast all-in-one FASTQ preprocessor. In: *Bioinformatics*, pp. i884–i890. <https://doi.org/10.1093/bioinformatics/bty560>
- Chifflet, S., Hernández, J.A., Grasso, S., 2005. A possible role for membrane depolarization in epithelial wound healing. *Am. J. Physiol. - Cell Physiol.* 288, 1420–1430. <https://doi.org/10.1152/ajpcell.00259.2004>
- Coffman, J.A., 2011. Information as a manifestation of development. *Information* 2(1), 102–116. <https://doi.org/10.3390/info2010102>
- Coffman, J.A., McCarthy, J.J., Dickey-Sims, C., Robertson, A.J., 2004. Oral-aboral axis specification in the sea urchin embryo: II. Mitochondrial distribution and redox state

- contribute to establishing polarity in *Strongylocentrotus purpuratus*. *Dev. Biol.* 273, 160–171. <https://doi.org/10.1016/j.ydbio.2004.06.005>
- Cohen, M.M., Sulik, K.K., 1992. Perspectives on holoprosencephaly: Part II. Central nervous system, craniofacial anatomy, syndrome commentary, diagnostic approach, and experimental studies. *J. Craniofac. Genet. Dev. Biol.* 12(4), 196–244.
- Conforti, L., 2012. Patch-clamp techniques. In: *Cell Physiology Source Book*. Academic Press, pp. 369–381. <https://doi.org/10.1016/B978-0-12-387738-3.00020-2>
- Crabb, D.W., Matsumoto, M., Chang, D., You, M., 2004. Overview of the role of alcohol dehydrogenase and aldehyde dehydrogenase and their variants in the genesis of alcohol-related pathology. *Proc. Nutr. Soc.* 63, 49–63.
<https://doi.org/10.1079/pns2003327>
- Croce, J.C., Wu, S.Y., Byrum, C., Xu, R., Duloquin, L., Wikramanayake, A.H., Gache, C., McClay, D.R., 2006. A genome-wide survey of the evolutionarily conserved Wnt pathways in the sea urchin *Strongylocentrotus purpuratus*. *Dev. Biol.* 300, 121–131. <https://doi.org/10.1016/j.ydbio.2006.08.045>
- Davidson, E.H., Rast, J.P., Oliveri, P., Ransick, A., Calestani, C., Yuh, C.H., Minokawa, T., Amore, G., Hinman, V., Arenas-Mena, C., Otim, O., Brown, C.T., Livi, C.B., Lee, P.Y., Revilla, R., Rust, A.G., Pan, Z.J., Schilstra, M.J., Clarke, P.J.C., Arnone, M.I., Rowen, L., Cameron, R.A., McClay, D.R., Hood, L., Bolouri, H., 2002. A genomic regulatory network for development. *Science* 295(5560), 1669–1678.
<https://doi.org/10.1126/science.1069883>

- Davidson, P.L., Guo, H., Wang, L., Berrio, A., Zhang, H., Chang, Y., Soborowski, A.L., McClay, D.R., Fan, G., Wray, G.A., 2020. Chromosomal-level genome assembly of the sea urchin *Lytechinus variegatus* substantially improves functional genomic analyses. *Genome Biol. Evol.* 12, 1080–1086.
<https://doi.org/10.1093/GBE/EVAA101>
- De Jonge, M.H., Zachman, R.D., 1995. The effect of maternal ethanol ingestion on fetal rat heart vitamin a: A model for fetal alcohol syndrome. *Pediatr. Res.* 37, 418–423.
<https://doi.org/10.1203/00006450-199504000-00006>
- Dobin, A., Davis, C.A., Schlesinger, F., Drenkow, J., Zaleski, C., Jha, S., Batut, P., Chaisson, M., Gingeras, T.R., 2013. STAR: Ultrafast universal RNA-seq aligner. *Bioinformatics* 29, 15–21. <https://doi.org/10.1093/bioinformatics/bts635>
- Dubey, A., Rose, R.E., Jones, D.R., Saint-Jeannet, J.P., 2018. Generating retinoic acid gradients by local degradation during craniofacial development: One cell's cue is another cell's poison. *Genesis* 56(2), e23091. <https://doi.org/10.1002/dvg.23091>
- Duboc, V., Lepage, T., 2008. A conserved role for the nodal signaling pathway in the establishment of dorso-ventral and left-right axes in deuterostomes. *J. Exp. Zool. Part B Mol. Dev. Evol.* 310, 41–53. <https://doi.org/10.1002/jez.b.21121>
- Duboc, V., Röttinger, E., Besnardeau, L., Lepage, T., 2004. Nodal and BMP2/4 signaling organizes the oral-aboral axis of the sea urchin embryo. *Dev. Cell* 6, 397–410.
[https://doi.org/10.1016/S1534-5807\(04\)00056-5](https://doi.org/10.1016/S1534-5807(04)00056-5)
- Duester, G., 1991. A Hypothetical Mechanism for Fetal Alcohol Syndrome Involving Ethanol Inhibition of Retinoic Acid Synthesis at the Alcohol Dehydrogenase Step.

- Alcohol. Clin. Exp. Res. 15, 568–572. <https://doi.org/10.1111/j.1530-0277.1991.tb00562.x>
- Duloquin, L., Lhomond, G., Gache, C., 2007. Localized VEGF signaling from ectoderm to mesenchyme cells controls morphogenesis of the sea urchin embryo skeleton. *Development* 134, 2293–2302. <https://doi.org/10.1242/dev.005108>
- Eberhart, J.K., Parnell, S.E., 2016. The Genetics of Fetal Alcohol Spectrum Disorders. *Alcohol. Clin. Exp. Res.* <https://doi.org/10.1111/acer.13066>
- Echelard, Y., Epstein, D.J., St-Jacques, B., Shen, L., Mohler, J., McMahon, J.A., McMahon, A.P., 1993. Sonic hedgehog, a member of a family of putative signaling molecules, is implicated in the regulation of CNS polarity. *Cell* 75, 1417–1430. [https://doi.org/10.1016/0092-8674\(93\)90627-3](https://doi.org/10.1016/0092-8674(93)90627-3)
- Emily-Fenouil, F., Ghiglione, C., Lhomond, G., Lepage, T., Gache, C., 1998. GSK3beta/shaggy mediates patterning along the animal-vegetal axis of the sea urchin embryo. *Development* 125, 2489–2498. <https://doi.org/10.1242/DEV.125.13.2489>
- Epps, D.E., Wolfe, M.L., Groppi, V., 1994. Characterization of the steady-state and dynamic fluorescence properties of the potential-sensitive dye bis-(1,3-dibutylbarbituric acid)trimethine oxonol (Dibac4(3)) in model systems and cells. *Chem. Phys. Lipids* 69, 137–150. [https://doi.org/10.1016/0009-3084\(94\)90035-3](https://doi.org/10.1016/0009-3084(94)90035-3)
- Ettensohn, C.A., 1990. The regulation of primary mesenchyme cell patterning. *Dev. Biol.* 140, 261–271. [https://doi.org/10.1016/0012-1606\(90\)90076-U](https://doi.org/10.1016/0012-1606(90)90076-U)

- Ettensohn, C.A., M., M., 1993. Size regulation and morphogenesis: a cellular analysis of skeletogenesis in the sea urchin embryo. *Development* 119, 155–167.
- Ettensohn, C.A., McClay, D.R., 1986. The regulation of primary mesenchyme cell migration in the sea urchin embryo: Transplantations of cells and latex beads. *Dev. Biol.* 117, 380–391. [https://doi.org/10.1016/0012-1606\(86\)90307-6](https://doi.org/10.1016/0012-1606(86)90307-6)
- Fink, R.D., McClay, D.R., 1985. Three cell recognition changes accompany the ingression of sea urchin primary mesenchyme cells. *Dev. Biol.* 107, 66–74. [https://doi.org/10.1016/0012-1606\(85\)90376-8](https://doi.org/10.1016/0012-1606(85)90376-8)
- Frank-Kamenetsky, M., Zhang, X.M., Bottega, S., Guicherit, O., Wichterle, H., Dudek, H., Bumcrot, D., Wang, F.Y., Jones, S., Shulok, J., Rubin, L.L., Porter, J.A., 2002. Small-molecule modulators of Hedgehog signaling: Identification and characterization of Smoothed agonists and antagonists. *J. Biol.* 1, 10. <https://doi.org/10.1186/1475-4924-1-10>
- Gil-Mohapel, J., Bianco, C.D., Cesconetto, P.A., Zamoner, A., Brocardo, P.S., 2019. Ethanol Exposure During Development, and Brain Oxidative Stress. In: *Neuroscience of Alcohol*. Academic Press, pp. 493–503. <https://doi.org/10.1016/b978-0-12-813125-1.00051-9>
- Gilliam, D., 2014. Embryo transfers between C57BL/6J and DBA/2J mice: Examination of a maternal effect on ethanol teratogenesis. *Front. Genet.* 5, 436. <https://doi.org/10.3389/fgene.2014.00436>
- Goodlett, C.R., Gilliam, D.M., Nichols, J.M., West, J.R., 1989. Genetic influences on brain growth restriction induced by development exposure to alcohol.

- Neurotoxicology 10, 321–334.
- Grainger, J.L., Winkler, M.M., 1987. Fertilization triggers unmasking of maternal mRNAs in sea urchin eggs. *Mol. Cell. Biol.* 7, 3947–3954.
<https://doi.org/10.1128/mcb.7.11.3947>
- Gur, M., Bendelac-Kapon, L., Shabtai, Y., Pillemer, G., Fainsod, A., 2022. Reduced Retinoic Acid Signaling During Gastrulation Induces Developmental Microcephaly. *Front. Cell Dev. Biol.* 10, 553. <https://doi.org/10.3389/fcell.2022.844619>
- Hänzelmann, S., Castelo, R., Guinney, J., 2013. GSVA: Gene set variation analysis for microarray and RNA-Seq data. *BMC Bioinformatics* 14, 1–15.
<https://doi.org/10.1186/1471-2105-14-7>
- Hardin, J., Armstrong, N., 1997. Short-range cell-cell signals control ectodermal patterning in the oral region of the sea urchin embryo. *Dev. Biol.* 182, 134–149.
<https://doi.org/10.1006/dbio.1996.8436>
- Hardin, J., Coffman, J.A., Black, S.D., McClay, D.R., 1992. Commitment along the dorsoventral axis of the sea urchin embryo is altered in response to NiCl₂. *Development* 116, 671–685.
- Harootunian, A.T., Kao, J.P.Y., Eckert, B.K., Tsien, R.Y., 1989. Fluorescence ratio imaging of cytosolic free Na⁺ in individual fibroblasts and lymphocytes. *J. Biol. Chem.* 264, 19458–19467. [https://doi.org/10.1016/s0021-9258\(19\)47322-5](https://doi.org/10.1016/s0021-9258(19)47322-5)
- Hemavathy, K., Ashraf, S.I., Ip, Y.T., 2000. Snail/Slug family of repressors: Slowly going into the fast lane of development and cancer. *Gene* 257(1), 1–12.
[https://doi.org/10.1016/S0378-1119\(00\)00371-1](https://doi.org/10.1016/S0378-1119(00)00371-1)

- Hibino, T., Ishii, Y., Levin, M., Nishino, A., 2006. Ion flow regulates left-right asymmetry in sea urchin development. *Dev. Genes Evol.* 216, 265–276.
<https://doi.org/10.1007/S00427-005-0051-6>
- Hogan, J.D., Keenan, J.L., Luo, L., Ibn-Salem, J., Lamba, A., Schatzberg, D., Piacentino, M.L., Zuch, D.T., Core, A.B., Blumberg, C., Timmermann, B., Grau, J.H., Speranza, E., Andrade-Navarro, M.A., Irie, N., Poustka, A.J., Bradham, C.A., 2020. The developmental transcriptome for *Lytechinus variegatus* exhibits temporally punctuated gene expression changes. *Dev. Biol.* 460, 139–154.
<https://doi.org/10.1016/j.ydbio.2019.12.002>
- Hong, M., Krauss, R.S., 2017. Ethanol itself is a holoprosencephaly-inducing teratogen. *PLoS One* 12, 8–10. <https://doi.org/10.1371/journal.pone.0176440>
- Hong, M., Krauss, R.S., 2012. Cdon Mutation and Fetal Ethanol Exposure Synergize to Produce Midline Signaling Defects and Holoprosencephaly Spectrum Disorders in Mice. *PLoS Genet.* 8, e1002999. <https://doi.org/10.1371/journal.pgen.1002999>
- Hooper, J.E., Scott, M.P., 2005. Communicating with hedgehogs. *Nat. Rev. Mol. Cell Biol.* 6, 306–317. <https://doi.org/10.1038/nrm1622>
- Horstadius, S., 1939. The mechanics of sea urchin development, studied by operative methods. *Biol. Rev.* 14, 132–179. <https://doi.org/10.1111/j.1469-185X.1939.tb00929.x>
- Howard-Ashby, M., Materna, S.C., Brown, C.T., Chen, L., Cameron, R.A., Davidson, E.H., 2006. Identification and characterization of homeobox transcription factor genes in *Strongylocentrotus purpuratus*, and their expression in embryonic

- development. *Dev. Biol.* 300, 74–89. <https://doi.org/10.1016/j.ydbio.2006.08.039>
- Hoyme, H.E., May, P.A., Kalberg, W.O., Kodituwakku, P., Gossage, J.P., Trujillo, P.M., Buckley, D.G., Miller, J.H., Aragon, A.S., Khaole, N., Viljoen, D.L., Jones, K.L., Robinson, L.K., 2005. A practical clinical approach to diagnosis of fetal alcohol spectrum disorders: Clarification of the 1996 institute of medicine criteria. *Pediatrics* 115, 39–47. <https://doi.org/10.1542/peds.2004-0259>
- Ingham, P.W., McMahon, A.P., 2001. Hedgehog signaling in animal development: paradigms and principles. *Genes Dev.* 15, 3059–3087. <https://doi.org/10.1101/GAD.938601>
- Ingham, P.W., Placzek, M., 2006. Orchestrating ontogenesis: Variations on a theme by sonic hedgehog. *Nat. Rev. Genet.* <https://doi.org/10.1038/nrg1969>
- Janesick, A., Wu, S.C., Blumberg, B., 2015. Retinoic acid signaling and neuronal differentiation. *Cell. Mol. Life Sci.* <https://doi.org/10.1007/s00018-014-1815-9>
- Jia, J., Jiang, J., 2006. Decoding the Hedgehog signal in animal development. *Cell. Mol. Life Sci.* <https://doi.org/10.1007/s00018-005-5519-z>
- Jiang, J., Hui, C. chung, 2008. Hedgehog Signaling in Development and Cancer. *Dev. Cell* 15(6), 801–812. <https://doi.org/10.1016/j.devcel.2008.11.010>
- Johnson, C.S., Zucker, R.M., Hunter, E.S., Sulik, K.K., 2007. Perturbation of retinoic acid (RA)-mediated limb development suggests a role for diminished RA signaling in the teratogenesis of ethanol. *Birth Defects Res. Part A - Clin. Mol. Teratol.* 79, 631–641. <https://doi.org/10.1002/bdra.20385>

- Johnson, J.D., Epel, D., Paul, M., 1976. Intracellular pH and activation of sea urchin eggs after fertilisation. *Nature* 262, 661–664. <https://doi.org/10.1038/262661a0>
- Johnson, W.E., Li, C., Rabinovic, A., 2007. Adjusting batch effects in microarray expression data using empirical Bayes methods. *Biostatistics* 8, 118–127. <https://doi.org/10.1093/biostatistics/kxj037>
- Khalid, O., Kim, J.J., Kim, H.-S., Hoang, M., Tu, T.G., Elie, O., Lee, C., Vu, C., Horvath, S., Spigelman, I., Kim, Y., 2014. Gene expression signatures affected by alcohol-induced DNA methylomic deregulation in human embryonic stem cells. *Stem Cell Res* 12, 791–806. <https://doi.org/10.1016/j.scr.2014.03.009>
- Kietzman, H.W., Everson, J.L., Sulik, K.K., Lipinski, R.J., 2014. The teratogenic effects of prenatal ethanol exposure are exacerbated by sonic Hedgehog or Gli2 haploinsufficiency in the mouse. *PLoS One* 9, 1–5. <https://doi.org/10.1371/journal.pone.0089448>
- Killian, C.E., Wilt, F.H., 2008. Molecular aspects of biomineralization of the Echinoderm endoskeleton. *Chem. Rev.* 108, 4463–4474. <https://doi.org/10.1021/cr0782630>
- Knapp, R.T., Wu, C.H., Mobilia, K.C., Joester, D., 2012. Recombinant Sea Urchin VEGF Directs Single Crystal Growth and Branching in vitro. *J. Am. Chem. Soc.* 17908–17911. <https://doi.org/10.1021/ja309024b>
- Kot-Leibovich, H., Fainsod, A., 2009. Ethanol induces embryonic malformations by competing for retinaldehyde dehydrogenase activity during vertebrate gastrulation. *DMM Dis. Model. Mech.* 2, 295–305. <https://doi.org/10.1242/dmm.001420>

- Kurrey, N.K., Amit, K., Bapat, S.A., 2005. Snail and Slug are major determinants of ovarian cancer invasiveness at the transcription level. *Gynecol. Oncol.* 97, 155–165. <https://doi.org/10.1016/j.ygyno.2004.12.043>
- Kwok, W.K., Ling, M.T., Lee, T.W., Lau, T.C.M., Zhou, C., Zhang, X., Chua, C.W., Chan, K.W., Chan, F.L., Glackin, C., Wong, Y.C., Wang, X., 2005. Up-regulation of TWIST in prostate cancer and its implication as a therapeutic target. *Cancer Res.* 65, 5153–5162. <https://doi.org/10.1158/0008-5472.CAN-04-3785>
- Lapraz, F., Besnardeau, L., Lepage, T., 2009. Patterning of the dorsal-ventral axis in echinoderms: Insights into the evolution of the BMP-chordin signaling network. *PLoS Biol.* 7, e1000248. <https://doi.org/10.1371/journal.pbio.1000248>
- Lapraz, F., Röttinger, E., Duboc, V., Range, R., Duloquin, L., Walton, K., Wu, S.Y., Bradham, C., Loza, M.A., Hibino, T., Wilson, K., Poustka, A., McClay, D., Angerer, L., Gache, C., Lepage, T., 2006. RTK and TGF- β signaling pathways genes in the sea urchin genome. *Dev. Biol.* 300, 132–152. <https://doi.org/10.1016/j.ydbio.2006.08.048>
- Latipää, P.M., Kärki, T.T., Hiltunen, J.K., Hassinen, I.E., 1986. Regulation of palmitoylcarnitine oxidation in isolated rat liver mitochondria. Role of the redox state of NAD(H). *Biochim. Biophys. Acta (BBA)/Lipids Lipid Metab.* 875, 293–300. [https://doi.org/10.1016/0005-2760\(86\)90179-7](https://doi.org/10.1016/0005-2760(86)90179-7)
- Leek, J.T., Johnson, W.E., Parker, H.S., Jaffe, A.E., Storey, J.D., 2012. The SVA package for removing batch effects and other unwanted variation in high-throughput experiments. *Bioinformatics* 28, 882–883.

<https://doi.org/10.1093/bioinformatics/bts034>

- Levin, M., Thorlin, T., Robinson, K.R., Nogi, T., Mercola, M., 2002. Asymmetries in H⁺/K⁺-ATPase and cell membrane potentials comprise a very early step in left-right patterning. *Cell* 111, 77–89. [https://doi.org/10.1016/S0092-8674\(02\)00939-X](https://doi.org/10.1016/S0092-8674(02)00939-X)
- Li, E., Cui, M., Peter, I.S., Davidson, E.H., 2014. Encoding regulatory state boundaries in the pregastrular oral ectoderm of the sea urchin embryo. *Proc. Natl. Acad. Sci. U. S. A.* 111. <https://doi.org/10.1073/pnas.1323105111>
- Li, X., Li, Y., Li, S., Li, H., Yang, C., Lin, J., 2021. The role of Shh signalling pathway in central nervous system development and related diseases. *Cell Biochem. Funct.* 39(2), 180–189. <https://doi.org/10.1002/cbf.3582>
- Li, Y.X., Yang, H.T., Zdanowicz, M., Sicklick, J.K., Qi, Y., Camp, T.J., Diehl, A.M., 2007. Fetal alcohol exposure impairs hedgehog cholesterol modification and signaling. *Lab. Investig.* 87, 231–240. <https://doi.org/10.1038/labinvest.3700516>
- Liao, Y., Smyth, G.K., Shi, W., 2014. FeatureCounts: An efficient general purpose program for assigning sequence reads to genomic features. *Bioinformatics* 30, 923–930. <https://doi.org/10.1093/bioinformatics/btt656>
- Logan, C.Y., Miller, J.R., Ferkowicz, M.J., McClay, D.R., 1998. Nuclear beta-catenin is required to specify vegetal cell fates in the sea urchin embryo. *Development* 126, 345–357.
- Longo, F.J., Lynn, J.W., McCulloh, D.H., Chambers, E.L., 1986. Correlative ultrastructural and electrophysiological studies of sperm-egg interactions of the sea urchin, *Lytechinus variegatus*. *Dev. Biol.* 118, 155–166.

[https://doi.org/10.1016/0012-1606\(86\)90083-7](https://doi.org/10.1016/0012-1606(86)90083-7)

Lou, H., Li, H., Huehn, A.R., Tarasova, N.I., Saleh, B., Anderson, S.K., Dean, M., 2020.

Genetic and epigenetic regulation of the smoothened gene (SMO) in cancer cells.

Cancers (Basel). 12, 1–19. <https://doi.org/10.3390/cancers12082219>

Love, M.I., Huber, W., Anders, S., 2014. Moderated estimation of fold change and

dispersion for RNA-seq data with DESeq2. *Genome Biol.* 15, 1–21.

<https://doi.org/10.1186/s13059-014-0550-8>

Luo, Y.J., Su, Y.H., 2012. Opposing Nodal and BMP Signals Regulate Left-Right

Asymmetry in the Sea Urchin Larva. *PLoS Biol.* 10, 1001402.

<https://doi.org/10.1371/journal.pbio.1001402>

Luxardi, G., Reid, B., Maillard, P., Zhao, M., 2014. Single cell wound generates electric

current circuit and cell membrane potential variations that requires calcium influx.

Integr. Biol. (United Kingdom) 6, 662–672. <https://doi.org/10.1039/c4ib00041b>

Lyons, D.C., Kaltenbach, S.L., Mcclay, D.R., 2012. Morphogenesis in sea urchin

embryos: Linking cellular events to gene regulatory network states. Wiley

Interdiscip. Rev. Dev. Biol. 1, 231–252. <https://doi.org/10.1002/wdev.18>

Malinda, K.M., Etensohn, C.A., 1994. Primary mesenchyme cell migration in the sea

urchin embryo: Distribution of directional cues. *Dev. Biol.* 164, 562–578.

<https://doi.org/10.1006/dbio.1994.1224>

Malinda, K.M., Fisher, G.W., Etensohn, C.A., 1995. Four-dimensional microscopic

analysis of the filopodial behavior of primary mesenchyme cells during gastrulation

in the sea urchin embryo. *Dev. Biol.* 172, 552–566.

<https://doi.org/10.1006/dbio.1995.8044>

Mann, K., Wilt, F.H., Poustka, A.J., 2010. Proteomic analysis of sea urchin (*Strongylocentrotus purpuratus*) spicule matrix. *Proteome Sci.* 8, 33.

<https://doi.org/10.1186/1477-5956-8-33>

Marrs, J.A., Clendenon, S.G., Ratcliffe, D.R., Fielding, S.M., Liu, Q., Bosron, W.F., 2010. Zebrafish fetal alcohol syndrome model: Effects of ethanol are rescued by retinoic acid supplement. *Alcohol* 44, 707–715.

<https://doi.org/10.1016/j.alcohol.2009.03.004>

Martin, V. V., Rothe, A., Gee, K.R., 2005. Fluorescent metal ion indicators based on benzoannelated crown systems: A green fluorescent indicator for intracellular sodium ions. *Bioorganic Med. Chem. Lett.* 15, 1851–1855.

<https://doi.org/10.1016/j.bmcl.2005.02.017>

Maruyama, Y.K., Nakaseko, Y., Yagi, S., 1985. Localization of cytoplasmic determinants responsible for primary mesenchyme formation and gastrulation in the unfertilized egg of the sea urchin *Hemicentrotus pulcherrimus*. *J. Exp. Zool.* 236, 155–163. <https://doi.org/10.1002/jez.1402360206>

Materna, S.C., Howard-Ashby, M., Gray, R.F., Davidson, E.H., 2006. The C2H2 zinc finger genes of *Strongylocentrotus purpuratus* and their expression in embryonic development. *Dev. Biol.* 300, 108–120. <https://doi.org/10.1016/j.ydbio.2006.08.032>

Materna, S.C., Ransick, A., Li, E., Davidson, E.H., 2013. Diversification of oral and aboral mesodermal regulatory states in pregastrular sea urchin embryos. *Dev. Biol.* 375, 92–104. <https://doi.org/10.1016/j.ydbio.2012.11.033>

- Mazari, E., Zhao, X., Migeotte, I., Collignon, J., Gosse, C., Perea-Gomez, A., 2014. A microdevice to locally electroporate embryos with high efficiency and reduced cell damage. *Development* 141, 2349–2359. <https://doi.org/10.1242/dev.106633>
- Mazia, D., 1937. The release of calcium in Arbacia eggs on fertilization. *J. Cell. Comp. Physiol.* 10, 291–304. <https://doi.org/10.1002/jcp.1030100304>
- McIntyre, D.C., Seay, N.W., Croce, J.C., McClay, D.R., 2013. Short-range Wnt5 signaling initiates specification of sea urchin posterior ectoderm. *Development* 140, 4881–4889. <https://doi.org/10.1242/dev.095844>
- Michael, K.L., Walt, D.R., 1999. Combined imaging and chemical sensing of fertilization-induced acid release from single sea urchin eggs. *Anal. Biochem.* 273, 168–178. <https://doi.org/10.1006/abio.1999.4173>
- Miller, E.W., 2016. Small molecule fluorescent voltage indicators for studying membrane potential. *Curr. Opin. Chem. Biol.* 33, 74–80. <https://doi.org/10.1016/j.cbpa.2016.06.003>
- Miller, J., Fraser, S.E., McClay, D., 1995. Dynamics of thin filopodia during sea urchin gastrulation. *Development* 121, 2501–2511.
- Mitoma, H., Manto, M., Shaikh, A.G., 2021. Mechanisms of ethanol-induced cerebellar ataxia: Underpinnings of neuronal death in the cerebellum. *Int. J. Environ. Res. Public Health* 18(6), 8678. <https://doi.org/10.3390/ijerph18168678>
- Modell, J.W., Bradham, C.A., 2011. Mitochondrial gradients and p38 activity in early sea urchin embryos. *Mol. Reprod. Dev.* 78, 225. <https://doi.org/10.1002/mrd.21302>

- Nam, J., Su, Y.H., Lee, P.Y., Robertson, A.J., Coffman, J.A., Davidson, E.H., 2007. Cis-regulatory control of the nodal gene, initiator of the sea urchin oral ectoderm gene network. *Dev. Biol.* 306, 860–869. <https://doi.org/10.1016/j.ydbio.2007.03.033>
- Negulescu, P.A., Machen, T.E., 1990. Intracellular Ion Activities and Membrane Transport in Parietal Cells Measured with Fluorescent Dyes. *Methods Enzymol.* 192, 38–81. [https://doi.org/10.1016/0076-6879\(90\)92062-I](https://doi.org/10.1016/0076-6879(90)92062-I)
- Nelson, C., Buttrick, B., Isoherranen, N., 2013. Therapeutic Potential of the Inhibition of the Retinoic Acid Hydroxylases CYP26A1 and CYP26B1 by Xenobiotics. *Curr. Top. Med. Chem.* 13, 1402–1428. <https://doi.org/10.2174/1568026611313120004>
- Nishioka, D., McGwin, N.F., 1980. Relationships between the release of acid, the cortical reaction, and the increase of protein synthesis in sea urchin eggs. *J. Exp. Zool.* 212, 215–223. <https://doi.org/10.1002/jez.1402120208>
- Nüsslein-volhard, C., Wieschaus, E., 1980. Mutations affecting segment number and polarity in drosophila. *Nature* 287, 795–801. <https://doi.org/10.1038/287795a0>
- Oliveri, P., Carrick, D.M., Davidson, E.H., Oliveri, P., 2002. A regulatory gene network that directs micromere specification in the sea urchin embryo. *Dev. Biol.* 246, 209–228. <https://doi.org/10.1006/dbio.2002.0627>
- Oliveri, P., Davidson, E.H., McClay, D.R., 2003. Activation of pmar1 controls specification of micromeres in the sea urchin embryo. *Dev. Biol.* 258, 32–43. [https://doi.org/10.1016/S0012-1606\(03\)00108-8](https://doi.org/10.1016/S0012-1606(03)00108-8)
- Oliveri, P., Tu, Q., Davidson, E.H., 2008. Global regulatory logic for specification of an embryonic cell lineage. *Proc. Natl. Acad. Sci. U.S.A.* 105(16), 5955–5962.

<https://doi.org/10.1073/pnas.0711220105>

- Ontko, J.A., 1973. Effects of ethanol on the metabolism of free fatty acids in isolated liver cells. *J. Lipid Res.* 14, 78–86. [https://doi.org/10.1016/s0022-2275\(20\)39332-9](https://doi.org/10.1016/s0022-2275(20)39332-9)
- Orr, C.W., Yoshikawa-Fukada, M., Ebert, J.D., 1972. Potassium: effect on DNA synthesis and multiplication of baby-hamster kidney cells: (cell cycle-membrane potential-synchronization-transformation). *Proc. Natl. Acad. Sci. U. S. A.* 69, 243–247. <https://doi.org/10.1073/pnas.69.1.243>
- Owen, C.S., 1992. Comparison of spectrum-shifting intracellular pH probes 5'(and 6')-carboxy-10-dimethylamino-3-hydroxyspiro[7H-benzo[c]xanthene-7, 1'(3'H)-isobenzofuran]-3'-one and 2',7'-biscarboxyethyl-5(and 6)-carboxyfluorescein. *Anal. Biochem.* 204, 65–71. [https://doi.org/10.1016/0003-2697\(92\)90140-3](https://doi.org/10.1016/0003-2697(92)90140-3)
- Peter, I.S., Davidson, E.H., 2011. A gene regulatory network controlling the embryonic specification of endoderm. *Nature* 474, 635–639. <https://doi.org/10.1038/nature10100>
- Peterka, D.S., Takahashi, H., Yuste, R., 2011. Imaging Voltage in Neurons. *Neuron* 69, 9–21. <https://doi.org/10.1016/j.neuron.2010.12.010>
- Petrelli, B., Bendelac, L., Hicks, G.G., Fainsod, A., 2019. Insights into retinoic acid deficiency and the induction of craniofacial malformations and microcephaly in Fetal Alcohol Spectrum Disorder. *Genesis* 1, e23278. <https://doi.org/10.1002/dvg.23278>
- Petryk, A., Graf, D., Marcucio, R., 2015. Holoprosencephaly: Signaling interactions between the brain and the face, the environment and the genes, and the phenotypic

- variability in animal models and humans. *Wiley Interdiscip. Rev. Dev. Biol.* 4(1), 17–32. <https://doi.org/10.1002/wdev.161>
- Piacentino, M.L., Chung, O., Ramachandran, J., Zuch, D.T., Yu, J., Conaway, E.A., Reyna, A.E., Bradham, C.A., 2016a. Zygotic LvBMP5-8 is required for skeletal patterning and for left-right but not dorsal-ventral specification in the sea urchin embryo. *Dev. Biol.* 412, 44–56. <https://doi.org/10.1016/j.ydbio.2016.02.015>
- Piacentino, M.L., Ramachandran, J., Bradham, C.A., 2015. Late Alk4/5/7 signaling is required for anterior skeletal patterning in sea urchin embryos. *Development* 142, 943–952. <https://doi.org/10.1242/dev.114322>
- Piacentino, M.L., Zuch, D.T., Fishman, J., Rose, S., Speranza, E.E., Li, C., Yu, J., Chung, O., Ramachandran, J., Ferrell, P., Patel, V., Reyna, A., Hameeduddin, H., Chaves, J., Hewitt, F.B., Bardot, E., Lee, D., Core, A.B., Hogan, J.D., Keenan, J.L., Luo, L., Coulombe-Huntington, J., Blute, T.A., Oleinik, E., Ibn-Salem, J., Poustka, A.J., Bradham, C.A., 2016b. RNA-Seq identifies SPGs as a ventral skeletal patterning cue in sea urchins. *Development* 143, 703–714. <https://doi.org/10.1242/dev.129312>
- Rahman, F.B., Yamauchi, K., 2006. Uncompetitive inhibition of *Xenopus laevis* aldehyde dehydrogenase 1A1 by divalent cations. *Zoolog. Sci.* 23, 239–244. <https://doi.org/10.2108/zsj.23.239>
- Range, R., Lapraz, F., Quirin, M., Marro, S., Besnardeau, L., Lepage, T., 2007. Cis-regulatory analysis of nodal and maternal control of dorsal-ventral axis formation by Univin, a TGF β related to Vg1. *Development* 134, 3649–3664. <https://doi.org/10.1242/dev.007799>

- Ransick, A., Davidson, E.H., 1995. Micromeres are required for normal vegetal plate specification in sea urchin embryos. *Development* 121, 3215–3222.
<https://doi.org/10.1242/dev.121.10.3215>
- Reid, B., Zhao, M., 2014. The Electrical Response to Injury: Molecular Mechanisms and Wound Healing. *Adv. Wound Care* 3, 184–201.
<https://doi.org/10.1089/wound.2013.0442>
- Reimers, M.J., Flockton, A.R., Tanguay, R.L., 2004. Ethanol- and acetaldehyde-mediated developmental toxicity in zebrafish. In: *Neurotoxicology and Teratology*. Elsevier Inc., pp. 769–781. <https://doi.org/10.1016/j.ntt.2004.06.012>
- Riddle, R.D., Ensini, M., Nelson, C., Tsuchida, T., Jessell, T.M., Tabin, C., 1995. Induction of the LIM homeobox gene *Lmx1* by WNT6a establishes dorsoventral pattern in the vertebrate limb. *Cell* 83, 631–640. [https://doi.org/10.1016/0092-8674\(95\)90103-5](https://doi.org/10.1016/0092-8674(95)90103-5)
- Rottinger, E., Saudemont, A., Duboc, V., Besnardeau, L., McClay, D., Lepage, T., 2008. FGF signals guide migration of mesenchymal cells, control skeletal morphogenesis and regulate gastrulation during sea urchin development. *Development* 135, 785–785. <https://doi.org/10.1242/dev.020016>
- Samanta, M.P., Tongprasit, W., Istrail, S., Cameron, R.A., Tu, Q., Davidson, E.H., Stolc, V., 2006. The transcriptome of the sea urchin embryo. *Science* 314, 960–962.
<https://doi.org/10.1126/science.1131898>
- Sarmah, S., Srivastava, R., McClintick, J.N., Janga, S.C., Edenberg, H.J., Marrs, J.A., 2020. Embryonic ethanol exposure alters expression of *sox2* and other early

- transcripts in zebrafish, producing gastrulation defects. *Sci. Rep.* 10.
<https://doi.org/10.1038/s41598-020-59043-x>
- Saudemont, A., Haillet, E., Mekpoh, F., Bessodes, N., Quirin, M., Lapraz, F., Duboc, V., Röttinger, E., Range, R., Oisel, A., Besnardeau, L., Wincker, P., Lepage, T., 2010. Ancestral regulatory circuits governing ectoderm patterning downstream of nodal and BMP2/4 revealed by gene regulatory network analysis in an echinoderm. *PLoS Genet.* 6, 1–31. <https://doi.org/10.1371/journal.pgen.1001259>
- Schatzberg, D., Lawton, M., Hadyniak, S.E., Ross, E.J., Carney, T., Beane, W.S., Levin, M., Bradham, C.A., 2015. H⁺/K⁺ ATPase activity is required for biomineralization in sea urchin embryos. *Dev. Biol.* 406, 259–270.
<https://doi.org/10.1016/j.ydbio.2015.08.014>
- Serio, R.N., Laursen, K.B., Urvalek, A.M., Gross, S.S., Gudas, L.J., 2019. Ethanol promotes differentiation of embryonic stem cells through retinoic acid receptor- γ . *J. Biol. Chem.* 294, 5536–5548. <https://doi.org/10.1074/jbc.RA118.007153>
- Sethi, A.J., Angerer, R.C., Angerer, L.M., 2009. Gene regulatory network interactions in sea urchin endomesoderm induction. *PLoS Biol.* 7, 0248–0264.
<https://doi.org/10.1371/journal.pbio.1000029>
- Shabtai, Y., Bendelac, L., Jubran, H., Hirschberg, J., Fainsod, A., 2018. Acetaldehyde inhibits retinoic acid biosynthesis to mediate alcohol teratogenicity. *Sci. Rep.* 8, 347.
<https://doi.org/10.1038/s41598-017-18719-7>
- Shen, S.S., Steinhardt, R.A., 1978. Direct measurement of intracellular pH during metabolic derepression of the sea urchin egg. *Nature* 272, 253–254.

<https://doi.org/10.1038/272253a0>

- Sherwood, D.R., McClay, D.R., 1999. LvNotch signaling mediates secondary mesenchyme specification in the sea urchin embryo. *Development* 126, 1703–1713. <https://doi.org/10.1242/dev.126.8.1703>
- Sidik, A., Dixon, G., Buckley, D.M., Kirby, H.G., Sun, S., Eberhart, J.K., 2021. Exposure to ethanol leads to midfacial hypoplasia in a zebrafish model of FASD via indirect interactions with the Shh pathway. *BMC Biol.* 19, 1–18. <https://doi.org/10.1186/s12915-021-01062-9>
- Singh, S., Arcaroli, J., Thompson, D.C., Messersmith, W., Vasiliou, V., 2015. Acetaldehyde and retinaldehyde-metabolizing enzymes in colon and pancreatic cancers. *Adv. Exp. Med. Biol.* 815, 281–294. https://doi.org/10.1007/978-3-319-09614-8_16
- Smith, S.M., Garic, A., Flentke, G.R., Berres, M.E., 2014. Neural crest development in fetal alcohol syndrome. *Birth Defects Res. Part C - Embryo Today Rev.* 102, 210–220. <https://doi.org/10.1002/bdrc.21078>
- Sodergren, E., Weinstock, G.M., Davidson, E.H., Cameron, R.A., Gibbs, R.A., Angerer, R.C., Angerer, L.M., Arnone, M.I., Burgess, D.R., Burke, R.D., Coffman, J.A., Dean, M., Elphick, M.R., Etensohn, C.A., Foltz, K.R., Hamdoun, A., Hynes, R.O., Klein, W.H., Marzluff, W., McClay, D.R., Morris, R.L., Mushegian, A., Rast, J.P., Smith, L.C., Thorndyke, M.C., Vacquier, V.D., Wessel, G.M., Wray, G., Zhang, L., Elsik, C.G., Ermolaeva, O., Hlavina, W., Hofmann, G., Kitts, P., Landrum, M.J., Mackey, A.J., Maglott, D., Panopoulou, G., Poustka, A.J., Pruitt, K., Sapozhnikov, V.,

Song, X., Souvorov, A., Solovyev, V., Wei, Z., Whittaker, C.A., Worley, K., Durbin, K.J., Shen, Y., Fedrigo, O., Garfield, D., Haygood, R., Primus, A., Satija, R., Severson, T., Gonzalez-Garay, M.L., Jackson, A.R., Milosavljevic, A., Tong, M., Killian, C.E., Livingston, B.T., Wilt, F.H., Adams, N., Bellé, R., Carbonneau, S., Cheung, R., Cormier, P., Cosson, B., Croce, J., Fernandez-Guerra, A., Genevière, A.M., Goel, M., Kelkar, H., Morales, J., Mulner-Lorillon, O., Robertson, A.J., Goldstone, J. V, Cole, B., Epel, D., Gold, B., Hahn, M.E., Howard-Ashby, M., Scally, M., Stegeman, J.J., Allgood, E.L., Cool, J., Judkins, K.M., McCafferty, S.S., Musante, A.M., Obar, R.A., Rawson, A.P., Rossetti, B.J., Gibbons, I.R., Hoffman, M.P., Leone, A., Istrail, S., Materna, S.C., Samanta, M.P., Stolc, V., Tongprasit, W., Tu, Q., Bergeron, K.F., Brandhorst, B.P., Whittle, J., Berney, K., Bottjer, D.J., Calestani, C., Peterson, K., Chow, E., Yuan, Q.A., Elhaik, E., Graur, D., Reese, J.T., Bosdet, I., Heesun, S., Marra, M.A., Schein, J., Anderson, M.K., Brockton, V., Buckley, K.M., Cohen, A.H., Fugmann, S.D., Hibino, T., Loza-Coll, M., Majeske, A.J., Messier, C., Nair, S. V, Pancer, Z., Terwilliger, D.P., Agca, C., Arboleda, E., Chen, N., Churcher, A.M., Hallböök, F., Humphrey, G.W., Idris, M.M., Kiyama, T., Liang, S., Mellott, D., Mu, X., Murray, G., Olinski, R.P., Raible, F., Rowe, M., Taylor, J.S., Tessmar-Raible, K., Wang, D., Wilson, K.H., Yaguchi, S., Gaasterland, T., Galindo, B.E., Gunaratne, H.J., Juliano, C., Kinukawa, M., Moy, G.W., Neill, A.T., Nomura, M., Raisch, M., Reade, A., Roux, M.M., Song, J.L., Su, Y.H., Townley, I.K., Voronina, E., Wong, J.L., Amore, G., Branno, M., Brown, E.R., Cavalieri, V., Duboc, V., Duloquin, L., Flytzanis, C., Gache, C., Lapraz, F., Lepage,

- T., Locascio, A., Martinez, P., Matassi, G., Matranga, V., Range, R., Rizzo, F., Röttinger, E., Wilson, K., Beane, W., Bradham, C., Byrum, C., Glenn, T., Hussain, S., Loza, M., Manning, G., Miranda, E., Thomason, R., Walton, K., Wikramanayke, A., Whittaker, C., Wu, S.Y., Xu, R., Brown, C.T., Chen, L., Gray, R.F., Lee, P.Y., Nam, J., Oliveri, P., Smith, J., Muzny, D., Bell, S., Chacko, J., Cree, A., Curry, S., Davis, C., Dinh, H., Dugan-Rocha, S., Fowler, J., Gill, R., Hamilton, C., Hernandez, J., Hines, S., Hume, J., Jackson, L.R., Jolivet, A., Kovar, C., Lee, S., Lewis, L., Miner, G., Morgan, M., Nazareth, L. V, Okwuonu, G., Parker, D., Pu, L.L., Thorn, R., Wright, R., 2006. The genome of the sea urchin *Strongylocentrotus purpuratus*. *Science* 314, 941–952. <https://doi.org/10.1126/science.1133609>
- Solomon, B.D., Mercier, S., Vélez, J.I., Pineda-Alvarez, D.E., Wyllie, A., Zhou, N., Dubourg, C., David, V., Odent, S., Roessler, E., Muenke, M., 2010. Analysis of genotype-phenotype correlations in human holoprosencephaly. *Am. J. Med. Genet. Part C Semin. Med. Genet.* 154C(1), 133–141. <https://doi.org/10.1002/ajmg.c.30240>
- Song, B., Zhao, M., Forrester, J., McCaig, C., 2004. Nerve regeneration and wound healing are stimulated and directed by an endogenous electrical field in vivo. *J. Cell Sci.* 117, 4681–4690. <https://doi.org/10.1242/jcs.01341>
- Soukup, V., Yong, L.W., Lu, T.M., Huang, S.W., Kozmik, Z., Yu, J.K., 2015. The Nodal signaling pathway controls left-right asymmetric development in amphioxus. *EvoDevo* 6. <https://doi.org/10.1186/2041-9139-6-5>
- Steinhardt, R.A., Epel, D., 1974. Activation of sea urchin eggs by a calcium ionophore. *Proc. Natl. Acad. Sci. U. S. A.* 71, 1915–1919.

<https://doi.org/10.1073/pnas.71.5.1915>

Stumpp, M., Hu, M.Y., Melzner, F., Gutowska, M.A., Dorey, N., Himmerkus, N., Holtmann, W.C., Dupont, S.T., Thorndyke, M.C., Bleich, M., 2012. Acidified seawater impacts sea urchin larvae pH regulatory systems relevant for calcification. *Proc. Natl. Acad. Sci. U. S. A.* 109, 18192–18197.

<https://doi.org/10.1073/pnas.1209174109>

Su, Y.H., Li, E., Geiss, G.K., Longabaugh, W.J.R., Krämer, A., Davidson, E.H., 2009. A perturbation model of the gene regulatory network for oral and aboral ectoderm specification in the sea urchin embryo. *Dev. Biol.* 329, 410–421.

<https://doi.org/10.1016/j.ydbio.2009.02.029>

Sulik, K.K., 2014. Fetal alcohol spectrum disorder: Pathogenesis and mechanisms, in: *Handbook of Clinical Neurology. Handb Clin Neurol*, pp. 463–475.

<https://doi.org/10.1016/B978-0-444-62619-6.00026-4>

Sun, M.R., Chung, H.M., Matsuk, V., Fink, D.M., Stebbins, M.J., Palecek, S.P., Shusta, E. V., Lipinski, R.J., 2020. Sonic Hedgehog Signaling in Cranial Neural Crest Cells Regulates Microvascular Morphogenesis in Facial Development. *Front. Cell Dev. Biol.* 8, 1055. <https://doi.org/10.3389/fcell.2020.590539>

<https://doi.org/10.3389/fcell.2020.590539>

Sun, Z., Etensohn, C.A., 2014. Signal-dependent regulation of the sea urchin skeletogenic gene regulatory network. *Gene Expr. Patterns* 16, 93–103.

<https://doi.org/10.1016/j.gep.2014.10.002>

Sundelacruz, S., Levin, M., Kaplan, D.L., 2009. Role of membrane potential in the regulation of cell proliferation and differentiation. *Stem Cell Rev. Reports* 5, 231–

246. <https://doi.org/10.1007/s12015-009-9080-2>
- Thomas, J.D., Warren, K.R., Hewitt, B.G., 2010. Fetal Alcohol Spectrum Disorders From Research to Policy. *Alcohol Res. Heal.* 33, 118–126.
<https://doi.org/10.3305/nh.2015.32.2.8373>
- Ulloa, F., Briscoe, J., 2007. Morphogens and the control of cell proliferation and patterning in the spinal cord. *Cell Cycle*. <https://doi.org/10.4161/cc.6.21.4822>
- Vieira, A.C., Reid, B., Cao, L., Mannis, M.J., Schwab, I.R., Zhao, M., 2011. Ionic components of electric current at rat corneal wounds. *PLoS One* 6, e17411.
<https://doi.org/10.1371/journal.pone.0017411>
- von Ubisch, L., 1937. Die Normale Skelettbildung bei *Echinocyamus pusillus* und *Psamechinus miliaris* und die Bedeutung dieser Vorgänge für die Analyse der Skelette von Keimblatt-Chimären. *Z Wiss. Zool* 149, 402–476.
- Walton, K.D., Croce, J.C., Glenn, T.D., Wu, S.Y., McClay, D.R., 2006. Genomics and expression profiles of the Hedgehog and Notch signaling pathways in sea urchin development. *Dev. Biol.* 300, 153–164. <https://doi.org/10.1016/j.ydbio.2006.08.064>
- Walton, K.D., Warner, J., Hertzler, P.H., McClay, D.R., 2009. Hedgehog signaling patterns mesoderm in the sea urchin. *Dev. Biol.* 331, 26–37.
<https://doi.org/10.1016/j.ydbio.2009.04.018>
- Wang, E., Yin, Y., Zhao, M., Forrester, J. V., McCaig, C.D., 2003. Physiological electric fields control the G1/S phase cell cycle checkpoint to inhibit endothelial cell proliferation. *FASEB J.* 17, 458–460. <https://doi.org/10.1096/fj.02-0510fje>

- Warner, J.F., McCarthy, A.M., Morris, R.L., McClay, D.R., 2014. Hedgehog signaling requires motile cilia in the sea urchin. *Mol. Biol. Evol.* 31, 18–22.
<https://doi.org/10.1093/molbev/mst176>
- Warner, J.F., Miranda, E.L., McClay, D.R., 2016. Contribution of hedgehog signaling to the establishment of left-right asymmetry in the sea urchin. *Dev. Biol.* 411, 314–324. <https://doi.org/10.1016/j.ydbio.2016.02.008>
- Wikramanayake, A.H., Huang, L., Klein, W.H., 1998. β -Catenin is essential for patterning the maternally specified animal-vegetal axis in the sea urchin embryo. *Proc. Natl. Acad. Sci. U. S. A.* 95, 9343–9348.
<https://doi.org/10.1073/pnas.95.16.9343>
- Wilson, G.F., Chiu, S.Y., 1993. Mitogenic factors regulate ion channels in Schwann cells cultured from newborn rat sciatic nerve. *J. Physiol.* 470, 501–520.
<https://doi.org/10.1113/jphysiol.1993.sp019872>
- Wilson, J.G., Roth, C.B., Warkany, J., 1953. An analysis of the syndrome of malformations induced by maternal vitamin a deficiency. Effects of restoration of vitamin a at various times during gestation. *Am. J. Anat.* 92, 189–217.
<https://doi.org/10.1002/aja.1000920202>
- Wilt, F.H., 2002. Biomineralization of the spicules of sea urchin embryos. *Zoolog. Sci.* 19(3), 253–261. <https://doi.org/10.2108/zsj.19.253>
- Wilt, F.H., 1999. Matrix and mineral in the sea urchin larval skeleton. *J. Struct. Biol.* 126, 216–226. <https://doi.org/10.1006/jsbi.1999.4105>

- Wolff, C., Fuks, B., Chatelain, P., 2003. Comparative study of membrane potential-sensitive fluorescent probes and their use in ion channel screening assays. *J. Biomol. Screen.* 8, 533–543. <https://doi.org/10.1177/1087057103257806>
- Wu, S.Y., McClay, D.R., 2007. The Snail repressor is required for PMC ingression in the sea urchin embryo. *Development* 134, 1061–1070.
<https://doi.org/10.1242/dev.02805>
- Wu, S.Y., Yang, Y.P., McClay, D.R., 2008. Twist is an essential regulator of the skeletogenic gene regulatory network in the sea urchin embryo. *Dev. Biol.* 319, 406–415. <https://doi.org/10.1016/j.ydbio.2008.04.003>
- Yaguchi, S., Yaguchi, J., Angerer, R.C., Angerer, L.M., Burke, R.D., 2010. TGFB signaling positions the ciliary band and patterns neurons in the sea urchin embryo. *Dev. Biol.* 347, 71–81. <https://doi.org/10.1016/j.ydbio.2010.08.009>
- Yaguchi, S., Yaguchi, J., Burke, R.D., 2006. Specification of ectoderm restricts the size of the animal plate and patterns neurogenesis in sea urchin embryos. *Development* 133, 2337–2346. <https://doi.org/10.1242/dev.02396>
- Yajima, M., Wessel, G.M., 2011. Small micromeres contribute to the germline in the sea urchin. *Development* 138, 237–243. <https://doi.org/10.1242/dev.054940>
- Yelin, R., Schyr, R.B.H., Kot, H., Zins, S., Frumkin, A., Pillemer, G., Fainsod, A., 2005. Ethanol exposure affects gene expression in the embryonic organizer and reduces retinoic acid levels. *Dev. Biol.* 279, 193–204.
<https://doi.org/10.1016/j.ydbio.2004.12.014>

- Yost, H.J., 2001. Establishment of left-right asymmetry. *Int. Rev. Cytol.* 203, 357–381.
[https://doi.org/10.1016/s0074-7696\(01\)03011-x](https://doi.org/10.1016/s0074-7696(01)03011-x)
- You, M., Arteel, G.E., 2019. Effect of ethanol on lipid metabolism. *J. Hepatol.* 70(1), 237–248. <https://doi.org/10.1016/j.jhep.2018.10.037>
- Zakhari, S., 2006. Overview: How is alcohol metabolized by the body? *Alcohol Res. Heal.* 29(4), 245–254. <https://www.ncbi.nlm.nih.gov/pmc/articles/PMC6527027/>
- Zernicka-Goetz, M., 2002. Patterning of the embryo: The first spatial decisions in the life of a mouse. *Development* 129(4), 815–829. <https://doi.org/10.1242/dev.129.4.815>
- Zhang, J., Liu, Z., Jia, J., 2021. Mechanisms of smoothed regulation in hedgehog signaling. *Cells* 10, 2138. <https://doi.org/10.3390/cells10082138>
- Zhao, M., Song, B., Pu, J., Wada, T., Reid, B., Tai, G., Wang, F., Guo, A., Walczysko, P., Gu, Y., Sasaki, T., Suzuki, A., Forrester, J. V., Bourne, H.R., Devreotes, P.N., McCaig, C.D., Penninger, J.M., 2006. Electrical signals control wound healing through phosphatidylinositol-3-OH kinase- γ and PTEN. *Nature* 442, 457–460.
<https://doi.org/10.1038/nature04925>
- Zuch, D.T., Bradham, C.A., 2019. Spatially mapping gene expression in sea urchin primary mesenchyme cells. In *Methods in Cell Biology*. Academic Press, pp. 433–442. <https://doi.org/10.1016/bs.mcb.2019.01.006>

CURRICULUM VITAE

